

RICE UNIVERSITY

Uncertainty in Regional Air Quality Modeling

by

Antara Digar

A THESIS SUBMITTED
IN PARTIAL FULFILLMENT OF THE
REQUIREMENTS FOR THE DEGREE

Doctor of Philosophy

APPROVED, THESIS COMMITTEE



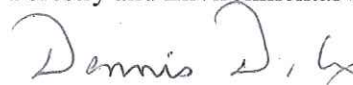
Daniel S. Cohan, Chair,
Assistant Professor, Civil and Environmental
Engineering, Rice University



Robert J. Griffin,
Associate Professor, Civil and Environmental
Engineering, Rice University



Michelle L. Bell,
Professor, Environmental Health, Yale School of
Forestry and Environmental Studies



Dennis D. Cox,
Professor, Statistics, Rice University

HOUSTON, TEXAS
February, 2012

ABSTRACT

Uncertainty in Regional Air Quality Modeling

by

Antara Digar

Effective pollution mitigation is the key to successful air quality management. Although states invest millions of dollars to predict future air quality, the regulatory modeling and analysis process to inform pollution control strategy remains uncertain. Traditionally deterministic 'bright-line' tests are applied to evaluate the sufficiency of a control strategy to attain an air quality standard. A critical part of regulatory attainment demonstration is the prediction of future pollutant levels using photochemical air quality models. However, because models are uncertain, they yield a false sense of precision that pollutant response to emission controls is perfectly known and may eventually mislead the selection of control policies. These uncertainties in turn affect the health impact assessment of air pollution control strategies.

This thesis explores beyond the conventional practice of *deterministic* attainment demonstration and presents novel approaches to yield *probabilistic* representations of pollutant response to emission controls by accounting for uncertainties in regional air quality planning. Computationally-efficient methods are developed and validated to characterize uncertainty in the prediction of secondary pollutant (ozone and particulate matter) sensitivities to precursor emissions in the

presence of uncertainties in model assumptions and input parameters. We also introduce *impact factors* that enable identification of model inputs and scenarios that strongly influence pollutant concentrations and sensitivity to precursor emissions. We demonstrate how these *probabilistic* approaches could be applied to determine the likelihood that any control measure will yield regulatory attainment, or could be extended to evaluate probabilistic health benefits of emission controls, considering uncertainties in both air quality models and epidemiological concentration–response relationships. Finally, ground-level observations for pollutant (ozone) and precursor concentrations (oxides of nitrogen) have been used to adjust probabilistic estimates of pollutant sensitivities based on the performance of simulations in reliably reproducing ambient measurements. Various observational metrics have been explored for better scientific understanding of how sensitivity estimates vary with measurement constraints. Future work could extend these methods to incorporate additional modeling uncertainties and alternate observational metrics, and explore the responsiveness of future air quality to project trends in emissions and climate change.

Acknowledgments

My Ph.D. journey has been remarkable! To be here at the final destination, I am grateful to all who have lent me their whole-hearted support all through my research. First and foremost I want to thank my advisor, Professor Daniel S. Cohan. It has been an honor to be his first Ph.D. student. His encouraging words, guidance and constant support, has helped me to think creatively and embrace challenges with a positive attitude. I am grateful to Professor Robert J. Griffin, Professor Michelle Bell and Professor Dennis D. Cox for their interests in my work and willingness to serve on my thesis committee. Their constructive critics and helpful feedbacks have added immense value to my research work. My sincere thanks to Dr. Kristen Foley (U.S. EPA), whose help, especially during the last part of my thesis has been invaluable. She has been very kind to my queries, giving me time whenever I wanted. I am thankful to my lab-mates Wei Tang, Xue Xiao and Wei Zhou for their all-possible help and cooperation.

I would also like to thank U.S. EPA Science To Achieve Results (STAR) (research grant R833665), Texas Air Quality Research Program (project 10-008) and National Science Foundation (grant 087386) for funding my research.

The acknowledgement cannot complete without expressing my deep indebtedness to my caring husband, Dipanjan, and my loving parents for their incredible support all through this journey, despite the painful distances. Finally I thank the Almighty for everything.

Contents

Acknowledgments	iii
Contents	iv
List of Figures	vii
List of Tables	xi
Nomenclature	xiii
Introduction	15
1.1. Background & Motivation	15
1.1.1. Air Pollution - Overview.....	15
<i>Tropospheric Ozone</i>	16
1.1.2. Air Quality Models	17
1.1.3. Uncertainties in Air Quality Modeling	19
1.1.4. Regulatory Applications of Air Quality Models	21
1.2. Scope of This Work.....	23
Reduced Form Model (RFM) to Characterize Parametric Uncertainty: Model Development and Validation	26
2.1. Introduction.....	26
2.2. Methods	29
2.2.1. Reduced Form Models for pollutant responsiveness.....	29
2.2.2. Photochemical Modeling Episode	36
2.3. Results and Discussion	38
2.3.1. Reduced Form Model evaluation	38
2.3.1.1. Selection of uncertain parameters	39
2.3.1.1. Evaluation of RFM in simulating transition regimes under a homogeneous uncertainty scenario	43
2.3.1.2. Evaluation of RFM in simulating transition regimes under a heterogeneous uncertainty scenario	55
2.3.1.3. Evaluation of RFM in simulating pollutant responsiveness in different ozone regimes	59
2.3.1.4. Evaluation of RFM in simulating pollutant impact under multiple controls	61

2.3.2. Computational efficiency and applicability of RFMs	62
Likelihood of achieving air quality targets under model uncertainties	67
3.1. Introduction.....	67
3.2. Methodology	70
3.2.1. Reduced Form Models.....	70
3.2.2. Probabilistic Framework and Reduction Targets.....	73
3.3. Application.....	77
3.3.1. Photochemical modeling episode	77
3.3.2. Control Strategies	78
3.3.3. Parameters for Uncertainty Analysis.....	82
3.4. Results and Discussion	83
3.4.1. Likelihood to Achieve a Fixed Target.....	84
3.4.2. Likelihood to Achieve Flexible Target	87
3.4.3. Relevance of Results	90
Uncertainties influencing health-based prioritization of ozone abatement options ...	92
4.1. Introduction.....	92
4.2. Methods	95
4.2.1. Air Quality Modeling.....	95
4.2.2. Health Benefit Estimation.....	98
4.2.3. Characterization of Uncertainty	99
4.2.3.1. <i>Structural Uncertainty</i>	99
4.2.3.2. Parametric Uncertainty.....	100
4.2.3.3. Epidemiological Uncertainty	104
4.3. Results and Discussion	104
Using observations to constrain probabilistic predictions of ozone-precursor responsiveness.....	114
5.1. Introduction.....	114
5.2. Photochemical Model description	117
5.2.1. Base Case Modeling.....	117
5.2.2. Model Uncertainty Scenarios	119
5.2.2.1. Structural Scenarios	119
5.2.2.2. Parametric Uncertainties	121

5.3. Ground-level Measurements of Ozone and its Precursors	122
5.4. Method	123
5.4.1. Model Uncertainty Analysis	123
5.4.1.1. Screening for Structural Uncertainty	124
5.4.1.2. Screening for Parametric Uncertainty	130
5.4.1.3. Joint consideration of structural and parametric uncertainty	133
5.4.2. Constraining Model Predictions using Measurements	133
5.4.2.1. Metric 1 (M1): Bayesian Analysis	135
5.4.2.2. Metric 2 (M2): Screening Based on Model Performance	137
5.4.2.3. Metric 3 (M3): Screening Based on Nonparametric Test	138
5.4.3. Adjusted Ozone Sensitivity	141
5.5. Results	141
5.6. Discussion	157
Conclusion	160
6.1. Major Findings and Contribution	160
6.1.1. Key factors influencing ozone-precursor responsiveness	160
6.1.2. Computationally efficient characterization of model uncertainties	161
6.1.3. Probabilistic framework for ozone attainment	162
6.2. Recommendations for Future Research	163
6.2.1. Additional Uncertainties	164
6.2.2. Observation-constrained Model Predictions	164
6.2.3. Economic Evaluation for Control Strategy Selection	165
6.2.4. Applicability	165
6.2.5. Valuable Extension	166
6.3. Closing Remarks	167
References	168
Appendix A	177
SUPPLEMENTARY INFORMATION TO CHAPTER 5:	177
Appendix B.....	183
PUBLICATIONS RELATED TO THE RESEARCH DESCRIBED IN THIS THESIS	183
Appendix C.....	184
PRESENTATIONS RELATED TO THE RESEARCH DESCRIBED IN THIS THESIS.....	184

List of Figures

Figure 1.1 – Formation pathway for O₃ in the troposphere.	17
Figure 1.2 – Schematic showing a 3-dimensional air quality model and its inputs	18
Figure 2.1 – The response of pollutant concentrations to reductions in emission rate E_j can change due to error in another input parameter (a) or in the base value of E_j itself (b).	31
Figure 2.2 – The 12-km resolution modeling domain (left) and the targeted Georgia emission regions (right)	37
Figure 2.3 – O₃ reduction (10 a.m. – 6 p.m.) due to 50% reduction in Atlanta NO_x (top) and 24-h average PM sulfate reduction due to 99.8% McDonough SO₂ control (bottom).	48
Figure 2.4 – O₃ reduction (10 a.m. – 6 p.m.) due to 50% reduction in Atlanta NO_x (top) and 24-h average PM sulfate reduction due to 99.8% McDonough SO₂ control (bottom).	51
Figure 2.5 – Ozone reduction due to 85% reduction in Plant McDonough NO_x, while domain-wide NO_x and VOC emissions and photolysis rates are increased by 50%, as simulated by brute-force (a), the discrete RFM neglecting (b) and accounting for (c) input parameter uncertainty. Results shown for 10 a.m.-6 p.m. on June 3.	52
Figure 2.6 – PM sulfate reduction due to 50% reduction in Atlanta SO₂, while domain-wide SO₂ and NH₃ emissions and photolysis rates are increased by 50%, as simulated by brute-force (a), the discrete RFM neglecting (b) and accounting for (c) input parameter uncertainty. Results shown for 24-hour average on June 3.	53
Figure 2.7 – PM ammonium reduction due to 50% reduction in Atlanta SO₂, while domain-wide SO₂ and NH₃ emissions and photolysis rates are increased by 50%, as simulated by brute-force (a), the discrete RFM neglecting (b) and accounting for (c) input parameter uncertainty. Results shown for 24-hour average on June 3.	54

Figure 2.8 – O₃ sensitivity coefficient without any parametric uncertainty (a) and adjusted coefficients when 6 input parameters are uncertain (b, c) (ANO_x: +40%, AVOC: -50%, RNO_x: +30%, RVOC: -40%, Rphoto: factor of 1.4, and R(NO₂+OH): +15%). Results are shown for 10 a.m.-6 p.m. in the urban regions of Atlanta on June 3.	57
Figure 2.9 – O₃ reductions due to 12% control in Atlanta NO_x in absence of parametric uncertainty (a, b) and when 6 input parameters are uncertain (c, d) (ANO_x: +40%, AVOC: -50%, RNO_x: +30%, RVOC: -40%, Rphoto: factor of 1.4, and R(NO₂+OH): +15%), as simulated by brute force finite differencing (left) and the reduced form model (right). Results are shown for 10 a.m.-6 p.m. in the urban regions of Atlanta on June 3.	58
Figure 2.10 – Reduction in ozone due to 50% reductions in NO_x (top) and VOC (bottom) emissions from HGB area in Texas, as simulated by brute-force (left) and the continuum RFM (right). Results are shown for 10 a.m. to 6 p.m. on September 2, 2006, when domain-wide NO_x, VOC, Rphoto and R(NO₂+OH) is +50% more.	60
Figure 2.11 – Reduction in ozone due to joint 50% reductions in NO_x emissions from both Atlanta and “Rest of Georgia”, as simulated by (a) brute-force, (b) summing the continuum RFM-predicted impacts for each region and (c) summing the continuum RFM-predicted impacts for each region with cross-sensitivity of O₃ sensitivity to emissions. Results are shown for 10 a.m. to 6 p.m. on June 3.	62
Figure 3.1 – Probabilistic framework for characterizing ozone response to a control strategy under model parametric uncertainty.	73
Figure 3.2 – Probability distribution of the O₃ impact at Confederate Avenue monitor due to a 12% reduction in Atlanta NO_x emissions and the likelihood that it will attain a flexible reduction target.	77
Figure 3.3 – Point sources and emission regions in Georgia considered for control strategy analyses.	79
Figure 3.4 – Predicted future O₃ design values (a) and likelihood of achieving a fixed (1.5 ppb) (b) or flexible (1.5 ± 3.0 ppb, 95% CI) (c) reduction target at Confederate Avenue monitor as a function of the percentage of Atlanta NO_x that is controlled under various scenarios for reducing NO_x emissions from other sources.	89

Figure 4.1 – CAMx Modeling Domain used for the study. [Source: TCEQ]	97
Figure 4.2 – Population density in the study region.....	97
Figure 4.3 – Probability density of averted premature mortalities per ozone season per ton per day reduction in anthropogenic NO_x or VOC emission from DFW under uncertain phi and/or beta. Modeling results are shown for 8-h O₃ metrics, averaged over the episode and integrated over the domain for the base-case simulation.....	105
Figure 4.4 – Max 8-h O₃ sensitivity to DFW emission and health benefits (averted mortalities) per ton of reduction in NO_x or VOCs for each of the 3 structural model scenarios when inputs are considered to be perfectly known. Episode average results are shown for the 4-km DFW sub-domain.....	106
Figure 4.5 – Health Impacts of 8-h O₃ reduction due to NO_x and VOC controls from DFW (9-county), considering uncertainties in photochemical modeling and in the health response relationship.....	108
Figure 4.6 – Relative health benefits from 8-h O₃ reduction due to (a) surface NO_x vs. elevated NO_x controls, and (b) total anthropogenic NO_x vs. VOC controls from DFW (9-county), considering uncertainties in photochemical modeling. The red dot denotes results from the deterministic modeling and pink regions represent negative impacts.....	109
Figure 4.7 – Diurnal profile of ozone concentrations and sensitivities for DFW sub-domain. Results are averaged over domain and episode.	110
Figure 4.8 – Averted mortalities per O₃ season due to 1 tpd reduction in NO_x or VOC emissions from various sources in DFW when both air quality model inputs (phi) and health risk estimates (beta) are uncertain. Results are averaged over the episode and integrated over the inner two modeling domains.	111
Figure 5.1 –Modeling domain used in the study [TCEQ, 2011a].	118
Figure 5.2 – Map showing the locations of the monitoring sites used in this study. The size of the circles are proportionate with their 2006 8-hour O₃ Design Values given in Table A.2 (Appendix A).....	123

Figure 5.3 – Diurnal profile of ozone sensitivities to DFW ANO_x (left) and AVOC (right) emissions, averaged over the episode and the grid-cells covering the DFW region.....	127
Figure 5.4 – Sensitivity of 8-hour O₃ to anthropogenic NO_x and VOC emissions from DFW for different structural model scenarios under default settings of input parameters. Episode average results are shown for the 4-km resolution domain.	129
Figure 5.5 – Flowchart for the observation-constrained Monte Carlo analysis.	134
Figure 5.6 – Weights assigned to the 4000 members of the full ensemble under the Bayesian Metric 1 using only 8-hour O₃, 24-hour NO_x and both (O₃ and NO_x) as the observational constraint.....	142
Figure 5.7 – Boxplot evaluating performance of model ensemble mean against 8-hour O₃ and 24-hour NO_x observations at each site-day within DFW.....	145
Figure 5.8 – PDFs for episode-average 8-hour ozone concentration at Denton (a)when observations from Denton were used to constrain the <i>a priori</i> results and (b) when observations from Denton were withheld.....	148
Figure 5.9 – Prior and posterior distributions of selected model input parameters.	151
Figure 5.10 – Probability density function of NO_x emission scaling factor showing results when only O₃ (left) or only NO_x (right) are used as observation constraints.....	152
Figure 5.11 – Comparison of 8-hour O₃ (top) and 24-hour NO_x (bottom) predictions against daily observations at all sites (left) and episode-average concentrations at each site (right).....	153
Figure 5.12 – <i>A priori</i> episode-average 8-hour ozone sensitivity results at Denton.....	155
Figure 5.13 – CDFs for the sensitivity of ozone at Denton monitor for the three metrics. Results are averaged over all days of the episode.	156

List of Tables

Table 1.1 –Sources of air quality model uncertainty.....	19
Table 2.1 – Uncertainties in selected photochemical model input parameters reported by previous published studies.....	42
Table 2.2 – Performance of the RFMs in predicting the impacts of emission reductions on 8-hour O₃ mixing ratios (10 a.m. – 6 p.m.) and 24-hr average PM sulfate concentrations, evaluated against brute force differencing of CMAQ runs.	46
Table 2.3 – Performance of the RFM in predicting the impacts of Atlanta regional emission reductions on 24-hr average PM ammonium concentrations, evaluated against brute force differencing of CMAQ runs. Results compared over all grid-cell-days in the episode.	49
Table 2.4 – Estimated computational time for Monte Carlo uncertainty analysis using continuum RFM or Brute Force for predicting pollutant response to emission controls under parametric uncertainty.....	64
Table 3.1 – Selection of uncertain input parameters for Monte Carlo analysis based on the impact analysis by <i>Digar and Cohan</i> [2010].....	74
Table 3.2 – NO_x control measures from AirControlNET[#] (based on the most stringent option available for each source).....	80
Table 3.3 – Additional NO_x control measures considered.....	81
Table 3.4 – Hypothetical NO_x emission control options in Georgia.	82
Table 3.5 – Reduction in 8-hour ozone at Atlanta Confederate Avenue monitor due to each emission control package.....	86
Table 4.1 – Uncertainties assumed in the input parameters for Monte Carlo analysis.	102
Table 5.1 – Screening test for the selection of uncertain model structural assumptions.....	128
Table 5.2 – Screening test for the selection of uncertain input parameters. .	132

Table 5.3 – Statistics for evaluating model performance in Metric 2 [USEPA, 2006b].	138
Table 5.4 – Posterior probability of the structural ensemble members.	143
Table 5.5 – Performance of the posterior model ensemble-mean against 8-hour O₃ at all site and days in DFW.	144
Table 5.6 – Comparison of prior and posterior episode average 8-hour ozone concentrations and sensitivities at Denton.	149

Nomenclature

Abbreviations:

USEPA	United States Environmental Protection Agency
NAAQS	National Ambient Air Quality Standard
SIP	State Implementation Plan
TCEQ	Texas Commission on Environmental Quality
EPD	Environmental Protection Division
CAMx	Comprehensive Air Quality Model with Extensions
CMAQ	Community Multiscale Air Quality Model
HDDM	High-order Decoupled Direct Method
O ₃	Ozone
PM	Particulate Matter
NO _x	Oxides of nitrogen
NO _y	Total reactive nitrogen
NO _z	Reaction products of NO _x (= NO _y - NO _x)
VOC	Volatile Organic Compounds
ppm	parts per million
ppb	parts per billion
NMB	Normalized Mean Bias
NME	Normalized Mean Error
RMSE	Root Mean Squared Error

Symbols:

C	Concentrations of pollutants (function of species, location, and time)
E_j	Base value of emission rate targeted for control
P_k	Base value of k^{th} uncertain input parameter
ε_j	Fractional change in targeted emission rate E_j
φ_k	Fractional error in input parameter P_k
C_B	Pollutant concentrations in base model
C_C	Pollutant concentrations in base model after controlling E_j
C_B^*	Pollutant concentrations adjusted for input errors φ_k
C_C^*	Pollutant concentrations with E_j controlled, adjusted for input parameter errors
ΔC	Pollutant response ($C_B - C_C$) to targeted emission reduction in base model
ΔC^*	Pollutant response ($C_B^* - C_C^*$) to targeted emission reduction after adjusting for input parameter errors
F_k	Response coefficient representing how response to a discrete emission reduction varies with changes in P_k (see Equation 9)
$S_j^{(1)}$	1 st -order sensitivity coefficient of pollutant concentrations to E_j
$S_j^{(2)}$	2 nd -order sensitivity coefficient of pollutant concentrations to E_j
$S_{j,k}^{(2)}$	2 nd -order cross-sensitivity coefficient of pollutant concentrations to E_j and P_k
μ	Mean
σ	Standard deviation

Chapter 1

Introduction

1.1. Background & Motivation

1.1.1. Air Pollution - Overview

Air pollution threatens human health. Concerns regarding the health effects of air pollution date back to the historic pollution episode - the “*Great Smog of 1952*” in London and consecutive severe smog events in New York and Los Angeles. Despite the continuous efforts of mitigating air pollution, large fractions of population all over the world are exposed to concentration levels that exceed the designated standards for air pollutants, the majority of which is due to ozone (O₃) and particulate matter (PM) [USEPA, 2011; European Environmental Agency, 2011]. These pollutants not only damage crop yield [Feng and Kobayashi, 2009; Renaut et al., 2009; Grantz et al., 2003] and reduce visibility [Malm et al., 1994], but also adversely affect human health. These effects may range from increased respiratory

illness such as aggravation of asthma [Brunekreef and Holgate, 2002; McConnell et al., 2002; Dockery and Pope, 1994] to causing premature mortality [Bell et al., 2004; Ito et al., 2005; Jerrett et al., 2009; NRC, 2008; Anderson et al., 2005; Hart et al., 2011]. Formulation of control strategies for ground-level O₃ and secondary PM is often challenging because these pollutants are not emitted directly into the atmosphere, instead they are formed as a result of nonlinear interactions between primary pollutants. Understanding the formation, transportation and removal processes of these secondary pollutants in the atmosphere is therefore critical for efficient management of ambient air quality. The subsequent section explains the complexity of secondary pollutant formation through a classic example for tropospheric O₃.

Tropospheric Ozone

In the troposphere, volatile organic compounds (VOCs) and oxides of nitrogen (NO_x), which denotes the sum of nitric oxide (NO) and nitrogen dioxide (NO₂), react to form O₃ in the presence of an oxidizing agent like hydroxyl radical (OH) [Lin et al., 1988; Seinfeld and Pandis, 2006; West et al., 1999]. Figure 1.1 elaborates the daytime formation pathway of O₃ in the troposphere. O₃ formation is influenced by the relative levels of NO_x and VOC emissions. Due to the complex nonlinear O₃-precursors relationship, reductions in NO_x emissions do not always lead to a proportional decrease of O₃ concentrations. Moreover, in regions where O₃ decreases with NO_x reductions, the ozone production efficiency of NO_x may vary with VOC concentrations, emission source, time and other meteorological factors

[Ryerson *et al.*, 2001; Lei *et al.*, 2008]. This complexity in O_3 - NO_x -VOC relationship demands a strong understanding of the underlying atmospheric photochemistry in order to formulate effective emission control strategies.

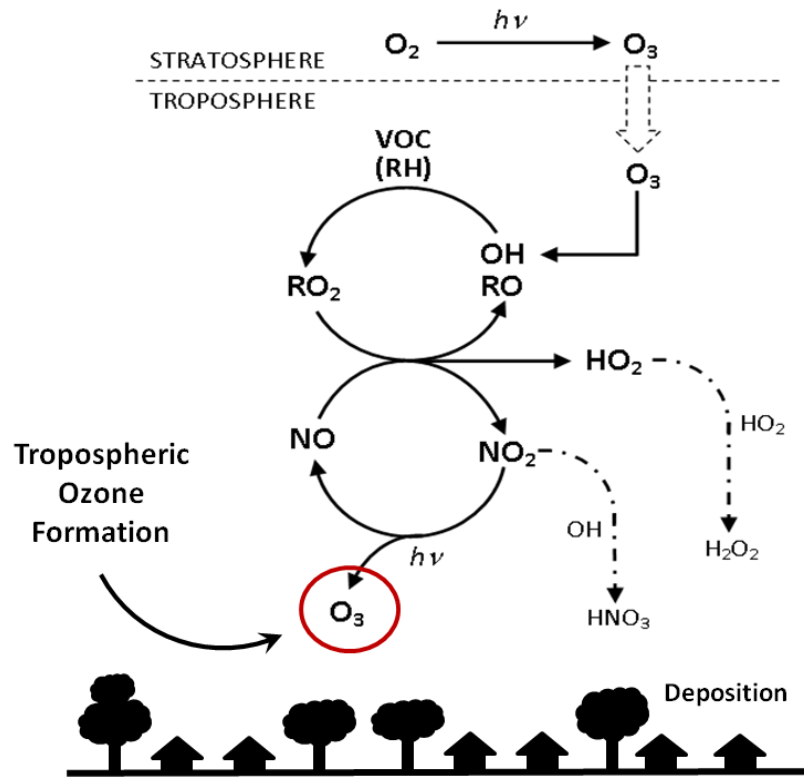


Figure 1.1 – Formation pathway for O_3 in the troposphere.

1.1.2. Air Quality Models

Air quality models are widely used to predict changes in secondary pollutant concentrations as a result of various precursor emission controls [Collins *et al.*, 1997; Derwent and Davies, 1994; Godowitch *et al.*, 2008; Harley *et al.*, 1997]. These models predict changes in concentration of pollutant i (C_i) in time t , due to emission rate E_i , based on the atmospheric advection-diffusion equation as follows,

$$\frac{\partial C_i}{\partial t} = \underbrace{-\nabla u C_i}_{\text{Advection}} + \underbrace{\nabla K \nabla C_i}_{\text{Diffusion}} + \underbrace{R_i}_{\text{Chemical Reaction}} + \underbrace{E_i}_{\text{Emission}} \quad (1.1)$$

where u represents the wind velocity, K is the coefficient for eddy diffusivity, and R_i denotes the rate of chemical reaction.

Figure 1.2 illustrates the schematic of a 3-dimensional air quality grid model and its key inputs. Since these models are based on simplified mathematical representations of the complex nonlinear physical and chemical processes in the atmosphere, relying on large datasets of model-estimated inputs, the resulting output is inherently uncertain.

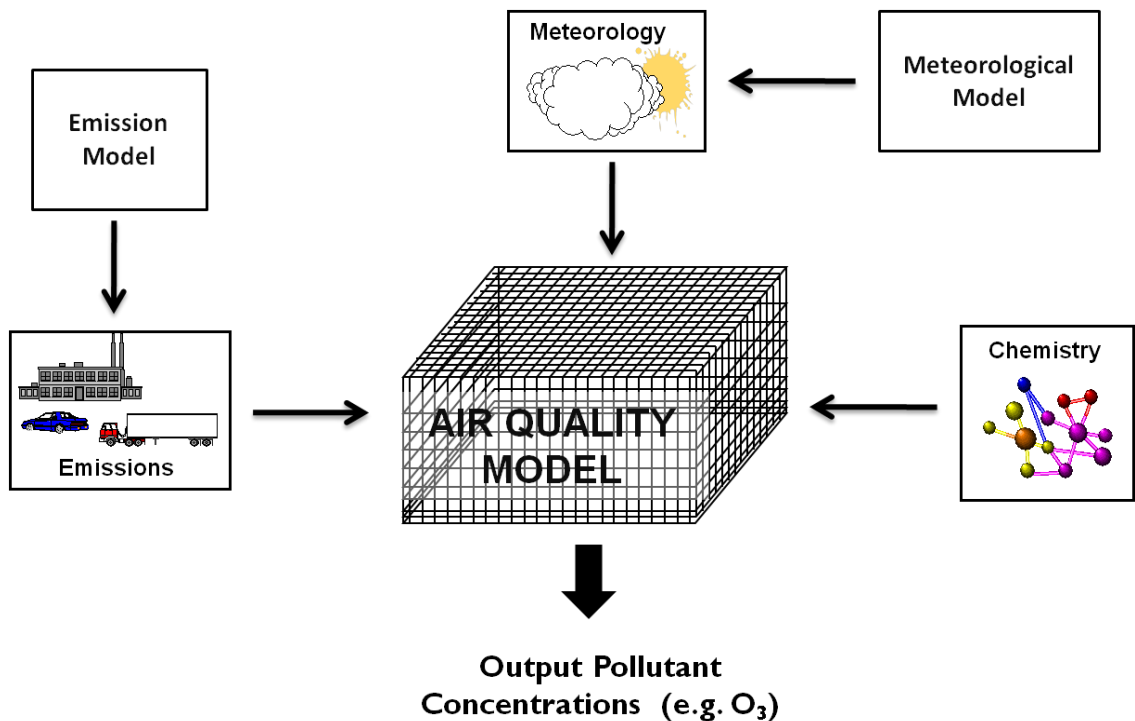


Figure 1.2 - Schematic showing a 3-dimensional air quality model and its inputs.

1.1.3. Uncertainties in Air Quality Modeling

Uncertainties in air quality models affect the accuracy of the predicted O₃ concentrations and responses to emissions changes. These uncertainties primarily arise from uncertain model formulation (*structural uncertainty*) and/or uncertain model input parameters (*parametric uncertainty*) [Fine et al., 2003; Russell and Dennis, 2000]. The key sources of photochemical model uncertainties as identified by these studies are listed in Table 1.1.

Structural Uncertainties	Parametric Uncertainties
Input Model Formulation (Emissions, Meteorology, Boundary Conditions, etc.)	Emission Rates
Chemical Mechanism	Reaction Rate Constants
Deposition Scheme	Deposition Velocity
Vertical Mixing Scheme	Boundary Conditions
Model Grid Resolution	Meteorological Parameters

Table 1.1 –Sources of air quality model uncertainty.

Considerable efforts have been made in the past to characterize how uncertainties in model input parameters influence model estimates of O₃ concentrations and their responses to fixed levels of emission reductions [Bergin et al., 1999; Moore and Londergan, 2001; Hanna et al., 2001]. These studies conducted Monte Carlo analysis of an air quality model for various input parameter settings by sampling parameter values (either randomly or using stratified sampling

techniques) from their estimated distribution defined by specific ranges of uncertainty. However, a key limitation of this type of uncertainty analysis for regulatory application involving numerous controls with extensive temporal and spatial resolution is its computational cost. A sophisticated and computationally efficient way to predict O₃ responses to flexible amounts of emissions changes is via sensitivity analysis [Cohan *et al.*, 2005; Yang *et al.*, 1997]. The Decoupled Direct Method (DDM) enables direct computation of O₃ sensitivity to multiple emission perturbations within a single model run [Dunker, 1981; Yang *et al.*, 1997]. Further extension of the DDM allows predicting the non-linearity in O₃-precursor relationship [Hakami *et al.*, 2003]. This method facilitates assessing the impact of perturbations in input parameters on predicted concentrations by computing 'sensitivity coefficients', which involves calculation of concentration gradient at any time as follows:

$$S_j^{(1)} = \frac{\partial C}{\partial \varepsilon_j} \quad (1.2)$$

$$S_j^{(2)} = \frac{\partial^2 C}{\partial \varepsilon_j^2} \quad (1.3)$$

$$S_{j,k}^{(2)} = \frac{\partial^2 C}{\partial \varepsilon_j \partial \varepsilon_k} \quad (1.4)$$

where, C denotes concentration, and ε_j and ε_k are the perturbations in parameters 'j' and 'k' respectively. $S_j^{(1)}$ and $S_{j,k}^{(2)}$ denote semi-normalized first- and second-order

sensitivities to parameters ' j ', and ρ_{jk} denotes cross-sensitivity between two input parameters ' j ' and ' k '.

Recent work by *Pinder et al.* [2009] introduced a reduced form model for O₃ concentration using DDM sensitivity coefficients by jointly considering both *parametric* and *structural* uncertainties. *Tian et al.* [2010] extended that approach to create a reduced form of a photochemical model to study the effect of uncertainties in emission inputs on O₃ response to various emission controls. However, neither study assessed the accuracy of these reduced form models.

1.1.4. Regulatory Applications of Air Quality Models

The Clean Air Act (CAA) necessitates the United States Environmental Protection Agency (US EPA) to impose standards, better known as National Ambient Air Quality Standards (NAAQS), on the concentration level of six criteria pollutants including O₃ and PM, for the betterment of environmental conditions and protection of human health. States with ambient monitors violating these standards must develop air pollution control strategies in order to attain the NAAQS by a future date. In attainment demonstrations, states use photochemical air quality models to deterministically evaluate whether an emission control strategy is sufficient to lower ambient pollutant concentrations below the regulatory NAAQS [USEPA, 2007]. However, recent studies have found that O₃ health effects are observed at concentrations even lower than the designated standard [Bell et al., 2006], which poses a serious question whether attainment of regulatory standards is fully protective of human health. A subsequent study by Cohan et al. [2006] reports that

the ranking of O₃ control options may differ based on the evaluation criteria of regulatory attainment and resulting health impacts. Therefore, evaluation of the relative health benefits of control options, along with their attainment implications could better inform control strategy selection and optimization of net benefits [Chestnut *et al.*, 2006].

Whether control strategies are assessed based on their relative health benefits or effectiveness of regulatory attainment, both assessments will largely depend on the accuracy of the regulatory models. However, uncertain air quality model results might mislead control strategy selection. Therefore, to yield results that are meaningful, one needs to account for these uncertainties while formulating air pollution abatement plans. *Hogrefe and Rao* [2001] suggests probabilistic analyses to supplement the pass/fail test of current regulatory practice. Probabilistic model uncertainty analysis considers multiple model simulations with varying model assumptions and input data, rather than a single “best-estimate” model setting. However, previous works focusing on uncertainty analysis of photochemical models have assumed all model scenarios to be equally probable [Bergin *et al.*, 1999; Moore and Londergan, 2001; Pinder *et al.*, 2009]. A Bayesian inference approach could be used to prioritize model simulations based on their relative performance in simulating observed pollutant concentrations [Bergin and Milford, 2000; Deguillaume *et al.*, 2007].

1.2. Scope of This Work

Following these footsteps, this thesis introduces and validates a computationally efficient Reduced Form Model (RFM) to represent how the responsiveness of pollutants to emission reductions in the underlying photochemical model varies with simultaneous perturbations in multiple model input parameters. This RFM is then used to develop a probabilistic framework for estimating the likelihood that an emission control strategy will achieve an air quality objective in the presence of uncertainties in a photochemical model. Methods have been discussed to prioritize O₃ control measures considering both NAAQS attainment requirements (considering model uncertainties) and maximum achievable levels of health benefits (considering uncertainties in health risk estimates). Finally, this thesis explores methods to constrain probabilistic estimates of O₃ sensitivities to NO_x and VOC emissions using ground-level observations of O₃ and its precursor concentrations.

Although this research extensively demonstrates application for O₃ abatement on specific regions and episodes, the methods can also be applied for other geographic locations, as well. Applicability of the RFM for particulate matter (PM) in Chapter 1 shows that the model can also be applied for other secondary pollutants like inorganic PM for which the underlying photochemical model is well developed.

The outline of the thesis is as follows:

- **Chapter 2, “Reduced Form Model (RFM) to characterize parametric uncertainty: development and validation”**, introduces two reduced form models (*Continuum* and *Discrete*) for efficiently representing air pollutant responsiveness to emissions controls under parametric uncertainty in photochemical models. To demonstrate the RFM, the Community Multiscale Air Quality (CMAQ) Model has been used, although this could be readily applied to any photochemical model. The accuracy and computational efficiency of the RFMs have been evaluated.
- **Chapter 3, “Probabilistic evaluation of ozone attainment considering parametric uncertainty”**, presents the methodology for evaluating the likelihood of attaining an air quality objective in light of parametric uncertainty in a photochemical model. Summertime episodes of high O₃ in the southeastern US, with particular focus on Georgia, have been considered as a case study. The method incorporates Monte Carlo simulations of the RFM to probabilistically predict the improvement in air quality due to emission control.
- **Chapter 4, “Prioritization of ozone abatement options considering health benefits”**, demonstrates methods to characterize uncertainties influencing health-benefits estimation of O₃ reduction (averted premature mortalities due to short-term exposure) in the Dallas-Fort Worth (DFW) region of Texas. The findings demonstrate that modeling of the relative health benefits of O₃ abatement options is greatly influenced by uncertainties

in photochemical modeling and the choice of temporal metric for characterizing health response to O₃ exposure.

- **Chapter 5, “Using observations to constrain probabilistic predictions of ozone-precursor responsiveness”**, aims at reliable estimation of O₃ sensitivities to precursor emissions by incorporating uncertainties in photochemical modeling and evaluating model performance based on ground-level observations of O₃ and NO_x. Weights based on a Bayesian inference technique, and screening based on model performance and statistical tests of significance are used to generate probabilistic representation of O₃ concentrations and its response to NO_x and VOCs.
- **Chapter 6** summarizes the research findings with concluding discussions and recommendations for future research.
- **Appendix A** furnishes supplemental information to Chapter 5.
- **Appendix B and C** lists all publications and presentations related to this research.

Adapted with permission from *Digar and Cohan*, Efficient Characterization of Pollutant-Emission Response under Parametric Uncertainty, *Environmental Science & Technology*, 44(17), 6724-6730, 2010. DOI: 10.1021/es903743t. Copyright © 2010, American Chemical Society.

Chapter 2

Reduced Form Model (RFM) to Characterize Parametric Uncertainty: Model Development and Validation

2.1. Introduction

Ground-level ozone (O_3) and particulate matter (PM) have long been leading targets of air quality management, due to their harmful effects on human health [Brunekreef and Holgate, 2002], natural ecosystems [Fuhrer, 2002], and visibility [Malm et al., 1994]. Control of these pollutants is complicated by the fact that they form from nonlinear interactions of multiple precursor compounds [Lin et al., 1988; West et al., 1999]. Accurate simulation of pollutant responsiveness to emission changes is critical to air quality management in the United States [Cohan et al., 2007; Hogrefe et al., 2008]. However, model predictions of pollutant-emission response

involve significant uncertainties due to errors in input parameters like emission rates, reaction rate constants, and initial and boundary conditions (*parametric uncertainty*) and due to errors in model assumptions and formulation (*structural uncertainty*). Parametric uncertainty plays a relatively large role for pollutants such as O₃ and inorganic PM for which the formation mechanism is generally well established but key input parameters are highly uncertain [*Fine et al., 2003; Pinder et al., 2009; Russell and Dennis, 2000*].

Recent studies have made considerable efforts to characterize how uncertainties in model input parameters influence model estimates of O₃ and PM concentrations and their sensitivities to emissions [*Bergin et al., 1999; Deguillaume et al., 2008; Fine et al., 2003; Hanna et al., 2001*]. Most of these studies used numerous model simulations with randomly sampled input parameters to characterize the probabilistic range of final outcomes. However, such an approach is immensely computationally intensive, making it unrealistic for characterizing uncertainty in regulatory applications that must consider several control measures at fine grid resolution for a long period of time with multiple uncertain parameters. Furthermore, most previous studies considered uncertainty of pollutant response only to fixed amounts of emission reductions. For attainment planning purposes, however, it may be desired to characterize the parametric uncertainty of pollutant response to controls of both variable size (e.g., regional sources with wide ranges of potential control levels) and fixed size (e.g., point sources with discrete control options) [*Cohan et al., 2006*]. The U.S. Environmental Protection Agency (U.S. EPA) has developed a response surface modeling approach for characterizing O₃ and

PM_{2.5} response to various emission categories, but has not probed the uncertainties in pollutant response that may result due to input uncertainties [Hill *et al.*, 2009; Hubbell, 2005].

Cohan *et al.* (2005) posited that second-order sensitivity coefficients could be applied to adjust concentration and first-order (incremental) sensitivity estimates to account for error in an input parameter [Cohan *et al.*, 2005]. Pinder *et al.* (2009) extended that approach to create a reduced form model (RFM) characterizing parametric uncertainty of pollutant concentrations, but not their responses to emission reductions [Pinder *et al.*, 2009]. Tian *et al.* (2010) [Tian *et al.*, 2010] extend that approach to create an RFM for O₃ response to a targeted emission reduction while multiple emission rates are uncertain. However, no previous works has assessed the accuracy of the RFMs relative to the underlying models or considered pollutants other than O₃. Gauging the accuracy of RFMs is crucial before such methods can be more widely adopted, given that secondary pollutant responsiveness could be influenced by nonlinear interactions among multiple input parameters.

This chapter assesses the accuracy of new computationally efficient approaches for estimating both O₃ and PM responsiveness to emission reductions of variable or fixed size while multiple input parameters are simultaneously perturbed. High-order sensitivity analysis is applied to develop analytical relationships (i.e., RFMs) between model outputs and changes in model inputs. These relationships characterize how the responsiveness of O₃ or PM to a control

option varies as model inputs are perturbed. The performance of the RFMs is evaluated by comparing the resulting response surfaces with traditional brute-force simulations for both O₃ and PM in a southeastern United States air pollution episode.

2.2. Methods

2.2.1. Reduced Form Models for pollutant responsiveness

Two analytical approaches are applied here, each aimed at characterizing uncertainty of modeled pollutant-emission response for a particular type of abatement scenario: (1) a comprehensive *Continuum Reduced Form Model (RFM)*, which uses local sensitivity coefficients computed by brute force or direct methods to develop equations that flexibly represent pollutant response to any level of emission reduction, analogous to the approach of ; and (2) a new simpler *Discrete RFM*, which uses brute force runs to explicitly simulate the impact of a pre-determined amount of emission reduction. Both RFMs yield analytical equations that can readily be applied to estimate pollutant response under any level of perturbed input parameters in the underlying model. The following section explains each of these models in detail.

- **Continuum RFM**

Suppose an emission rate, E_j , is perturbed by a factor ε_j such that,

$$E'_j = E_j + \Delta E_j = (1 + \varepsilon_j)E_j \quad (2.1)$$

The perturbation factor ε_j can be positive or negative, though attainment planning typically focuses on emissions controls (i.e., $\varepsilon_j < 0$). It is straightforward to estimate the resulting changes in pollutant levels, $\Delta\mathbf{C}$, by differencing concentrations under base (\mathbf{C}_B) and controlled (\mathbf{C}_C) conditions in two runs of a photochemical model. Note that \mathbf{C} (i.e., $C_i(X,t)$) represents concentrations of all modeled species i at all modeled locations X and times t , but the notations for space and time are dropped for simplicity. Previous studies [Cohan *et al.*, 2005; Hakami *et al.*, 2004] have demonstrated that $\Delta\mathbf{C}$ can also be approximated for flexible levels of ε_j by using Taylor expansions of local first- and second order sensitivity coefficients,

$S_j^{(1)} = \frac{\partial\mathbf{C}}{\partial\varepsilon_j}$ and $S_j^{(2)} = \frac{\partial^2\mathbf{C}}{\partial\varepsilon_j^2}$, as shown in Equation 2.2:

$$\Delta\mathbf{C} = \mathbf{C}_B - \mathbf{C}_C \approx - \left[\varepsilon_j S_j^{(1)} + \frac{1}{2} \varepsilon_j^2 S_j^{(2)} + \text{HOT} \right] \quad (2.2)$$

where HOT denotes higher-order terms (neglected here). The first- and second-order sensitivity coefficients may be computed by the high-order decoupled direct method (HDDM) [Dunker, 1984; Hakami *et al.*, 2003] or by finite differencing of brute force photochemical model runs.

Predictions of pollutant response to emissions perturbations become more complicated when input parameters are acknowledged to be uncertain. Uncertainties in model inputs affect predicted pollutant concentrations and their responsiveness to control measures due to the nonlinearity of secondary pollutant

formation processes (Figure 2.1) [Cohan et al., 2005; Hakami et al., 2004; Lin et al., 1988]. Consider a case when one or more input parameters have actual values, P_k^* , that differ from their modeled values, P_k , as described by Equation 3:

$$P_k^* = (1 + \phi_k)P_k \quad \text{for } k = 1, \dots, K \quad (2.3)$$

where ϕ_k is the fractional error (negative or positive) in model input P_k and the asterisk (*) is used throughout this paper to denote conditions after correcting for errors in input parameters. The uncertain input parameters may include the base level of the targeted emission rate E_j (Figure 2.1b).

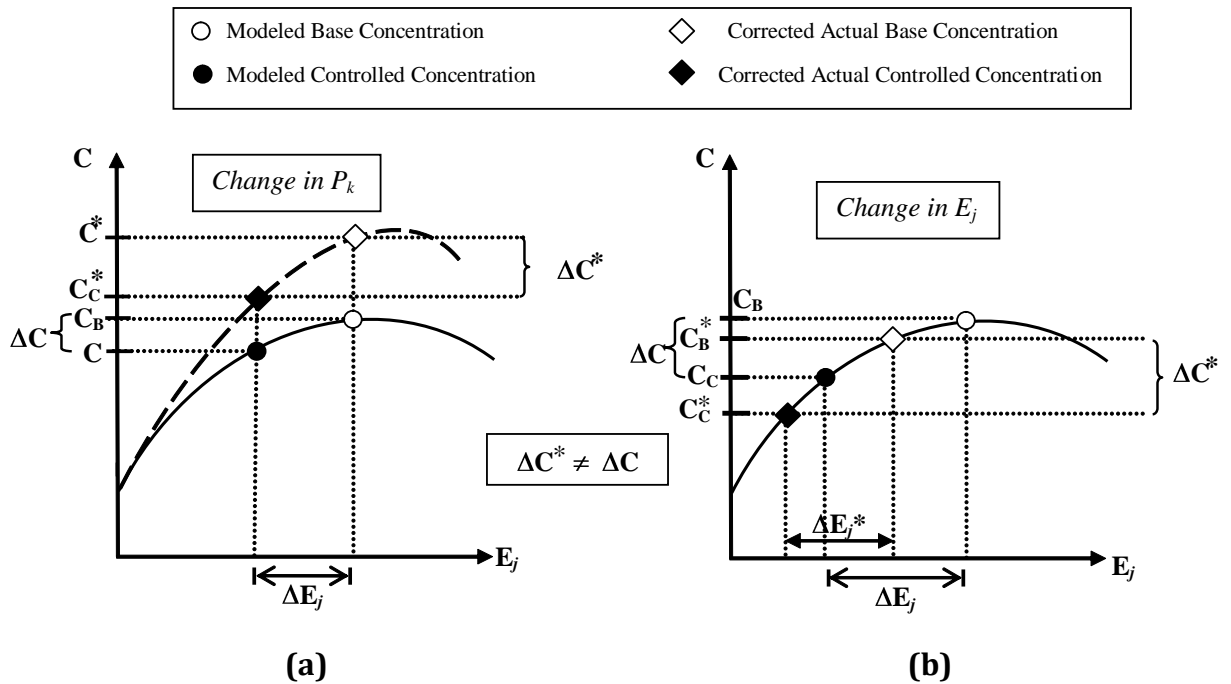


Figure 2.1 - The response of pollutant concentrations to reductions in emission rate E_j can change due to error in another input parameter (a) or in the base value of E_j itself (b).

After correcting for errors in the input parameters, the base and emission-controlled concentrations C_B and C_C would have error-corrected values C_B^* and C_C^* , leading to a new estimate of pollutant response ΔC^* (Figure 2.1). However, it would be computationally prohibitive to directly compute ΔC^* for all possible values of the uncertain input parameters and the emission perturbation amount in the three-dimensional model. Instead, the continuum RFM computes first- and second-order sensitivity coefficients, $S_j^{(1)}$ and $S_j^{(2)}$, with respect to the perturbed emission rate, and second-order cross-sensitivity coefficients, $S_{j,k}^{(2)} = \partial^2 C / \partial \varepsilon_j \partial \phi_k$, involving the perturbed emission rate and each of the uncertain input parameters. First-order, second-order, and cross-sensitivity coefficients can be computed directly by HDDM [Hakami *et al.*, 2003; 2004], or by finite differencing of multiple brute force runs via Equations 2.4(a-c):

$$S_j^{(1)} \approx \frac{C_{+\varepsilon_j E_j} - C_{-\varepsilon_j E_j}}{2\varepsilon_j} \quad (2.4a)$$

$$S_j^{(2)} \approx \frac{C_{+\varepsilon_j E_j} - 2C_B + C_{-\varepsilon_j E_j}}{\varepsilon_j^2} \quad (2.4b)$$

$$S_{j,k}^{(2)} \approx \frac{(C_{+\varepsilon_j E_j, +\phi_k P_k} - C_{+\varepsilon_j E_j, -\phi_k P_k}) - (C_{-\varepsilon_j E_j, +\phi_k P_k} - C_{-\varepsilon_j E_j, -\phi_k P_k})}{4\varepsilon_j \phi_k} \quad (2.4c)$$

where $C_{+\varepsilon_j E_j, +\phi_k P_k}$ denotes concentrations when emission rate E_j is perturbed by fraction ε_j and input parameter P_k is perturbed by fraction ϕ_k , with signs denoting

direction of perturbation. In this work, HDDM was used to compute sensitivity coefficients for O_3 , and perturbations of +/-10% were used to compute the finite difference sensitivity coefficients for PM, for which second-order HDDM is currently unavailable in CMAQ [Napelenok *et al.*, 2006].

The continuum RFM then uses these sensitivity coefficients in second-order Taylor series expansions to estimate the following terms: C_B^* , the concentrations that the model would predict after adjusting for the errors due to uncertainties in input parameters P_k , but without specifically adjusting E_j (Equation 2.5); C_C^* , the concentrations that the model would predict after adjusting for the errors in input parameters P_k , and with E_j perturbed by fraction ε_j (Equation 2.6); and hence, ΔC^* , the error-corrected pollutant response to the targeted emission perturbation ε_j (Equation 2.7):

$$C_B^* \approx C_B + \sum_k \varphi_k S_k^{(1)} + \frac{1}{2} \sum_k \varphi_k^2 S_k^{(2)} + \text{HOT} \quad (2.5)$$

$$C_C^* \approx C_B^* + \varepsilon_j S_j^{(1)} + \frac{1}{2} \varepsilon_j^2 S_j^{(2)} + \varepsilon_j \sum_k \varphi_k S_{j,k}^{(2)} + \text{HOT} \quad (2.6)$$

$$\Delta C^* = C_B^* - C_C^* \approx - \left[\varepsilon_j S_j^{(1)} + \frac{1}{2} \varepsilon_j^2 S_j^{(2)} + \varepsilon_j \sum_k \varphi_k S_{j,k}^{(2)} + \text{HOT} \right] \quad (2.7)$$

Equation 2.7 assumes that the base level of the targeted emission rate E_j has no uncertainty (i.e., $j \notin K$). If the actual base emission rate E_j differs from the

originally modeled rate, then the error-corrected pollutant response can then be expressed as:

$$\Delta C^* \approx - \left[(1 + \varphi_j) \varepsilon_j S_j^{(1)} + \frac{1}{2} (1 + \varphi_j)^2 \varepsilon_j^2 S_j^{(2)} + (1 + \varphi_j) \varepsilon_j \sum_k \varphi_k S_{j,k}^{(2)} + \text{HOT} \right] \quad (2.8)$$

The $(1 + \varphi_j)$ terms in Equation 8 reflect the fact that due to input error, the targeted *fractional* perturbation in emissions (ε_j) will correspond to more or less *tons* of emission perturbation than originally anticipated due to φ_j . Note that Equation 2.8 enables flexible estimation of ΔC^* for any amount of emission perturbation ε_j and any level of error in each input parameter P_k . If the equation proves accurate, it would enable near instantaneous characterization of pollutant-emission response over wide ranges of input uncertainty through Monte Carlo sampling of input parameters, as will be explored in subsequent chapters.

Two aspects of Equation 2.8 motivate the need for accuracy testing before wider application is pursued. First, the equation considers only first- and second-order sensitivity coefficients computed with respect to a base case, neglecting higher-order terms or discontinuities that could arise for very large perturbations in input parameters and/or targeted emission rates. Furthermore, the equation makes the simplifying assumption that the impacts of multiple uncertain input parameters on ΔC^* are additive, as indicated by the summation term. Previous studies applying HDDM coefficients to characterize the impact of parametric error on pollutant-emission response have considered only one uncertain parameter at a time [*Cohan*

et al., 2005]. Equations analogous to the continuum RFM for multiple input parameters were introduced for O₃ by Tian *et al.* [Tian *et al.*, 2010], but the accuracy was not tested.

• Discrete RFM

The Discrete RFM is a new approach that aims to accurately and efficiently characterize the parametric uncertainty of pollutant-emission response for cases in which the targeted amount of emission reduction is known in advance. For example, attainment plan options often include particular control technologies that would result in specific amounts of emission reduction at major point sources [Boylan *et al.*, 2006; Cohan *et al.*, 2006]. To develop pollutant response equations for this type of *Yes/No* control choice, we introduce a new parameter, the *response coefficient*, F_k , defined by Equation 2.9:

$$F_k = \frac{\Delta C_{\phi_k P_k} - \Delta C_{\text{base}}}{\phi_k} = \frac{(C_{B,+\phi_k P_k} - C_{C,+\phi_k P_k}) - (C_B - C_C)}{\phi_k} \quad (2.9)$$

where $C_{C,+\phi_k P_k}$ and $C_{B,+\phi_k P_k}$ denote concentrations modeled under an arbitrary small change ϕ_k in one input parameter P_k while the targeted emitter is at its controlled and base rates, respectively. In this study, $\phi_k = -10\%$ was used to calculate the response coefficients for the discrete RFM, to provide independence from the positive input parameter perturbations considered in the accuracy testing scenarios.

The Discrete RFM then scales each response coefficient by the actual amount of error Φ_k in each input parameter to adjust the original estimates of pollutant response and derive error-corrected estimates of actual pollutant response to the targeted emission reduction:

$$\Delta C^* = \Delta C + \sum_k \Phi_k F_k \quad (2.10)$$

Note that Equation 2.10 allows the user to flexibly consider a different level of error Φ_k for each uncertain input parameter, but that the base and the control emission rates of the targeted emitter must be pre-determined. This is appropriate for point sources such as power plants for which the base emission rates are accurately measured by continuous emission monitoring systems (CEMS) [*Frost et al., 2006*] and the potential control efficiencies of specific technologies are well characterized [*Srivastava and Jozewicz, 2001; Srivastava et al., 2005*]. Again, however, accuracy testing is crucial, because Equation 2.10 makes the simplifying assumptions that (1) influences of the input parameters are additive and (2) linear scaling of the response coefficients is sufficient to characterize the nonlinear impacts.

2.2.2. Photochemical Modeling Episode

We assess the abilities of the RFMs to represent O_3 and PM concentration-emission responses under an ensemble of uncertain inputs by considering a 6-day summer episode (May 29 to June 03, 2002) for a southeastern United States

modeling domain with 19 vertical layers of increasing thickness and 12-km grid resolution (Figure 2.2). The first three days were discarded for model initialization, leaving three days for accuracy testing. Photochemical modeling was conducted using CMAQ v4.5 [Byun and Schere, 2006] with the Chemical Bond 4 mechanism [Gery *et al.*, 1989] with aerosol and aqueous updates, to match the modeling used in recent Georgia SIP modeling. Meteorological conditions were taken from 5th generation Mesoscale Model (MM5) [Grell *et al.*, 1994] simulations conducted by the Georgia Environmental Protection Division (GA EPD) for its recent State Implementation Plan (SIP) modeling; emissions were taken from the Visibility and Improvements State and Tribal Association of the Southeast (VISTAS) year 2009 projections (projected from a 2002 base inventory), with updates to Georgia emissions projections based on GA EPD SIP modeling. Details on VISTAS specific model set-up, execution and evaluation are documented elsewhere [MACTEC Engineering and Consultancy, 2008; Morris *et al.*, 2008; Olerud and Sims, 2004].

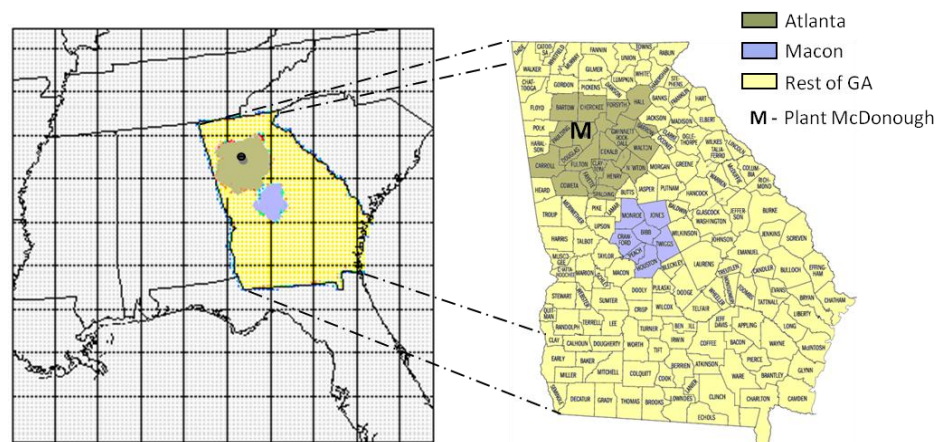


Figure 2.2 - The 12-km resolution modeling domain (left) and the targeted Georgia emission regions (right).

2.3. Results and Discussion

2.3.1. Reduced Form Model evaluation

The accuracy and computational efficiency of CMAQ-HDDM for calculating first- and second-order sensitivities of O_3 to a single input parameter have been reported elsewhere [Cohan *et al.*, 2005; Napelenok *et al.*, 2008] and was confirmed for the current episode. Cohan *et al.* (2005) introduced methods for adjusting pollutant-emission response based on changes in a single input parameter, but did not test its accuracy. Here we focus on the ability of the continuous and discrete RFMs (Equations 2.8 and 2.10, respectively) to predict the responses of pollutant concentrations to targeted emissions reductions in the presence of multiple simultaneous input parameter perturbations in the underlying model. Since the emissions reductions and input parameter perturbations cannot be directly realized in the real world, pollutant response to altered inputs in the underlying CMAQ model is the ultimate benchmark available for accuracy testing.

Case studies for accuracy testing were developed by considering scenarios of potential relevance to O_3 and PM attainment planning in Georgia. The Atlanta region exceeds federal standards for ambient levels of O_3 and fine PM. Most of the modeling domain is characterized by forests with high levels of biogenic VOC emissions [Guenther *et al.*, 2000], resulting in predominately NO_x -limited O_3 formation conditions that are relatively insensitive to VOC emission perturbations [Hagerman *et al.*, 1997; Sillman *et al.*, 1995]. Sulfate, ammonium, and nitrate are major components of PM in the region [Solomon *et al.*, 2003], and their formation

processes are thought to be better characterized in air quality models than those for the other leading component of PM, organic carbon [*Fine et al.*, 2008]. Thus, our accuracy testing focuses on the ability of the RFMs to represent O₃ response to NO_x emission controls, and inorganic PM responses to SO₂ emission controls, while multiple input parameters are uncertain.

2.3.1.1. Selection of uncertain parameters

To develop scenarios of input parameter perturbations, a literature review of previous parametric uncertainty studies [*Bergin et al.*, 1999; *Deguillaume et al.*, 2008; *Fine et al.*, 2003; *Gao et al.*, 1996; *Hanna et al.*, 2001; *Russell and Dennis*, 2000] was conducted to identify key uncertain input parameters that are likely to affect O₃ and PM responsiveness to emission perturbations. In order to select parameters for the uncertainty analysis, we specifically focused on three Monte Carlo studies that characterized the relative importance of individual parameters in contributing to uncertainty in ozone and its sensitivity to emissions [*Bergin et al.*, 1999; *Gao et al.*, 1996; *Hanna et al.*, 2001]. The 19 parameters selected for analysis (Table 2.1) have each been found by at least one of those studies to be among the leading contributors to uncertainty. All photolysis reactions are considered jointly because of their shared dependency on actinic flux. We then used the most recent reported estimates of the uncertainty factors of those parameters [*Beekmann and Derognat*, 2003; *Deguillaume et al.*, 2007; *Hanna et al.*, 2001; *Sander S P*, 2006] as detailed in Table 2.1.

HDDM cross-sensitivity coefficients were computed to assess the relative impact of each of the 19 targeted input parameters on O_3 sensitivity to Atlanta NO_x emissions. The impact factor, $\sigma S_{j,k}^{(2)} / S_j^{(1)}$, denotes the fractional change in first-order sensitivity due to a 1σ change in each input parameter. Results are presented for the maximum 8-hour average in the “nearby” (3x3 array centered on the monitor) cells surrounding Confederate Avenue monitor (the grid-cell with worst ozone for the episode), averaged over the episode (Table 2.1). Uncertain domain-wide (both biogenic and anthropogenic) VOC emissions and photolysis rates (positive impact), and uncertain domain-wide NO_x emissions (negative impact) generate several times more uncertainty in O_3 response to Atlanta NO_x controls than any other parameter (Table 2.1).

Parameter	Reported Uncertainty ¹	Factor of Uncertainty L-N (1 σ) ²	Sigma ³	Reference	Cross-sensitivity ⁴ (ppb)	Impact Factor ⁵
<i>Emission Rates:</i>						
Domain-wide NO _x	± 40% (1 σ)	1.40	0.336	[<i>Deguillaume et al., 2007</i>]	-32.92	-0.762
Domain-wide Anthropogenic VOC	± 40% (1 σ)	1.40	0.336	[<i>Deguillaume et al., 2007</i>]	4.70	0.109
Domain-wide Biogenic VOC	± 50% (1 σ)	1.50	0.405	[<i>Deguillaume et al., 2007</i>]	17.58	0.491
<i>Reaction Rate Constants:</i>						
All Photolysis Frequencies	Factor of 2 (2 σ)	1.41	0.347	[<i>Hanna et al., 2001</i>]	16.45	0.393
R(All VOCs+OH)	± 10% (1 σ)	1.10	0.095	[<i>Hanna et al., 2001</i>], [<i>Deguillaume et al., 2007</i>]	8.24	0.054
R(OH+NO ₂)	± 30% (2 σ)	1.14	0.131	[<i>Sander S P, 2006</i>]	-9.30	-0.084
R(NO+HO ₂)	± 10% (1 σ)	1.10	0.095	[<i>Deguillaume et al., 2007</i>]	5.48	0.036
R(HO ₂ +HO ₂)	± 10% (1 σ)	1.10	0.095	[<i>Deguillaume et al., 2007</i>]	-0.86	-0.006
R(NO+O ₃)	± 10% (1 σ)	1.10	0.095	[<i>Hanna et al., 2001</i>]	-9.39	-0.061
R(NO ₃ +NO)	Factor of 1.8 (2 σ)	1.34	0.294	[<i>Hanna et al., 2001</i>]	-0.10	-0.002
R(RO ₂ +HO ₂)	± 30% (1 σ)	1.30	0.262	[<i>Deguillaume et al., 2007</i>]	-0.54	-0.010
R(RO ₂ +NO)	± 30% (1 σ)	1.30	0.262	[<i>Deguillaume et al., 2007</i>]	0.40	0.007
R(HCHO+NO ₃)	Factor of 1.8 (2 σ)	1.34	0.294	[<i>Hanna et al., 2001</i>]	0.00	0.000

Parameter	Reported Uncertainty ¹	Factor of Uncertainty L-N (1 σ) ²	Sigma ³	Reference	Cross-sensitivity ⁴ (ppb)	Impact Factor ⁵
R(C ₂ O ₃ +NO)	Factor of 1.4 (2 σ)	1.20	0.182	[Hanna et al., 2001], [Deguillaume et al., 2007]	1.98	0.025
R(C ₂ O ₃ +HO ₂)	Factor of 1.8 (2 σ)	1.34	0.294	[Hanna et al., 2001]	-0.67	-0.014
R(PAN decomposition)	± 30% (1 σ)	1.30	0.262	[Deguillaume et al., 2007]	1.33	0.024
Boundary Conditions:						
Boundary Cond. O ₃	± 50% (2 σ)	1.23	0.203	[Deguillaume et al., 2007]	0.41	0.006
Boundary Cond. NO _y	Factor of 3 (2 σ)	1.73	0.549	[Deguillaume et al., 2007]	-0.10	-0.004
Others:						
Dry deposition velocity (all gaseous species)	± 25% (1 σ)	1.25	0.223	[Beekmann and Derognat, 2003]	-2.42	-0.037

¹All distributions are log-normal; ²Uncertainties converted to the same unit (expressed as Factors); ³For 1 σ L-N distribution, $\sigma = \ln(\text{Factor})$; ⁴Cross-sensitivity of O₃ to Atlanta anthropogenic non-EGU NO_x emissions and each uncertain parameter, evaluated at the grid-cell with maximum daily 8-hour average O₃ in a 3x3 array centered on the Confederate Avenue monitor, averaged over the episode; ⁵Impact factor: The fractional change in first-order sensitivity of ozone to emissions, due to a 1 σ change in an input parameter. Computed as Impact Factor = $\sigma S_{j,k}^{(2)} / S_j^{(1)}$, where $S_j^{(1)}$ is the 1st order sensitivity of O₃ to Atlanta NO_x and $S_{j,k}^{(2)}$ is the cross sensitivity of $S_j^{(1)}$ with an uncertain parameter.

Table 2.1 – Uncertainties in selected photochemical model input parameters reported by previous published studies.

2.3.1.1. Evaluation of RFM in simulating transition regimes under a homogeneous uncertainty scenario

For O₃ sensitivity to NO_x emissions (Table 2.1), analysis using HDDM coefficients identified three of 19 parameters considered to be leading contributors to uncertainty: domain-wide (1) NO_x, (2) VOC emission rates, and (3) all photolysis frequencies. Therefore, we selected these three parameters to be the focus of accuracy testing of the RFMs for ozone. For inorganic PM and its sensitivity to SO₂ emissions, we consider uncertainty in domain-wide (1) SO₂, (2) NH₃ emission rates, and (3) all photolysis frequencies. We consider three distinct scenarios for accuracy testing of the continuum and discrete RFMs: 10%, 30%, and 50% simultaneous increases in all the selected input parameters (Table 2.2), with the upper levels roughly corresponding to the 1 σ input uncertainties reported by previous studies (Table 2.1). Although for illustrative purposes we choose uniform perturbations across the parameters, the RFMs (Equations 2.8 and 2.10) can flexibly consider any combination of perturbations in inputs and targeted emission rates.

The continuum RFM is designed for cases in which a flexible range of percentage emission reductions may be under consideration. This is similar in attainment planning to the multiple control options that may be available for controlling regional emission rates. Thus, for studying O₃-NO_x and inorganic PM-SO₂ responses, the continuum RFM is applied and tested for the Atlanta region (defined as the 20-county O₃ non-attainment region). For analysis purposes, uniform emission reductions of 10, 30, and 50% were considered, and were paired with

corresponding percentage increases in the selected uncertain input parameters described above (Table 2.2). For the continuum model only, we applied the percentage increases in the uncertain domain-wide input parameters to the base and controlled levels of the targeted regional emission rates. In other words, for a base regional emission rate of X tons, the (+50% error in domain-wide emissions, -50% control of targeted regional emissions) case would consider the impact of reducing regional emissions from 1.5X tons to 0.75X tons (Equation 2.8).

The discrete model is intended for cases in which a predetermined large amount of emission reduction is targeted. As a case study for the discrete model, we consider the decision by Georgia Power to repower its coal-fired McDonough power plant with natural gas, which is expected to reduce that facility's NO_x emissions by 85% and its SO₂ emissions by 99.8% below the levels originally modeled for 2009 (J. Boylan, Georgia EPD, personal communication). These targeted emission reductions are considered with the same scenarios of error in selected input parameters as described above (Table 2.2). Whereas in the continuum model we assume that the tons reduced for a given percentage regional emission reduction depended on the input parameter adjustments, in the discrete model we assume that both the percent and tons of emissions reduction at the power plant are known because the base emission levels are well-established by point source CEMS measurements [Frost *et al.*, 2006]. Alternate assumptions could be applied readily if desired.

Pollutant responses ΔC^* predicted by the continuum and discrete RFMs (via Equations 2.8 and 2.10) are compared to the actual (brute force) response of the

underlying photochemical model, computed in Equation 2.11 as the difference between two simulations in which the targeted emitter is set at base and controlled levels while the perturbations are applied to the uncertain input parameters:

$$\Delta C_{\text{BruteForce}}^* = C_{\text{B},+\phi_k P_k} - C_{\text{C},+\phi_k P_k} \quad (2.11)$$

Statistical analysis is conducted by comparing the RFMs and Equation 2.11 results for each grid-cell-day over the entire domain and episode, after excluding the initialization days (Table 2.2). The O₃ response results are evaluated based on changes in daily 8-hour average mixing ratios from 10 a.m. to 6 p.m. (*computing O₃ results on a peak, rather than fixed, 8-hour basis would introduce slight additional error, because the peak 8-hour time interval can shift as emission rates and other input parameters are perturbed*), and PM sulfate results are evaluated based on changes in 24-hr average concentrations, corresponding to temporal metrics of interest for attainment planning [US-EPA, 2007]. Normalized mean bias (NMB) and normalized mean error (NME) in the predictions of pollutant impact were computed (Table 2.2).

	Pollutant Metric	Targeted Emission Source	Change in Targeted Emission	Uncertain Input Parameters	Change in Input parameters	Impact of Control	Statistical Analysis		Linear Regression Analysis		
							Bias (NMB ^b)	Error (NME ^c)	R ²	Slope	Intercept
Continuum RFM	8-hr O3	Atlanta Region NO _x (316 tpd ^a)	-10%	Domainwide E _{NO_x} , E _{VOC} , and J _{phot}	+10%	0.07 ppb	1.6%	7.5%	0.993	1.002	1.0E-06
			-30%		+30%	0.27 ppb	3.2%	8.0%	0.993	1.012	5.0E-06
			-50%		+50%	0.55 ppb	6.0%	9.7%	0.992	1.034	1.0E-05
	24-hr SO ₄	Atlanta Region SO ₂ (57 tpd ^a)	-10%	Domainwide E _{SO₂} , E _{NH₃} , and J _{phot}	+10%	15.92 ng/m ³	-2.5%	2.5%	1.000	0.997	-3.0E-04
			-30%		+30%	61.65 ng/m ³	-3.3%	3.5%	1.000	0.998	-2.0E-03
			-50%		+50%	129.09 ng/m ³	-2.9%	3.7%	1.000	1.002	-4.1E-03
Discrete RFM	8-hr O3	Plant McDonough NO _x (10 tpd ^a)	-10%	Domainwide E _{NO_x} , E _{VOC} , and J _{phot}	+10%	0.0095 ppb	0.3%	1.8%	1.000	1.008	-5.0E-08
			-85%		+30%	0.0093 ppb	1.5%	6.5%	0.997	1.039	-2.0E-07
					+50%	0.0091 ppb	3.3%	13.1%	0.993	1.083	-5.0E-07
	24-hr SO ₄	Plant McDonough SO ₂ (55 tpd ^a)	-10%	Domainwide E _{SO₂} , E _{NH₃} , and J _{phot}	+10%	14.73 ng/m ³	-0.1%	0.9%	1.000	0.998	2.0E-05
			-99.8%		+30%	15.93 ng/m ³	-0.5%	2.4%	0.999	0.993	3.0E-05
					+50%	17.10 ng/m ³	-0.7%	3.9%	0.998	0.990	4.0E-05

^a Average tons per day for the episode,

^b Normalized mean bias = , ^c Normalized mean error =

Table 2.2 – Performance of the RFMs in predicting the impacts of emission reductions on 8-hour O3 mixing ratios (10 a.m. – 6 p.m.) and 24-hr average PM sulfate concentrations, evaluated against brute force differencing of CMAQ runs.

The continuum RFM predicts the O₃ impact of a 50 percent reduction in Atlanta NO_x, while input parameters (domain-wide photolysis frequencies and NO_x and VOC emissions) are perturbed upward by 50 percent, with 6.0% NMB and 9.7% NME (Table 2.2). Linear regression analysis of the continuum model against finite differenced brute force results shows an R² of 0.992 and a slope of 1.03. Performance statistics were slightly better for cases with smaller emissions reductions and input parameter perturbations. Errors do not converge to 0% due to imperfections in the HDDM coefficients [Cohan *et al.*, 2005; Napelenok *et al.*, 2008] and because the impact magnitude declines with the targeted perturbation. Spatially, the continuum model accurately represents the “plume” of O₃ reductions resulting from reductions in Atlanta NO_x emissions (Figure 2.3). The high levels of accuracy are achieved even though the continuum model for O₃ uses only HDDM sensitivity coefficients generated from within a single base simulation of the CMAQ model.

The continuum model achieves even better accuracy for simulating PM sulfate response to 50 percent reductions in Atlanta SO₂ emissions (NMB = -2.9%, NME = 3.7%, R² = 1.000), again with 50 percent perturbations in relevant input parameters (Table 2.2). Slightly more scatter occurs in simulating the response of PM ammonium to SO₂ emission reductions (Table 2.3). Both the concentrations of PM nitrate and its response to changes in SO₂ emissions are modeled to be very small during this episode, so statistical comparisons are not meaningful.

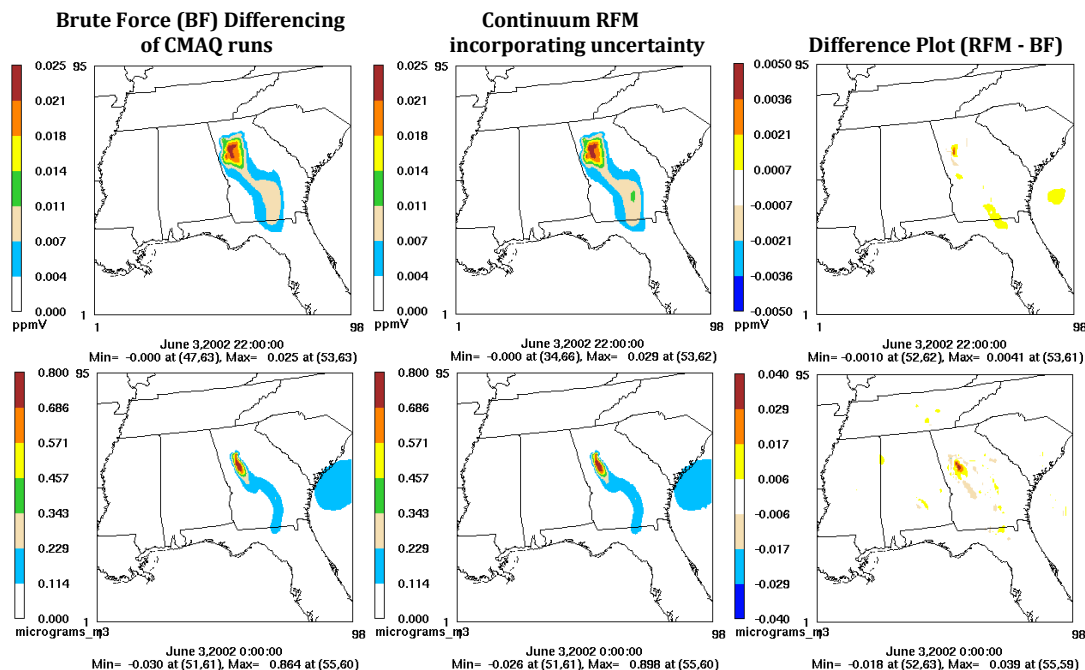


Figure 2.3 – O₃ reduction (10 a.m. – 6 p.m.) due to 50% reduction in Atlanta NO_x (top) and 24-h average PM sulfate reduction due to 99.8% McDonough SO₂ control (bottom).

Note: For O₃ simulation, domain-wide NO_x, VOC emissions and photolysis rates are assumed to be uncertain by + 50%, and for PM, domain-wide SO₂, NH₃ emissions and photolysis rates are increased by +50%. The left hand plots show results from brute force (a, d), the middle plots show continuum RFM results (b, e) and the right hand plots show the differences in results (c, f). Results are shown for June 3.

Pollutant Metric	Targeted Emission Source	Change in Targeted Emission	Uncertain Input Parameters	Change in Input parameters	$\Delta C_{BruteForce}^*$ Impact of Control	Statistical Analysis		Linear Regression Analysis		
						Bias (NMB ^b)	Error (NME ^c)	R ²	Slope	Intercept
24-hr NH ₄	Atlanta Region SO ₂ (57 tpd ^a)	-10%	Domainwide E _{SO2} , E _{NH3} , and J _{phot}	+10%	15.92 ng/m ³	-2.5%	2.5%	1.000	0.997	-3.0E-04
		-30%		+30%	61.65 ng/m ³	-3.3%	3.5%	1.000	0.998	-2.0E-03
		-50%		+50%	129.09 ng/m ³	-2.9%	3.7%	1.000	1.002	-4.1E-03
	Plant McDonough SO ₂ (55 tpd ^a)	+10%	Domainwide E _{SO2} , E _{NH3} , and J _{phot}	+10%	3.14 ng/m ³	-0.0%	2.9%	0.999	1.004	-1.0E-05
		+30%		+30%	3.36 ng/m ³	0.2%	8.1%	0.992	1.012	-4.0E-05
		+50%		+50%	3.55 ng/m ³	1.1%	13.3%	0.981	1.026	-5.0E-05

^a Average tons per day for the episode, ^b Normalized mean bias, ^c Normalized mean error

Table 2.3 – Performance of the RFM in predicting the impacts of Atlanta regional emission reductions on 24-hr average PM ammonium concentrations, evaluated against brute force differencing of CMAQ runs. Results compared over all grid-cell-days in the episode.

The discrete RFM achieves similar performance statistics (Table 2.2), despite simulating even larger percentage reductions in a single point source. The discrete model does show slightly more degradation in performance as the size of the input parameter perturbations are increased, most likely reflecting the fact that its computations are extrapolated from response coefficients computed for only -10% changes in each input parameter.

For both the regional and point-source emission controls, by correcting for input errors the RFMs yield far more accurate predictions of pollutant-emission response than if those errors had been neglected (Figure 2.4-Figure 2.7).

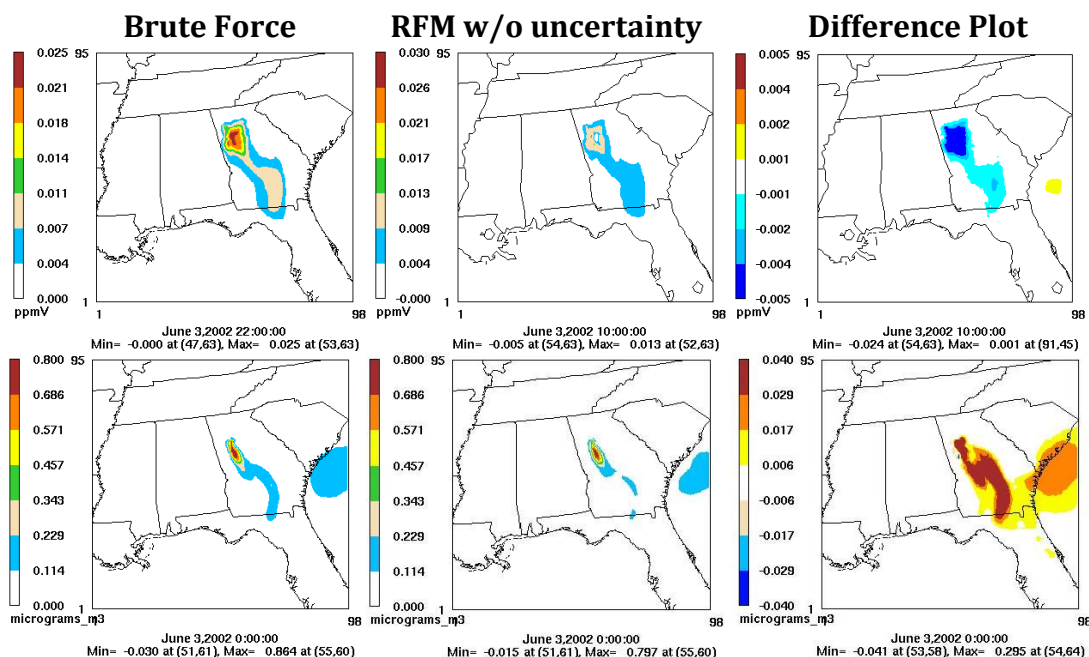


Figure 2.4 – O₃ reduction (10 a.m. – 6 p.m.) due to 50% reduction in Atlanta NO_x (top) and 24-h average PM sulfate reduction due to 99.8% McDonough SO₂ control (bottom).

Note: For O₃ simulation, domain-wide NO_x, VOC emissions and photolysis rates are assumed to be uncertain by + 50%, and for PM, domain-wide SO₂, NH₃ emissions and photolysis rates are increased by +50%. The left hand plots show results from brute force (a, d), the middle plots show continuum RFM results neglecting parametric uncertainty (b, e) and the right hand plots show the differences in results (c, f). Results are shown for June 3.

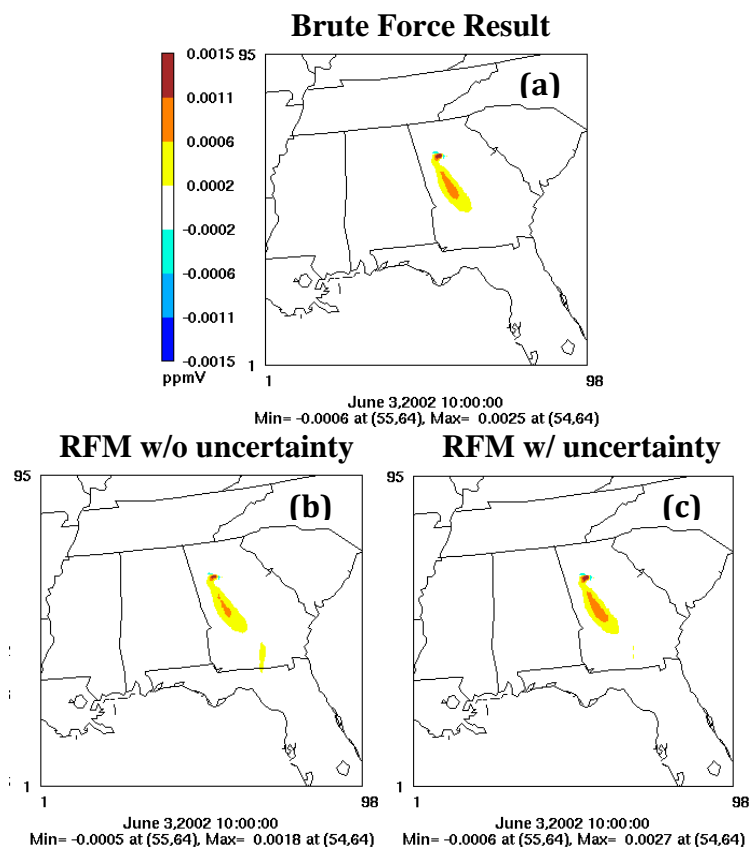


Figure 2.5 - Ozone reduction due to 85% reduction in Plant McDonough NO_x , while domain-wide NO_x and VOC emissions and photolysis rates are increased by 50%, as simulated by brute-force (a), the discrete RFM neglecting (b) and accounting for (c) input parameter uncertainty. Results shown for 10 a.m.-6 p.m. on June 3.

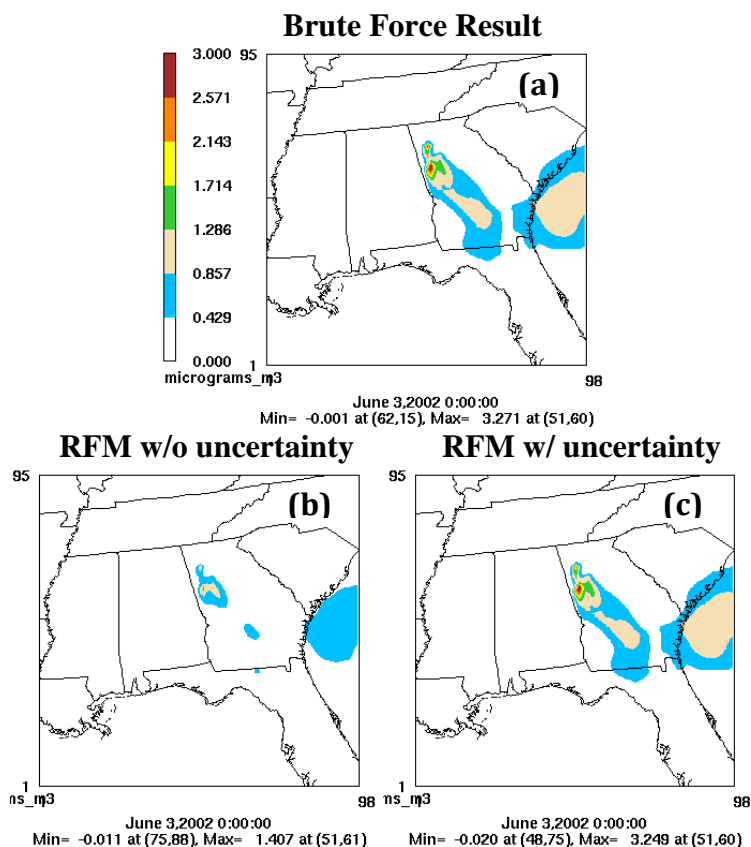


Figure 2.6 - PM sulfate reduction due to 50% reduction in Atlanta SO₂, while domain-wide SO₂ and NH₃ emissions and photolysis rates are increased by 50%, as simulated by brute-force (a), the discrete RFM neglecting (b) and accounting for (c) input parameter uncertainty. Results shown for 24-hour average on June 3.

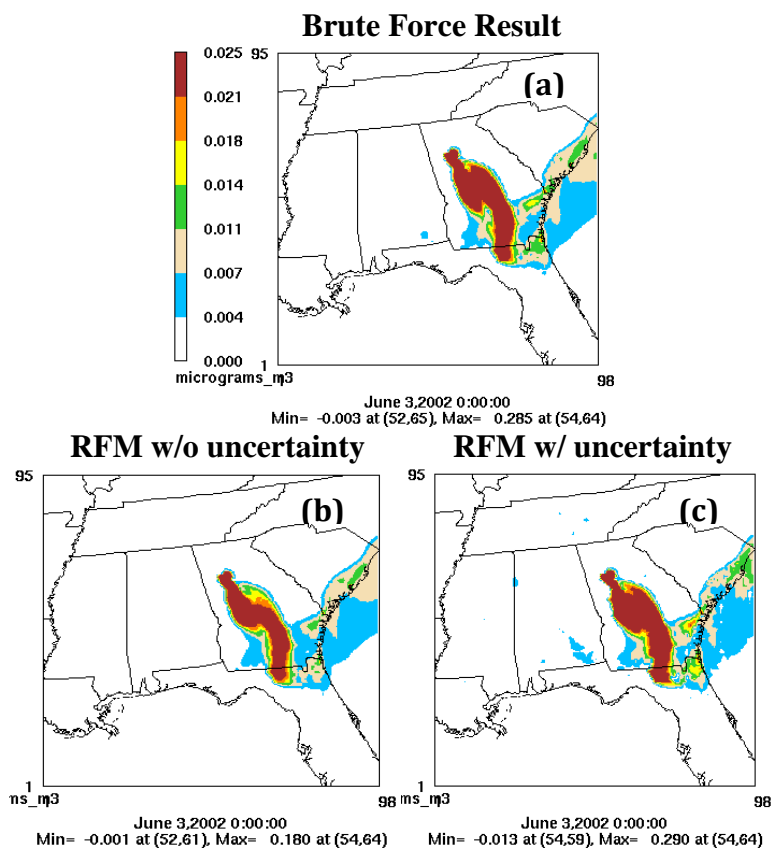


Figure 2.7 – PM ammonium reduction due to 50% reduction in Atlanta SO_2 , while domain-wide SO_2 and NH_3 emissions and photolysis rates are increased by 50%, as simulated by brute-force (a), the discrete RFM neglecting (b) and accounting for (c) input parameter uncertainty. Results shown for 24-hour average on June 3.

2.3.1.2. Evaluation of RFM in simulating transition regimes under a heterogeneous uncertainty scenario

The primary accuracy tests described above consider homogeneous levels of perturbation in the input parameters and a base scenario that was dominated by NO_x -sensitive ozone conditions. An additional test was developed to ensure that similar performance is achieved under heterogeneous parametric uncertainty and in transitional conditions between NO_x - and VOC-limited ozone chemistry. The testing scenario described below applies heterogeneous perturbations simultaneously to 6 input parameters, with perturbation magnitudes roughly comparable to the 1σ uncertainty levels described in Table 2.1.

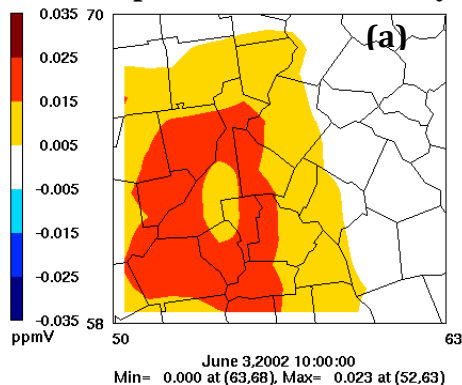
- Perturbations to uncertain input parameters
 - Atlanta NO_x (ANO_x) is 40% more than modeled
 - Atlanta VOC (AVOC) is 50% less than modeled
 - Rest-of-domain (i.e., domain – Atlanta) NO_x (RNO_x) is 30% more than modeled
 - Rest-of-domain VOC (RVOC) is 40% less than modeled
 - All photolysis frequencies (Rphoto) are 1.4 times more than modeled
 - $\text{R}(\text{NO}_2+\text{OH})$ is 15% more than modeled
- Targeted emission reduction: 12% reduction in Atlanta NO_x

In absence of the above uncertainties, O_3 is found to be sensitive to Atlanta NO_x (Figure 2.8(a)); however, by increasing baseline NO_x and decreasing baseline VOC, these perturbations shift the model to predict NO_x -saturated (Figure 2.8(b))

and VOC-limited (Figure 2.8(c)) conditions in the innermost Atlanta counties, surrounded by NO_x-limited conditions elsewhere.

This provides an especially rigorous test, because the targeted emission reduction (and hence ozone impact) is small compared to the input perturbations and the RFM relies solely on sensitivity coefficients computed under starkly different base-case conditions. Nevertheless, the RFM successfully simulates the spatial patterns and magnitudes of the resultant O₃ impact and captures the correct flips in O₃-precursor sensitivities in the transition regimes as the input parameters are perturbed (Figure 2.9; normalized mean bias (NMB) = 7.3%, normalized mean error (NME) = 19.3% and R² = 0.964), bolstering confidence that the RFM can be reliably applied over heterogeneous input parameter and ozone chemistry conditions.

**O₃ sensitivity to Atlanta NO_x
without parametric uncertainty**



Corrected O₃ sensitivity considering parametric uncertainty

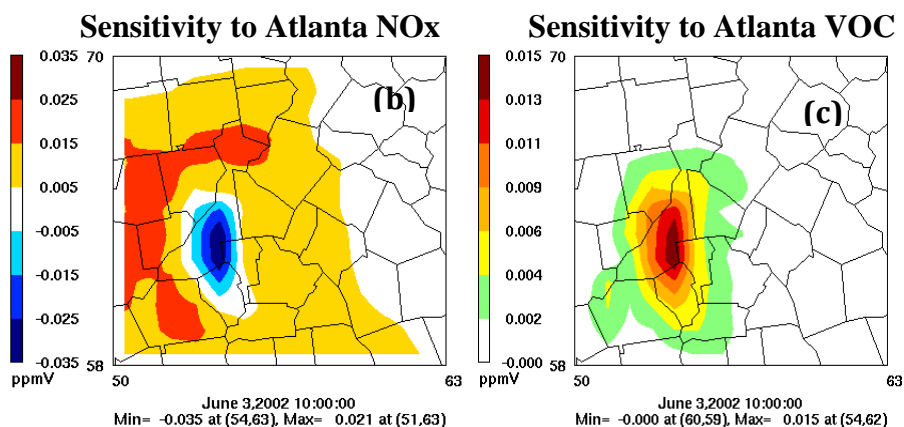


Figure 2.8 - O₃ sensitivity coefficient without any parametric uncertainty (a) and adjusted coefficients when 6 input parameters are uncertain (b, c) (ANO_x: +40%, AVOC: -50%, RNO_x: +30%, RVOC: -40%, Rphoto: factor of 1.4, and R(NO₂+OH): +15%). Results are shown for 10 a.m.-6 p.m. in the urban regions of Atlanta on June 3.

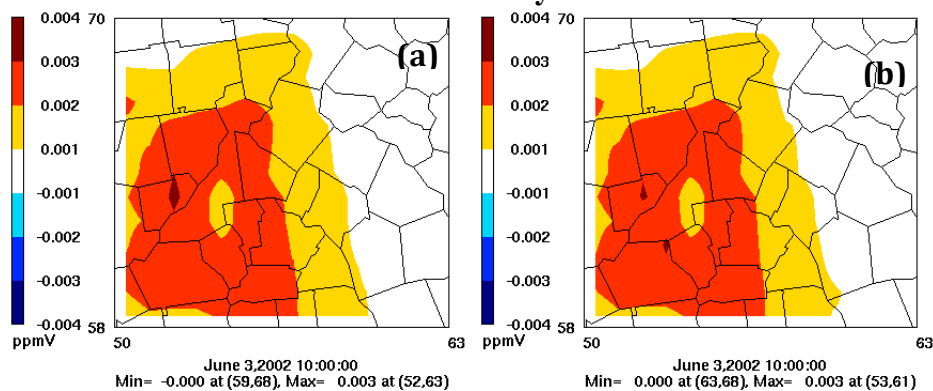
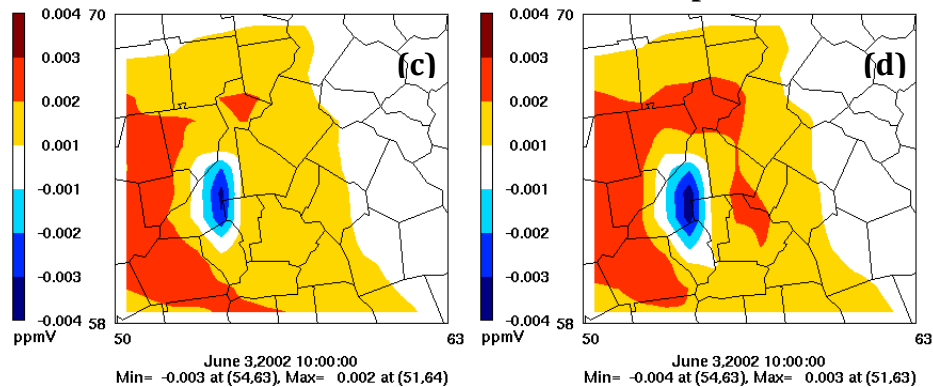
Brute Force**Reduced Form Model****O₃ reduction due to 12% control in Atlanta NO_x in absence of parametric uncertainty****O₃ reduction due to 12% control in Atlanta NO_x under parametric uncertainty**

Figure 2.9 - O₃ reductions due to 12% control in Atlanta NO_x in absence of parametric uncertainty (a, b) and when 6 input parameters are uncertain (c, d) (ANO_x: +40%, AVOC: -50%, RNO_x: +30%, RVOC: -40%, Rphoto: factor of 1.4, and R(NO₂+OH): +15%), as simulated by brute force finite differencing (left) and the reduced form model (right). Results are shown for 10 a.m.-6 p.m. in the urban regions of Atlanta on June 3.

2.3.1.3. Evaluation of RFM in simulating pollutant responsiveness in different ozone regimes

So far, we have applied the RFM to a single region characterized mostly by NO_x-limited conditions, apart from the testing case above that pushed conditions to be VOC-limited in the Atlanta urban core. To evaluate whether similar performance would be achieved elsewhere, we also applied the RFM to a Houston, Texas region characterized by transitional conditions between NO_x- and VOC-limited ozone chemistry.

We apply the RFM to the 4-km modeling of a TexAQS-II (Texas Air Quality Study-part 2) episode during August - September 2006, from Rappengluck et al. (2009) [Rappengluck, 2009]. Results are evaluated for three days (September 1-3) following two model initialization days. The continuum RFM is tested for assessing ozone responsiveness to a 50% reduction in NO_x and VOC emission from Harris-Galveston-Brazoria (HGB) area when domain-wide NO_x and VOC emissions and rate constants for all photolysis reactions and the termination reaction (NO₂+OH) are considered to be 50% more than reported. NMB of -9.6% and -9.1%, NME of 7.4% and 13.2% and R² of 0.994 and 0.973 were obtained for simulating the ozone impact of controlling NO_x and VOC respectively. Figure 2.10 shows the performance of the RFM for this TexAQS-II case study, demonstrating a strong spatial match between RFM and brute force results.

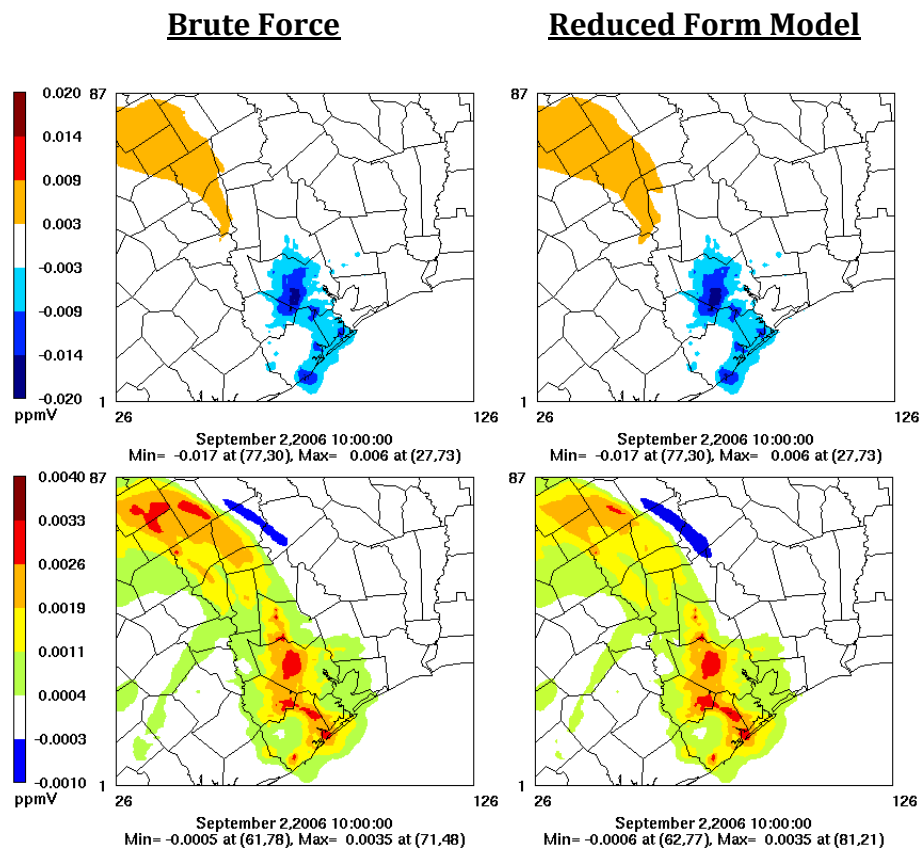


Figure 2.10 - Reduction in ozone due to 50% reductions in NO_x (top) and VOC (bottom) emissions from HGB area in Texas, as simulated by brute-force (left) and the continuum RFM (right). Results are shown for 10 a.m. to 6 p.m. on September 2, 2006, when domain-wide NO_x , VOC, R_{photo} and $R(\text{NO}_2+\text{OH})$ is +50% more.

2.3.1.4. Evaluation of RFM in simulating pollutant impact under multiple controls

Since the RFMs accurately simulate the underlying model's responsiveness to isolated reductions in regional or point source emissions under parametric uncertainty, it may be asked whether those impacts can be summed to predict the overall benefits of a combined strategy. Additional simulations were conducted to test the accuracy of the RFM equations in estimating the pollutant responsiveness to multiple control strategies applied simultaneously under parametric uncertainties. We define a new region, "Rest-of-Georgia" consisting of all Georgia counties *excluding* both the Atlanta ozone non-attainment region and the seven counties centered on the city of Macon (Figure 2.2). We evaluate RFM predictions for ozone responsiveness as a result of the combined effect of NO_x reductions in Atlanta and Rest-of-Georgia, under the same +50% parametric uncertainties considered earlier (domain-wide NO_x, VOC and photolysis rates).

A summation of the 8-hour ozone responses to NO_x controls from each region predicts the joint effect with a high degree of accuracy even for a 50% change in each term (Figure 2.11(b), NMB = -0.85%, NME = 8.6%, and R² = 0.985, comparing all grid-cell-days for the episode). In theory, it would be expected that accuracy could be improved even further by incorporating a term for the cross-sensitivity of ozone to emissions from each region (i.e., $\partial^2 O_3 / \partial \epsilon_{j1} \partial \epsilon_{j2}$) into the Taylor expansions, especially for a case such as this in which the plumes have substantial opportunity to interact. However, the incorporation of a cross-sensitivity term between the two

controls (RFMx) does not significantly improve the accuracy of results for the case examined here (Figure 2.11(c), $R^2 = 0.985$, NMB = 0.97%, and NME = 8.2%). Further testing would be needed to examine the importance of cross-sensitivity interactions in other cases.

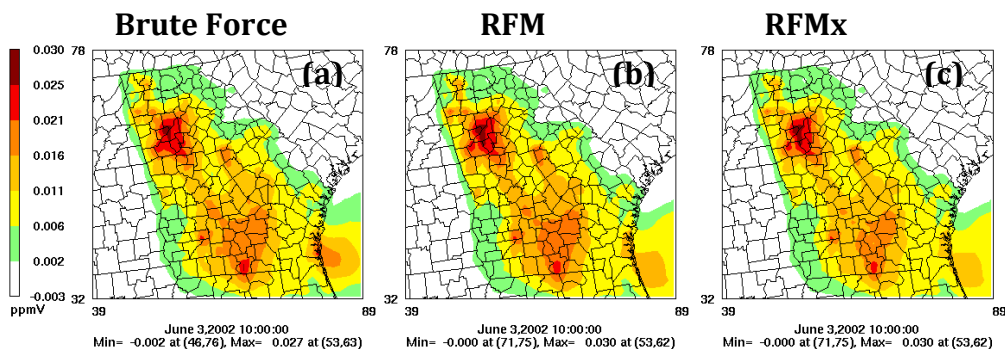


Figure 2.11 – Reduction in ozone due to joint 50% reductions in NO_x emissions from both Atlanta and “Rest of Georgia”, as simulated by (a) brute-force, (b) summing the continuum RFM-predicted impacts for each region and (c) summing the continuum RFM-predicted impacts for each region with cross-sensitivity of O₃ sensitivity to emissions. Results are shown for 10 a.m. to 6 p.m. on June 3.

2.3.2. Computational efficiency and applicability of RFMs

The computational efficiency of the RFMs is a key motivator for their use as substitutes for traditional brute-force methods in parametric uncertainty characterization. The computational requirements of the RFMs can be described by considering a case in which it is desired to characterize pollutant responses to J control options while K input parameters are uncertain. A traditional Monte Carlo Latin Hypercube Sampling (LHS) method would require sufficient sampling (say, N samples, typically $N=10 \times \text{input dimension}$ [Loeppky *et al.*, 2009]) of photochemical

model simulations from this $(J \times K)$ parameter space to characterize pollutant responsiveness to all the E_j 's, likely requiring $(1+J) \times 10K$ model runs [Bergin *et al.*, 1999; Hanna *et al.*, 1998; Rodriguez and Dabdub, 2003]. On the other hand, the continuum RFM requires $2J$ sensitivity coefficients ($S_j^{(1)}$ and $S_j^{(2)}$) to the targeted emissions, plus $J \times K$ cross-sensitivity coefficients ($S_{j,k}^{(2)}$) between the targeted emissions and the uncertain parameters. If HDDM is available, then this total of $J(K+2)$ sensitivity coefficients can be computed within the base model itself. Depending on the capabilities of the computer and the size of the modeling domain, dozens of HDDM sensitivity coefficients may be computed within a single simulation, albeit requiring much more time than a base simulation (see [Koo *et al.*, 2007a; Koo *et al.*, 2007b; Napelenok *et al.*, 2008; Yang *et al.*, 1997] for examinations of the computational efficiency of DDM and HDDM). The comparison of CPU time needed for the continuous RFM-Monte Carlo analysis against the traditional Monte Carlo LHS technique of the base model is presented in Table 2.4.

Number of parameters ¹	Description of uncertain parameters	Number ² of Monte Carlo (LHS ³) Simulations	Monte Carlo (LHS ³) of RFM			Monte Carlo (LHS ³) of Air Quality Model (minutes)
			Required number of sensitivity coefficients ⁴	CPU time using HDDM to compute sensitivity coefficients (minutes)	CPU time using Brute Force to compute sensitivity coefficients (minutes)	
$j = 1; k = 2$	2 emission rate	20(base) + 20(control)	3 (4)	156	275	1568
$j = 1; k = 10$	3 emission, 2 boundary conditions, 1 deposition velocity and 4 reaction rates	100(base) + 100(control)	11 (20)	436	1530	7840
$j = 2; k = 34$	6 emissions, 25 reaction rate constants, 3 deposition velocities	340(base) + 340(control) + 340(control)	68 (100)	2177	10271	39984

¹ j denotes number of control scenarios and k denotes number of uncertain parameters; ²We assume that the sample size needed for LHS is 10 times the input dimension [Loeppky *et al.*, 2009]; ³LHS stands for Latin Hypercube Sampling; ⁴number in parenthesis denotes the total number of sensitivities that HDDM needs to compute in order to compute the required number of sensitivity coefficients required by the RFM.

Note: Time is calculated on the basis of a single-day simulation period for a 12-km CMAQ grid with 98x95 cells, using an Intel Xeon 5150 processor (CPU speed - 2.66 GHz, FSB speed - 1333 MHz, and system RAM - 8 GB).

Table 2.4 – Estimated computational time for Monte Carlo uncertainty analysis using continuum RFM or Brute Force for predicting pollutant response to emission controls under parametric uncertainty.

Modelers may also choose to compute sensitivity coefficients by brute force, if HDDM is unavailable or if a slightly higher level of accuracy is desired. Calculation of the $J \times K$ cross-sensitivity coefficients by Equation 2.4 requires $4(J \times K)$ brute force model runs, along with the $2J+1$ simulations needed to compute coefficients $S_j^{(1)}$ and $S_j^{(2)}$ by brute force. While more computationally burdensome than HDDM, this approach still requires much fewer model simulations than would typically be conducted for Monte Carlo sampling of the input parameter space (Table 2.4). The ability to apply the RFM methods in the absence of HDDM is important, because it is highly time-consuming to implement and update HDDM in air quality models, and many regulatory modelers lack experience in its application. Brute force methods, on the other hand, can readily be applied in any air quality model.

However the continuum RFM is applied, the result is an analytical equation expressing pollutant response to targeted emission reductions as a function of the fractional changes in targeted emissions and in input parameters. The equation allows near instantaneous calculation of a virtually unlimited number of combinations of perturbations to the targeted emission rates and the input parameters, enabling efficient characterization of parametric uncertainty.

The discrete RFM operates only by brute force, and requires a total of $J(K+1)$ perturbed simulations to compute the required response coefficients. This easy-to-apply method may be useful in attainment planning if the size of the targeted emission reduction is known in advance, while a flexible range of input parameters is desired for uncertainty analysis. Like the continuum model, it enables near-

instantaneous Monte Carlo characterization of pollutant-response, although in the discrete model only the uncertain input parameters (and not the targeted amount of emission reduction) can be varied.

The high level of accuracy demonstrated for both RFMs lends confidence to their application for scientific and air quality management purposes such as parametric uncertainty analysis and the development of attainment strategies. Despite significant nonlinearities in O₃ and inorganic PM formation, the responses of each pollutant to large emission reductions can be well-characterized over large perturbations in multiple important input parameters using only first- and second-order sensitivity relationships from the base model. The RFM analytical equations can hence serve as effective surrogates for far more complex photochemical models, of course with the crucial caveat that their results can only be as accurate as the underlying model itself in representing pollutant-emission response. Subsequent chapters explore the application of the RFMs to characterize the parametric uncertainty of secondary pollutant responses to emission reductions and to assess the likelihood that an attainment plan will achieve a desired pollutant reduction target. Future research could also consider the role of meteorological uncertainties together with the parametric uncertainties considered here.

Adapted with permission from *Digar et al.*, Likelihood of Achieving Air Quality Targets under Model Uncertainties, *Environmental Science & Technology*, 45(1), 189-196, 2011. DOI: 10.1021/es102581e. Copyright © 2011, American Chemical Society.

Chapter 3

Likelihood of achieving air quality targets under model uncertainties

3.1. Introduction

The United States Environmental Protection Agency (U.S. EPA) sets national ambient air quality standards (NAAQS) for ozone (O₃) and other criteria pollutants. States with ambient monitors violating those standards must develop State Implementation Plans (SIPs) for attaining the NAAQS by a future date. Recent proposed rules to tighten the NAAQS for O₃ and fine particulate matter (PM_{2.5}) will likely prompt a wave of new SIP development [*USEPA*, 2010; March, 2010].

In order to demonstrate future attainment, States use photochemical models to simulate the response of ambient pollution to projected reductions at emission sources. The current framework for SIP attainment demonstrations applies a *bright-line test* to deterministically evaluate whether an emission control program is

sufficient [USEPA, 2007]. In this process, photochemical models simulate pollutant concentrations under ‘controlled’ (future-year) and ‘base’ (base-year) emission rates, applying identical base-year meteorological episodes in each case. The ratio of future to base pollutant concentrations is termed the relative reduction factor (RRF). This process enables the use of model results in a *relative* rather than an *absolute* sense. The RRF is then multiplied by the measured base-year design value (DVB) for each monitor to estimate the future design value (DVF), which determines whether the monitor is projected to attain the NAAQS with the considered set of control measures [USEPA, 2007]. Although U.S. EPA also advocates consideration of other “weight of evidence” factors in close cases, the deterministic *bright-line test* forms the core of most SIP attainment demonstrations.

However, photochemical model results are known to be uncertain due to uncertain model formulation (structural uncertainty) and uncertain input parameters (parametric uncertainty) [Fine et al., 2003; Pinder et al., 2009; Russell and Dennis, 2000]. Thus, RRFs computed by photochemical models will be uncertain [Jones et al., 2005]. Moreover, future meteorology will differ from the past, and those changes will impact pollutant concentrations [Cox and Chu, 1993]. Whether a given control strategy will be sufficient is thus a probabilistic rather than a deterministic question, but the current *bright-line test* fails to quantify the likelihood that attainment will actually be achieved. In fact, many regions have failed to attain NAAQS by the targeted year despite SIP modeling that predicted attainment [USEPA, 2011].

Hogrefe and Rao (2001) suggested that probabilistic analyses should supplement the pass/fail test of current regulatory practice [Hogrefe and Rao, 2001]. However, most previous efforts to characterize the probabilistic response of air pollutants to emission controls have relied upon numerous Monte Carlo photochemical model simulations [Bergin et al., 1999; Deguillaume et al., 2008; Hanna et al., 2001], which is impractical for extensive SIP modeling. New methods would be needed to enable States to objectively characterize the attainment likelihood of various potential control packages in a computationally efficient manner.

This chapter introduces methods for estimating the likelihood that a given level of emission reductions will achieve a targeted improvement in air quality, in light of parametric uncertainties in the photochemical model. Two types of targeted pollutant reduction are considered: a *fixed* amount of air pollution reduction needed at a monitor, and a *flexible* function acknowledging that unknown future meteorology and uncertain projections of emission trends generate uncertainty in how much additional improvement is needed. The new methods are applied to recent attainment modeling from the Atlanta, Georgia, 8-hour O₃ SIP to assess the likelihood that additional emission controls would achieve targeted amounts of air quality improvement.

3.2. Methodology

3.2.1. Reduced Form Models

Recent work has shown that high-order sensitivity analysis of a photochemical model can be applied to construct reduced form models (RFMs) that represent how perturbations in multiple input parameters (e.g. emission rates, reaction rate constants, boundary conditions, and deposition velocities) influence the responsiveness of pollutant concentrations to precursor emissions [Digar and Cohan, 2010; Tian et al., 2010]. These RFMs provide analytical representations for the amount of ambient pollutant reduction that would be achieved as a function of the fractional changes (ϵ_j) in targeted emission rates $j=1,2,\dots,J$, and the fractional perturbations ϕ_k needed to adjust uncertain parameters $k=1,2,\dots,K$ to their 'actual' values. Digar and Cohan (2010) introduced methods for efficiently computing the impacts of emissions perturbations while input parameters are perturbed [Digar and Cohan, 2010]. The Continuum RFM considers adjustable fractional perturbations in emissions, while the Discrete RFM is applicable when the tonnage of emission perturbation is pre-determined (e.g., a specific control technology at a point source).

For the Continuum RFM, the change in concentrations (ΔC^*) resulting from fractional emission perturbation (ϵ_j) while input parameters P_k are perturbed by fractions ϕ_k is given by,

$$\Delta C^* = C_{\varphi_k P_k} - C_{\varphi_k P_k, \varepsilon_j E_j} \approx - \left[\varepsilon_j S_j^{(1)} + \frac{1}{2} \varepsilon_j^2 S_j^{(2)} + \varepsilon_j \sum_k \varphi_k S_{j,k}^{(2)} \right] \quad (3.1a)$$

where $C_{\varphi_k P_k}$ denotes concentrations under the input perturbations and $C_{\varphi_k P_k, \varepsilon_j E_j}$ are the corresponding concentrations when emission rate E_j is perturbed by fraction ε_j

. $S_j^{(1)} \left(= \frac{\partial C}{\partial \varepsilon_j} \right)$ and $S_j^{(2)} \left(= \frac{\partial^2 C}{\partial \varepsilon_j^2} \right)$ are the local first- and second order sensitivity

coefficients of 'C' to the targeted emission rate, and $S_{j,k}^{(2)} \left(= \frac{\partial^2 C}{\partial \varepsilon_j \partial \varphi_k} \right)$ is the cross-

sensitivity between parameter j and k . These coefficients are computed using the

high-order decoupled direct method (HDDM) [Dunker, 1984; Hakami et al., 2003],

except for $S_{j,k}^{(2)}$ involving deposition velocities, which is computed by finite

differencing of model runs. If the targeted emission rate E_j is also uncertain then eq

1a can be re-written as

$$\Delta C^* = - \left[1 + \varphi_j \varepsilon_j S_j^{(1)} + \frac{1}{2} 1 + \varphi_j^2 \varepsilon_j^2 S_j^{(2)} + 1 + \varphi_j \varepsilon_j \sum_k \varphi_k S_{j,k}^{(2)} \right] \quad (3.1b)$$

The $1 + \varphi_j$ terms accounts for the influence of the uncertain emission inventory on the amount of tons controlled by fractional perturbation ε_j . For our

analysis, ε_j represents emission control (i.e. $\varepsilon_j < 0$), so $C_{\varphi_k P_k, \varepsilon_j E_j}$ is typically less

than $C_{\varphi_k P_k}$ and positive values of ΔC^* indicate pollutant reduction. Extensive testing

of eq 1 (a and b) showed that ΔC^* is accurately predicted (normalized mean bias \approx

6%, normalized mean error $\approx 10\%$) even for 50% emission controls under 50% simultaneous perturbations in 3 parameters [Digar and Cohan, 2010].

The Discrete RFM allows accurate (normalized mean bias $\approx 3\%$ and error $\approx 13\%$ for 50% perturbations in 3 input parameters [Digar and Cohan, 2010]) and efficient estimation of concentration response under input uncertainty when the magnitude of the emission reduction is pre-determined. It computes the error-adjusted concentration response ΔC^* to an emission control by computing a function F_k , that represents how concentration response to targeted emission change $\varepsilon_j E_j$ varies with change φ_k in parameter k [Digar and Cohan, 2010]:

$$F_k = \Delta C_{\text{perturbed}} - \Delta C_{\text{base}} / \varphi_k \quad (3.2)$$

where $\Delta C_{\text{perturbed}} (= C_{\varphi_k P_k} - C_{\varphi_k P_k, \varepsilon_j E_j})$ and $\Delta C_{\text{base}} (= C_{\text{base}} - C_{\varepsilon_j E_j})$ represent concentration response under perturbed and base input conditions, respectively.

Finite differencing of model runs with 10% input perturbations ($\varphi_k = 0.1$) was used to compute F_k . ΔC^* is then calculated by the following Discrete RFM,

$$\Delta C^* \approx \Delta C_{\text{base}} + \sum_k \varphi_k F_k \quad (3.3)$$

in which input perturbations can be set by Monte Carlo sampling of φ_k .

3.2.2. Probabilistic Framework and Reduction Targets

The Continuum (eq 1) and Discrete (eq 3) RFMs are analytical equations that can be evaluated readily for any perturbations Φ_k in uncertain parameters \mathbf{k} , in contrast to direct Monte Carlo simulation of a photochemical model [Bergin *et al.*, 1999; Deguillaume *et al.*, 2008; Hanna *et al.*, 2001]. Here, we conduct Monte Carlo simulations of these RFMs, treating each input parameter as an independent log-normally distributed random variable with 1σ uncertainty listed in Table 3.1 based on earlier studies [Beekmann and Derognat, 2003; Deguillaume *et al.*, 2007; Digar and Cohan, 2010; Hanna *et al.*, 2001; Sander *et al.*, 2006]. The basis for selecting the input parameters is explained later. One million Monte Carlo sampling of Φ_k are made to generate a probability distribution of the concentration reduction resulting from each targeted emission perturbation ε_j (Figure 3.1).

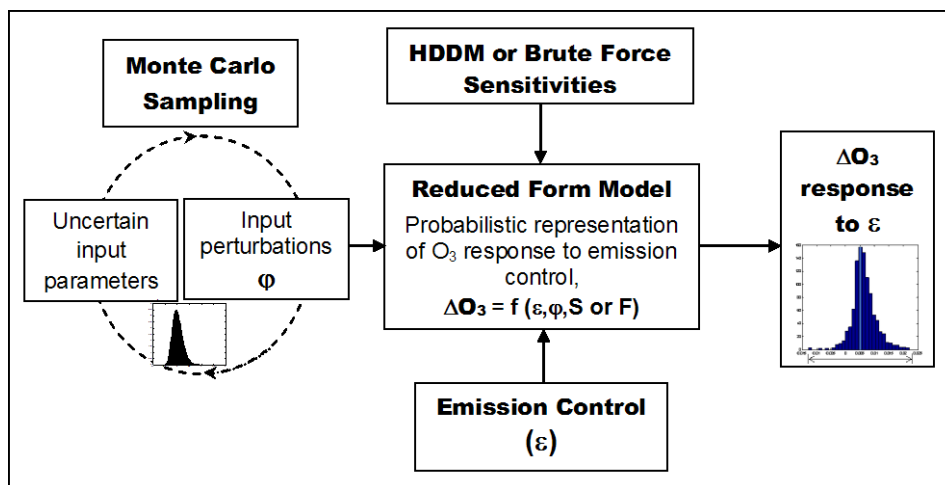


Figure 3.1 – Probabilistic framework for characterizing ozone response to a control strategy under model parametric uncertainty.

Parameter	Uncertainty in parameter ¹ (1 σ)	Cross- sensitivity ² (ppb)	Impact on O ₃ sensitivity ³
Emission Rates:			
Domain-wide NO _x	0.336	-32.92	-0.762
Domain-wide Biogenic VOC	0.405	17.58	+0.491
Domain-wide Anthropogenic VOC	0.336	4.70	+0.109
Reaction Rate Constants:			
All Photolysis Frequencies	0.347	16.45	+0.393
R(OH+NO ₂)	0.131	-9.30	-0.084
R(NO+O ₃)	0.095	-9.39	-0.061
R(All VOCs+OH)	0.095	8.24	+0.054
R(NO+HO ₂)	0.095	5.48	+0.036
R(C ₂ O ₃ +NO)	0.182	1.98	+0.025
R(PAN decomposition)	0.262	1.33	+0.024
R(C ₂ O ₃ +HO ₂)	0.294	-0.67	-0.014
R(RO ₂ +HO ₂)	0.262	-0.54	-0.010
R(RO ₂ +NO)	0.262	0.40	+0.007
R(HO ₂ +HO ₂)	0.095	-0.86	-0.006
R(NO ₃ +NO)	0.294	-0.10	-0.002
R(HCHO+NO ₃)	0.294	0.00	+0.000
Boundary Conditions:			
Boundary Cond. O ₃	0.203	0.41	+0.006
Boundary Cond. NO _y	0.549	-0.10	-0.004
Others:			
Dry deposition velocity (all gaseous species)	0.223	-2.42	-0.037

¹All distributions are log-normal [Beekmann and Derognat, 2003; Deguillaume et al., 2007; Digar and Cohan, 2010; Hanna et al., 2001; Sander et al., 2006];

²Cross-sensitivity of O₃ to Atlanta anthropogenic non-EGU NO_x emissions and each uncertain parameter, evaluated at the grid-cell with maximum daily 8-hour average O₃ in a 3x3 array centered on the Confederate Avenue monitor, averaged over the episode;

³Impact factor: The fractional change in first-order sensitivity of ozone to emissions, due to a 1 σ change in an input parameter. Computed as Impact Factor = $\sigma S_{j,k}^{(2)} / S_j^{(1)}$, where $S_j^{(1)}$ is the 1st order sensitivity of O₃ to Atlanta NO_x and $S_{j,k}^{(2)}$ is the cross sensitivity of $S_j^{(1)}$ with an uncertain parameter.

Table 3.1 – Selection of uncertain input parameters for Monte Carlo analysis based on the impact analysis by Digar and Cohan [2010].

Our goal is to estimate the probability that a control strategy would actually achieve an air quality target in light of parametric uncertainty in the photochemical model. In this study, two types of pollutant reduction targets are considered:

A *fixed* reduction target (T_{fixed}) which assumes that the amount of additional pollutant reduction needed for achieving the air quality improvement target is perfectly known, and only the impact (ΔC^*) of the control measures is uncertain due to input uncertainty. Thus, likelihood of attainment (L_{fixed}) is simply the probability that ΔC^* is greater than or equal to T_{fixed} , i.e.,

$$L_{\text{fixed}} = p \Delta C^* \geq T_{\text{fixed}} \quad (3.4)$$

A *flexible* reduction target (T_{flexible}) which recognizes that the needed amount of ambient pollutant reduction (ΔC^*) cannot be predicted perfectly because factors such as future weather and emission trends are unpredictable. In this case, likelihood of attainment (L_{flexible}) is assumed to be a function that increases with the amount of pollutant reduction (ΔC^*) that is achieved. Though various target functions could be posited, for analysis purposes we define a target function, $T(\Delta C^*)$, based on a cumulative distribution (cdf) of a Gaussian function as follows,

$$T(\Delta C^*) = \int_{-\infty}^{\Delta C^*} N(x) dx \quad (3.5)$$

where, $N(x) = \frac{1}{\sigma\sqrt{2\pi}} e^{-\frac{x-\mu}{2\sigma^2}}$. The mean reduction target μ (at which a strategy would have 50% likelihood to be sufficient) and standard deviation $\pm\sigma$ can be assigned values depending on the case under consideration. In this study, an uncertainty of ± 3 ppb (95% confidence interval) has been used, because current EPA methodology requires weight of evidence analysis if the deterministic attainment modeling results are within 3 ppb of the standard [USEPA, 2007]. Moreover, uncertainties in O_3 DVFs have been estimated to be 3-5 ppb due to variation in emission inventories and photochemical models [Sistla et al., 2004] and 2-4 ppb due to variability in meteorology and chemical mechanisms [Jones et al., 2005]. The final likelihood of attainment (L_{flexible}) for given emission controls under parametric uncertainty with the flexible reduction target (Figure 3.2) can then be calculated using the probability density as,

$$L_{\text{flexible}} = \int_{-\infty}^{+\infty} P(\Delta C^* \leq T - \Delta C^*) d\Delta C^* \quad (3.6)$$

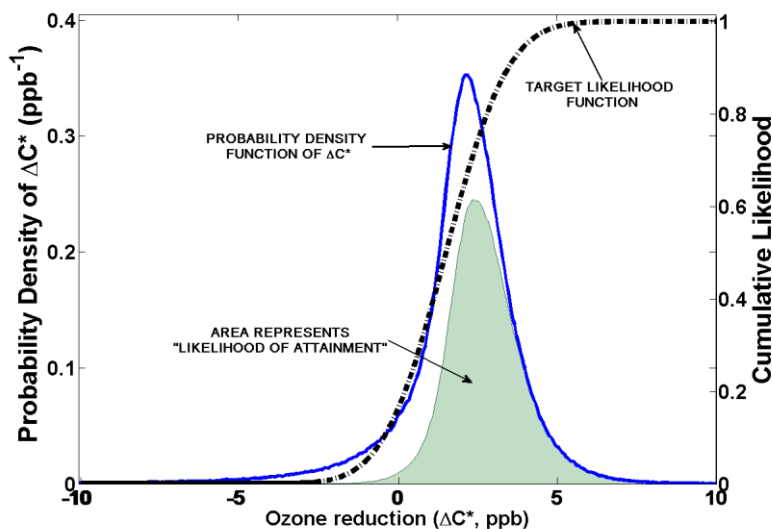


Figure 3.2 - Probability distribution of the O₃ impact at Confederate Avenue monitor due to a 12% reduction in Atlanta NO_x emissions and the likelihood that it will attain a flexible reduction target.

3.3. Application

3.3.1. Photochemical modeling episode

We demonstrate this method by applying it to reconsider attainment modeling from a recent 8-hour O₃ SIP for Atlanta, Georgia [Georgia Department of Natural Resources, 2009]. Modeling is conducted for an 18-day summer episode (May 30 to June 16, 2002; first three days discarded for model initialization) for a southeastern U.S. modeling domain with 12 km grid resolution and 19 vertical layers of increasing thickness, covering Alabama, Georgia, Mississippi, South Carolina, Tennessee, and parts of Kentucky, North Carolina and Florida. The episode is a subset of the full ozone season simulated for the Georgia SIP. Otherwise,

modeling methods mimicked those of the Georgia SIP, including use of the Community Multiscale Air Quality (CMAQ) Model v4.5 [Byun and Schere, 2006] with Carbon Bond 4 (CB-IV) mechanism [Gery *et al.*, 1989] with aerosol and aqueous updates; input meteorological conditions from the 5th generation Mesoscale Model (MM5) [Georgia Department of Natural Resources, 2009; Grell *et al.*, 1994; Olerud and Sims, 2004] simulations; and input emissions from Visibility and Improvements State and Tribal Association of the Southeast (VISTAS) year 2009 projections (projected from a 2002 base inventory) [MACTEC Engineering and Consultancy, 2008; Morris *et al.*, 2008], with updates to Georgia emissions projections based on GA EPD SIP modeling [Georgia Department of Natural Resources, 2009]. Accuracy of O₃ predictions for the 2002 base case was thoroughly tested in Georgia SIP modeling and found to be well within U.S. EPA benchmarks [Georgia Department of Natural Resources, 2009].

3.3.2. Control Strategies

Ozone in Georgia is predominantly sensitive to NO_x emissions because of the dense forest cover leading to high biogenic VOC emissions [Guenther *et al.*, 2000]; our modeling showed O₃ in the region to be at least an order of magnitude more sensitive to NO_x than to VOCs, consistent with earlier studies [Cohan *et al.*, 2005]. Hence, for the selection of control options, NO_x emission reductions were emphasized. For simplicity, Georgia is divided into three broad regions (see Figure 3.3): Atlanta (the 20 county O₃ non-attainment region), Macon (5 counties), and the Rest of GA (= Georgia – Atlanta – Macon).

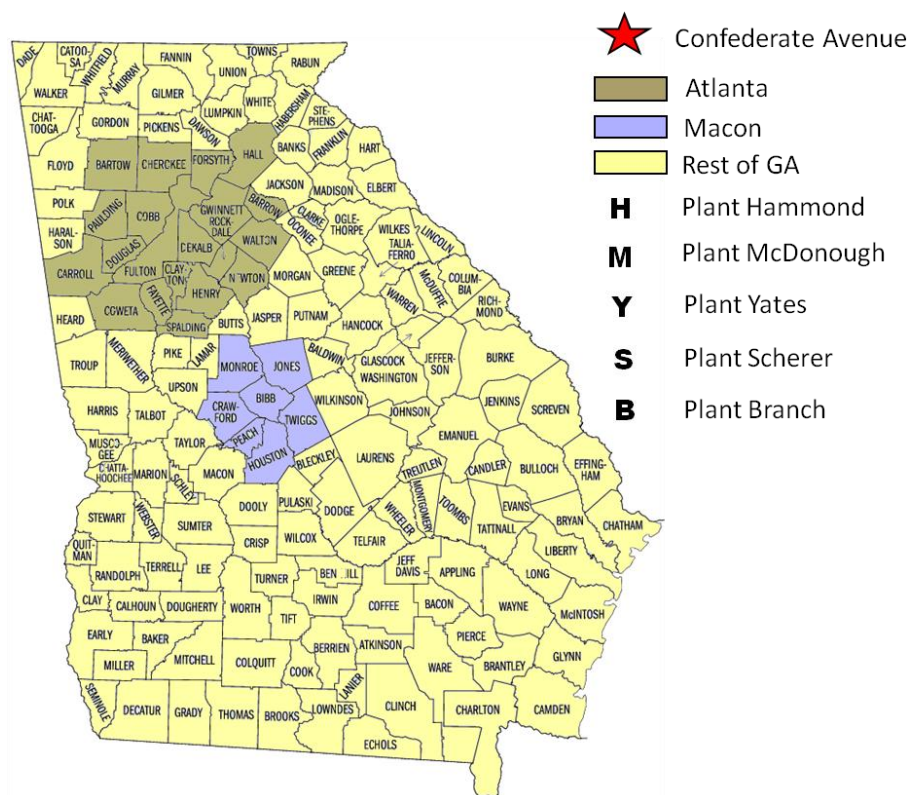


Figure 3.3 – Point sources and emission regions in Georgia considered for control strategy analyses.

Our analysis sought to identify scenarios of control measures that could be implemented at the state level within a SIP time frame. These scenarios were constructed by applying AirControlNET v. 3.2 [E. H. P. Associates, 2005] to identify potential control options for the emission inventory. [A limited list of control technologies and associated control efficiencies obtained from AirControlNET is furnished in Table 3.2. Additional potential measures were also incorporated as described in Table 3.3]. The maximum percent emission reduction from applying all identified control options in each region is tabulated in Table 3.2.

Source	Control Measures	Efficiency of Emission Reduction
Internal Combustion Engines - Gas	L-E (Medium Speed)	87%
Industrial NG/Coal/Oil Combustion	RACT to 25/50 tpy (LNB)	31%
Iron & Steel Mills - Reheating	LNB + FGR	77%
Residential/Commercial NG	Water Heater + LNB Space Heaters	7%
ICI Boilers - Coal/Wall/Stoker/Coke/Natural Gas/Residual Oil/Process Gas; Cement Manufacturing - Dry; Lime Kilns; Sulfate Pulping - Recovery Furnaces; Ammonia - NG-Fired Reformers	SCR	80 - 95%
Rich Burn Internal Combustion Engines - Oil	NSCR	90%
In-Process; Bituminous Coal; Cement Kilns	SNCR - Urea Based	50%
Nitric Acid Manufacturing	SNCR	98%
In-Process Fuel Use; Natural Gas	LNB	50%
Combustion Turbines - Natural Gas	SCR + Steam Injection	95%
Process Heaters - Natural Gas/Process Gas	LNB + SCR	88%

[#] Cost and effectiveness assumptions in AirControlNET are documented by E. H. Pechan & Associates. AirControlNET Version 3.2 documentation report. Prepared for U.S. EPA. 2003.

List of abbreviations:

LNB = Low NO_x Burner
 ICI = Industrial, Commercial and Institutional
 L-E = Low-Excess Air
 RACT = Reasonably Available Control Technologies
 FGR = Flue Gas Recirculation
 SCR = Selective Catalytic Reduction
 NSCR = Non-Selective Catalytic Reduction
 SNCR = Selective Non-Catalytic Reduction

Table 3.2 – NO_x control measures from AirControlNET[#] (based on the most stringent option available for each source).

Source	Control Measures	Emission Reduction	Reference/ Source
Power Plants:			
Scherer Yates Hammond Branch	SCR	50% of EGU NO _x	GA EPD analysis using EPA IPM
		80% of EGU NO _x	
		63.7% of EGU NO _x	
		80% of EGU NO _x	
McDonough	Convert from Coal to Natural Gas + SCR	85% of EGU NO _x	GA EPD
Others: Locomotives	Low-Sulfur Diesel; Genset Locomotives	78-98% of mobile NO _x	[1]
Vehicles	Inspection & Maintenance	6% of mobile NO _x	[1]
Truck Stops	Truck Stop Electrification	2.6% of heavy- duty vehicle emissions	[1]
Diesel Engines	Retrofit Incentives	13.2 tpd* NO _x	[2]
Light-duty vehicles	Distance-based car insurance pricing	10% of light-duty vehicle emissions	[3]

Table 3.3 – Additional NO_x control measures considered.

Power plant emissions are excluded from the regional categories and considered separately. Specifically we consider five large coal-fired power plants, which are among the largest NO_x point-sources near Atlanta and lacked selective catalytic reduction (SCR) control for NO_x when the Georgia SIP was being developed. Potential emission reductions at the power plants were computed by applying control efficiencies from U.S. EPA Integrated Planning Model methodology [USEPA, 2006a] to the inventoried emission rates, accounting for pre-existing control technologies where applicable (Table 3.4). Note that power plant controls

are based on fixed tonnage reductions, whereas regional emission controls are based on percentage reductions.

Control Scenario	Description	Emission Controlled¹
<i>Regional Sources:</i>		<i>Fixed % reduction of total emission</i>
ATL(12)	Maximum available anthropogenic NO _x control in Atlanta	12% (42.7 tpd ²)
ATL(6)	Half of available anthropogenic NO _x control in Atlanta	6% (21.3 tpd)
MAC	Maximum available anthropogenic NO _x control in Macon	20% (10.7 tpd)
REST	Maximum available anthropogenic NO _x control in Rest of Georgia (i.e. Georgia – Atlanta – Macon)	15% (81.5 tpd)
<i>Point Sources (EGU):</i>		<i>Fixed tonnage reduction</i>
EGU(M)	Convert Plant McDonough from coal to gas plus SCR	10.0 tpd (85%)
EGU(S)	Add SCR ³ at Plant Scherer	26.5 tpd (50%)
EGU(Y)	Add SCR at Plant Yates	29.8 tpd (80%)
EGU(H)	Add SCR to units 1-3 at Plant Hammond	11.6 tpd (63%)
EGU(B)	Add SCR at Plant Branch	51.7 tpd (80%)

¹The basis for emission control estimates is explained in Table 3.2 and Table 3.3;

²tpd – tons per day;

³SCR – Selective Catalytic Reduction.

Table 3.4 – Hypothetical NO_x emission control options in Georgia.

3.3.3. Parameters for Uncertainty Analysis

Table 3.1 shows the input parameters that were targeted for uncertainty analysis due to the following reasons. Uncertainties in domain-wide NO_x and VOC emissions rates and in boundary conditions of O₃ and total reactive nitrogen (NO_y = NO_x and its oxidation

products) have been shown to substantially influence the sensitivities of O₃ to NO_x emissions [Bergin *et al.*, 1999; Deguillaume *et al.*, 2008; Fine *et al.*, 2003; Gao *et al.*, 1996; Hanna *et al.*, 2001; Russell and Dennis, 2000]. Past studies have also shown that reaction rates for NO₂+OH [D'Ottonne *et al.*, 2005; Hippler *et al.*, 2006; Tonnesen, 1999] and the photolysis reactions [Cohan *et al.*, 2010; Jin *et al.*, 2008] and several other uncertain reactions [Deguillaume *et al.*, 2007; Hanna *et al.*, 2001] can also significantly influence ozone sensitivity (Table 3.1). We also consider dry deposition velocities of all gaseous species jointly as an uncertain input parameter [Wesely and Hicks, 2000].

Chapter 2 evaluates the relative impacts of the 19 input parameters in Table 2.1 on estimates of O₃-precursor sensitivity in this region [Digar and Cohan, 2010]. For this study, we consider 10 of the 19 uncertain parameters marked in bold in Table 3.1, limiting the uncertain reaction rate constants to the four that most influenced O₃ sensitivity.

3.4. Results and Discussion

Based on the standard U.S. EPA attainment demonstration methodology [USEPA, 2007], Georgia's 2009 SIP modeling predicted that one monitor (Confederate Avenue, AIRS ID: 13-121-0055, for location see Figure 3.3) would exceed the 1997 8-hour O₃ NAAQS of 85 ppb (Ref. Table 6-1 on page 133 of [Georgia Department of Natural Resources, 2009]). The SIP reports additional modeling and weight of evidence analyses to argue that attainment would actually be achieved. However, it can be computed that an additional 1.5 ppb reduction in modeled 2009 8-hour O₃ would have been needed to reduce the relative reduction factor (RRF) in the Georgia SIP (Ref Table 6-1 on page 133 of [Georgia

Department of Natural Resources, 2009]) sufficiently to demonstrate NAAQS attainment using the standard methodology. Hence for this study, we consider the hypothetical scenario that an additional 1.5 ppb of improvement is necessary at this monitor, and explore various control scenarios available in Georgia for reaching that target.

3.4.1. Likelihood to Achieve a Fixed Target

We first assess the likelihood that each control scenario will achieve at least 1.5 ppb reduction in 8-hour O_3 at the grid-cell corresponding to the Confederate Avenue monitor, averaged over the six days with O_3 in the base year 2002 exceeding 80 ppb (Table 3.5). The deterministic results are from the base model ($\phi_k = 0$), with the standard deviation of the daily O_3 reductions shown as an indicator of the variability in results due to day-to-day changes in emissions and meteorology. The probabilistic results reflect 1 million Monte Carlo samplings of the input ϕ_k 's for the RFMs. A Continuum RFM was constructed to predict the impact of each regional control scenario and a Discrete RFM for each power plant option, under parametric uncertainties in the 10 selected parameters from Table 3.4. Impacts of jointly controlling NO_x from multiple regions or power plants were assumed to be additive. This is a conservative assumption that may slightly underpredict joint impacts, since controlling NO_x in one place makes O_3 more sensitive to NO_x from elsewhere [*Cohan et al., 2005*]. The error caused by this assumption is small for controls of these magnitudes [*Digar and Cohan, 2010*].

These ranking reversals occur in part because the parametric uncertainty analysis methods applied here show regional NO_x controls to have more uncertain O_3 impact than

power plant-only controls (as indicated by the 90% confidence intervals for O₃ reduction in Table 3.5) for three reasons. First, the tonnage reduced is assumed to be perfectly known for the power plants (whose baseline emissions are well-established by continuous emission monitors [*Frost et al.*, 2006]) but to vary with uncertainty in domain-wide NO_x for the regional controls, which are set on a percentage basis. Second, power plant controls have a consistently positive impact on O₃ reduction at a faraway monitor because aged, diluted NO_x plumes produce O₃ under a wide range of input parameter conditions. By contrast, local emissions can have a titrating or inhibiting effect on urban O₃ under certain input perturbations, especially if domain-wide NO_x emissions are much larger than originally modeled (Figure 3.2).

Control Strategy ¹	Description	Deterministic O ₃ reduction ² (ppb)	Day-to-day variation (σ) of deterministic O ₃ reduction ³ (ppb)	O ₃ reduction under parametric uncertainty, mean (5 th , 95 th percentiles) ⁴ (ppb)	Likelihood to Achieve T _{fixed} ⁵	Likelihood to Achieve T _{flexible} ⁶
C1	ATL(6)	1.1	0.4	1.0 (-0.7, 2.1)	19.6%	37.5%
C2	EGUs (B, S)	1.2	1.1	1.2 (0.7, 1.7)	4.4%	41.1%
C3	ATL(6) + MAC + REST	1.4	0.4	1.2 (-0.4, 2.5)	37.1%	44.9%
C4	ATL(6) + EGU(M)	<u>1.7</u>	0.8	1.5 (-0.6, 3.2)	57.8%	52.5%
C5	EGUs (B, S, H)	<u>1.7</u>	1.7	1.7 (1.2, 2.3)	77.9%	56.1%
C6	ATL(6) + EGUs (B, S)	<u>2.2</u>	1.3	2.1 (0.1, 3.6)	78.4%	63.5%
C7	ATL(12)	<u>2.3</u>	0.8	2.0 (-1.2, 4.5)	71.7%	62.6%
C8	EGUs (M, B, H, S)	<u>2.3</u>	1.1	2.4 (1.5, 3.3)	94.4%	70.6%
C9	ATL(12) + MAC + REST	<u>2.6</u>	0.8	2.3 (-0.9, 5.0)	78.0%	67.8%
C10	ATL(12) + EGU(M)	<u>2.8</u>	1.2	2.7 (-1.1, 5.6)	79.9%	71.9%
C11	EGUs (M, B, H, S, Y)	<u>2.9</u>	2.8	2.9 (1.2, 7.6)	99.9%	81.7%
C12	ATL(12) + EGUs (B, S)	<u>3.4</u>	1.6	3.2 (-0.3, 6.0)	86.6%	79.0%
C13	ATL(12) + EGUs (B, H, S)	<u>4.0</u>	2.1	3.7 (0.3, 6.4)	90.3%	84.5%
C14	ATL(12) + EGUs (M, B, H, S, Y)	<u>5.1</u>	3.2	5.0 (1.1, 8.1)	94.0%	91.5%

¹In ascending order based on deterministic O₃ reduction; ²Mean of the impacts among the high ozone days in episode; underlining indicates O₃ reduction ≥ 1.5 ppb; ³Standard deviation of the daily impacts within the high O₃ days of the episode; ⁴90% confidence intervals; ⁵Fixed reduction target of 1.5 ppb; ⁶Flexible reduction target of 1.5 ppb with 3 ppb uncertainty (95% confidence).

Table 3.5 – Reduction in 8-hour ozone at Atlanta Confederate Avenue monitor due to each emission control package.

Finally, the likelihood calculations considered uncertainty in model parameters but not in meteorology, and used results averaged over all high O₃ days of the episode. Distant power plant plumes have greater day-to-day variability in impacts (indicated by standard deviation in column 4 of Table 3.5) than regional sources because fluctuating wind fields determine whether the plume reach the monitor. For example, the C5 strategy controlling three distant power plants exhibits more than twice the day-to-day variability of C7, which controls only local Atlanta emissions. Longer episodes with classification and regression tree analysis [Breiman *et al.*, 1984] could be used to ensure that a representative range of high O₃ meteorological conditions have been modeled.

3.4.2. Likelihood to Achieve Flexible Target

The impacts of the control packages are re-assessed for a *flexible* air pollutant reduction target, corresponding to eq 3.6 and Figure 3.2, to reflect the fact that meteorological variability and other factors may make the needed amount of improvement uncertain. The results in Table 3.5 and Figure 3.4 show that when the reduction target is not accurately known, the chances of attainment are less responsive to the amount of emission control. For example, strengthening Atlanta NO_x controls from 6% to 12% (strategies C1 and C7) increases the L_{fixed} by 52 percentage points, but increases L_{flexible} by only 25 percentage points (Table 3.5). Similar trends can be seen in the flatter lines of Figure 3.4(c) than Figure 3.4(b). This occurs because a *flexible* reduction target blurs the distinction between strategies

that achieve just more or just less than 1.5 ppb of reduction. However, the results approach the *fixed* target results as the σ used to define T_{flexible} is narrowed.

The likelihood rankings remain largely consistent under the *flexible* and *fixed* reduction targets, but with some exceptions (Table 3.5 and Figure 3.4). For example, strategy C8 (four power plant controls) ranks second under the *fixed* reduction target but only sixth under the *flexible* reduction target. The relatively narrow uncertainty of power plant control impacts, modeled to occur for reasons explained above, is more helpful in achieving a *fixed* than a *flexible* reduction target, provided that the mean impact is above 1.5 ppb.

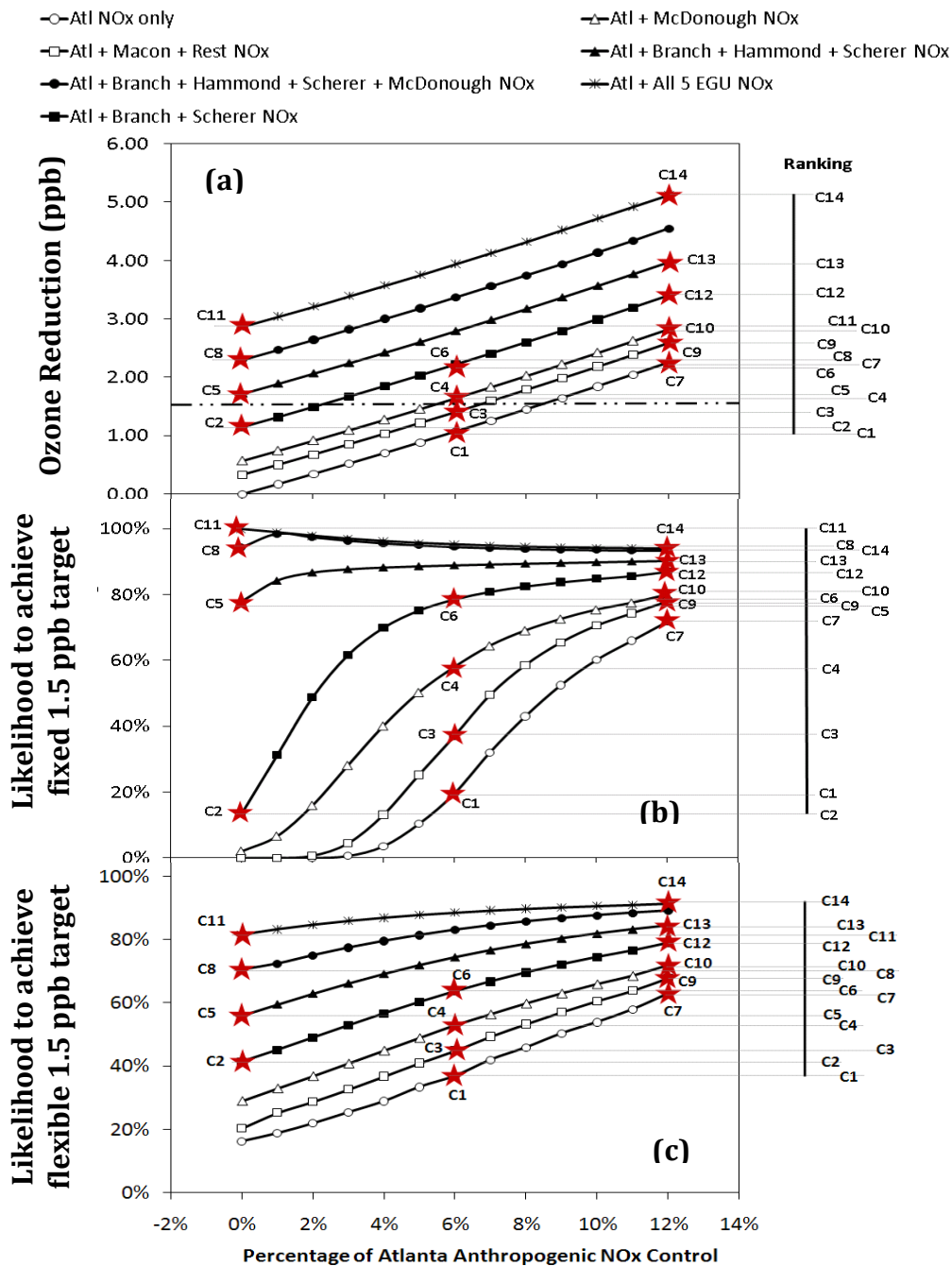


Figure 3.4 - Predicted future O₃ design values (a) and likelihood of achieving a fixed (1.5 ppb) (b) or flexible (1.5 ± 3.0 ppb, 95% CI) (c) reduction target at Confederate Avenue monitor as a function of the percentage of Atlanta NO_x that is controlled under various scenarios for reducing NO_x emissions from other sources.

3.4.3. Relevance of Results

The approaches introduced here enable probabilistic prediction of the likelihood that a control package will be sufficient to achieve a *fixed* or *flexible* air quality improvement target in the presence of parametric uncertainties in the photochemical model. Both targets may usefully inform environmental decision-making, depending on how the policy issue is framed. The *fixed* target is apt if the needed amount of additional ozone reduction is clearly defined; for example, if regulatory approval of an attainment plan depends on demonstrating an additional increment of ozone abatement. A *flexible* target, meanwhile, is more attuned to predicting the likelihood of future attainment at monitors, which increases with the amount of control but is also influenced by external factors such as meteorological variation. Although the *flexible* target may obscure the distinctions between relative efficacies of control strategies, it avoids unrealistic expectations that a State's control choices could be so determinative of future attainment at monitors.

Results from these approaches could be linked with control cost estimates to maximize the likelihood of attainment, subject to practical or budgetary constraints, or may supplement deterministic approaches to inform the prioritization of control strategies [Cohan *et al.*, 2006]. Actual selection of control measures depends upon a whole host of practical, economic, and political considerations, but our approaches could usefully inform strategy selection. Probabilistic approaches may also be used as additional 'weight of evidence' analyses in attainment demonstrations. However, probabilistic approaches are unlikely to supplant deterministic bright-line tests as

the primary arbiter of attainment plan sufficiency, because to do so would require subjective judgments about which model uncertainties to consider, the form of the target function, and what likelihood of attainment is sufficient.

Although only 8-hour O₃ attainment was considered here, this method can also be applied for assessing control strategies for other pollutants. Application to particulate matter (PM) would need to account for differences in model performance among PM species and use an alternative method to compute sensitivity coefficients, since high-order DDM is currently unavailable for PM in CMAQ.

This analysis represents an important yet incomplete step towards comprehensive likelihood assessment because it considered uncertainties only in the photochemical model parameters and in the reduction target. The specific *flexible* target considered here is just one of many ways that such a target could be formulated. Structural uncertainties in the photochemical model, uncertainties in the meteorological inputs, and the representativeness of the meteorological episode were overlooked. Additional important uncertainties include control measure effectiveness (i.e., the percent or tons of emissions actually reduced by the abatement measures) and the accuracy of predicted baseline emission trends (e.g., due to economic and population growth, vehicle fleet turnover, etc.). Future work could incorporate these uncertainties into the likelihood assessments and explore alternate formulations of the target functions.

Adapted with permission from *Digar et al.*, Uncertainties Influencing Health-Based Prioritization of Ozone-Abatement Option, *Environmental Science & Technology*, 45(18), 7761-7767, 2011. DOI: 10.1021/es200165n. Copyright © 2011, American Chemical Society.

Chapter 4

Uncertainties influencing health-based prioritization of ozone abatement options

4.1. Introduction

Tropospheric ozone (O_3) causes threats to human health such as aggravating asthma and other respiratory illness. Several studies, including a review by the National Research Council (NRC) have found statistical associations between short-term O_3 exposure and premature mortality [*Bell et al.*, 2004; *Ito et al.*, 2005; *Jerrett et al.*, 2009; *NRC*, 2008]. For the protection of public health, which is the primary objective of air quality management, control policies are formulated to mitigate O_3 . This is often challenging because O_3 is a secondary pollutant formed as a result of complex nonlinear chemistry between various primary pollutants. Photochemical

models are therefore used to predict the relative impacts of controlling various O₃ precursor emissions for regulatory attainment purposes.

Most studies of control strategy optimization [Shih *et al.*, 1998; Wang and Milford, 2001; Yang *et al.*, 2006] or the relative impacts of O₃ control options [Digar *et al.*, 2011] have focused on attainment of standards at ambient monitors, in line with the standard regulatory practice for attainment demonstrations in the United States [USEPA, 2007]. However, attainment of regulatory standards may not be fully protective of human health, since effects have been observed at low levels [Bell *et al.*, 2006]. Evaluation of the relative health benefits of control options along with their attainment implications could better inform strategy selection and optimization of net benefits [Chestnut *et al.*, 2006], because the ranking of controls options on health and attainment bases may differ [Cohan *et al.*, 2006].

Various studies have quantified the health benefits of O₃ abatement by linking O₃ concentration-response (C-R) relationships from epidemiological studies with baseline health incidence data, population distributions, and model estimates of O₃ reductions [Hubbell *et al.*, 2004; Ostro *et al.*, 2006]. Health benefits estimation may be uncertain due to (a) *photochemical uncertainty* - the uncertainty of the air quality models used to compute the O₃ concentrations and sensitivities to emission changes, and/or (b) *epidemiological uncertainty* - the uncertainty in the magnitude and form of the C-R relationships. Photochemical model predictions of O₃ response to emission changes are known to be uncertain [Fine *et al.*, 2003], and recent studies have introduced efficient methods for characterizing these model uncertainties

[Digar and Cohan, 2010; Pinder et al., 2009; Tian et al., 2010]. However, not much effort has been made to study the effect of these uncertainties on the estimation of health benefits. Most studies that have presented confidence intervals for O₃-health impacts have considered uncertainty only in the C-R functions, not in the photochemical modeling of O₃ changes [Bell et al., 2007; US-EPA, 1999; Zhou et al., 2010].

Moreover, apart from the uncertainty in the magnitude of C-R relationships, there is also the question of which temporal metric of O₃ concentrations (e.g. 1-h or 8-h daily maximum, or 24-h average) is most determinative of health responses [NRC, 2008]. The U.S. EPA has modified the metric of O₃ health-based regulations from the 24-h to the daily 1-h maximum to the 8-h maximum in response to epidemiological evidence on which metric is most associated with health. Epidemiological meta-analyses of O₃ health effects convert these metrics using standard conversion ratios, in order to draw from a larger pool of C-R results reported on disparate temporal metrics [Bell et al., 2005a; Ito et al., 2005]. Such scaling has generally been deemed a reasonable approach for estimating the health impacts of total O₃ concentrations, despite some variations in temporal ratios with season and location [Anderson and Bell, 2008]. However, converting across temporal metrics may be more problematic for O₃ sensitivity to controls, since diurnal patterns of responsiveness can differ sharply depending on the emission that is targeted [Cohan et al., 2005]. Bell et al. [2005b] showed that the choice of temporal metric can strongly influence overall rankings of air pollution policies.

This manuscript characterizes how uncertain photochemical modeling and uncertain C-R relationships influence predictions of the relative health benefits of O₃ precursor emission control options in the Dallas-Fort Worth region of Texas. Although idealized abatement options have been considered here, this method can be easily extended for actual O₃ abatement strategies and may serve as a tool for prioritizing control options. While the main results are presented based on the standard 8-h O₃ metrics, efforts have also been made to explore the effects of alternate temporal metrics.

4.2. Methods

4.2.1. Air Quality Modeling

The high-order decoupled direct method (HDDM) [Dunker, 1984; Hakami *et al.*, 2003] within the Comprehensive Air Quality Model with Extensions (CAMx) v5.32 developed by ENVIRON Corporation [ENVIRON, 2010] is used to compute O₃ sensitivities to its precursor emissions. The modeling domain (Figure 4.1) used for this study was taken from the Texas Commission on Environmental Quality's (TCEQ) O₃ SIP modeling for the Dallas-Fort Worth (DFW) region [TCEQ, 2011a], which consists of a 36-km coarse grid covering the eastern US, with a nested 12-km grid covering eastern Texas and a 4-km grid centered on the DFW 9-county region (Collin, Dallas, Denton, Tarrant, Parker, Johnson, Ellis, Kaufman and Rockwall). The 12-km domain contains 89x89 grids with a total population of 32.5 million (Figure 4.2). The 74x65 grid cells of the 4-km sub-domain comprise about 20% of this total

population. Model simulation was conducted for a full month, May 31 to July 02, 2006, within the summer O₃ season. The first three days of the episodes were discarded for model initialization. Input meteorological conditions for the model simulations were taken from the MM5 mesoscale model [Dudhia, 1993] using simulations developed by TCEQ for its actual attainment modeling [Emery et al., 2009]. Detailed performance evaluation of the June 2006 meteorological modeling is documented in Appendix A of TCEQ report [TCEQ, 2011a]. Input emissions for the anthropogenic sources obtained from EPA MOBILE6.2 emission factor model and EPA's National Mobile Inventory Model (NMIM) / the Texas NONROAD (TexN) mobile source models, were processed by TCEQ using version-3 of the Emission Processing System (EPS3) [ENVIRON, 2007]. The biogenic inventories for the Base Case modeling were generated using Global Biosphere Emissions and Interaction System (GloBEIS, v3.1) [Yarwood et al., 1999]. Details of model set-up can be found in the TCEQ attainment demonstration and its progress report.[TCEQ, 2011a; b]

We compare the relative benefits of controlling emissions from the following sources within the DFW 9-county region: anthropogenic NO_x (ANO_x), 314.24 metric tons per day (tpd), subdivided as surface NO_x (SNO_x), 301.50 tpd, and elevated NO_x (ENO_x), 12.74 tpd; and anthropogenic VOC (AVOC), 300.72 tpd. To facilitate comparisons between emission control options, the change in O₃ concentrations (ΔC , in ppb) per one incremental tpd of emission reduction is computed by dividing the semi-normalized sensitivity coefficients output from CAMx-DDM[Dunker et al., 2002] by the size of the emission category.

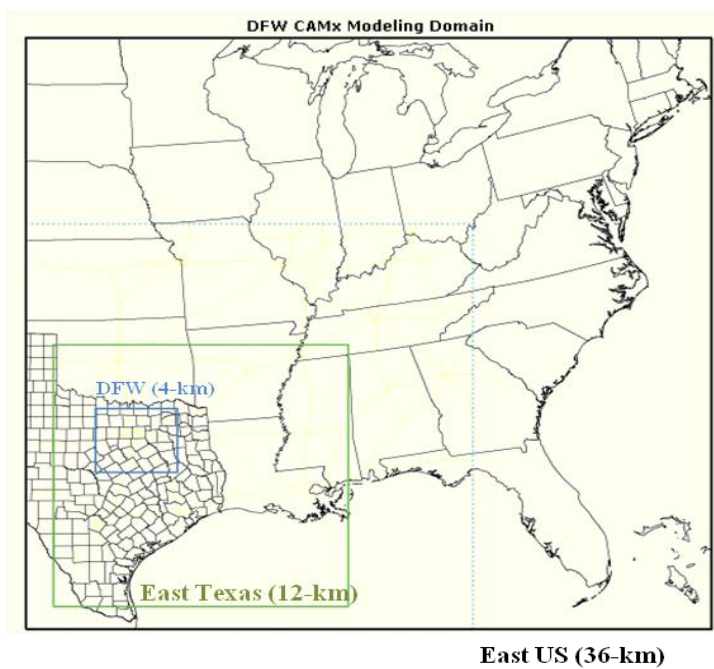


Figure 4.1 – CAMx Modeling Domain used for the study. [Source: TCEQ]

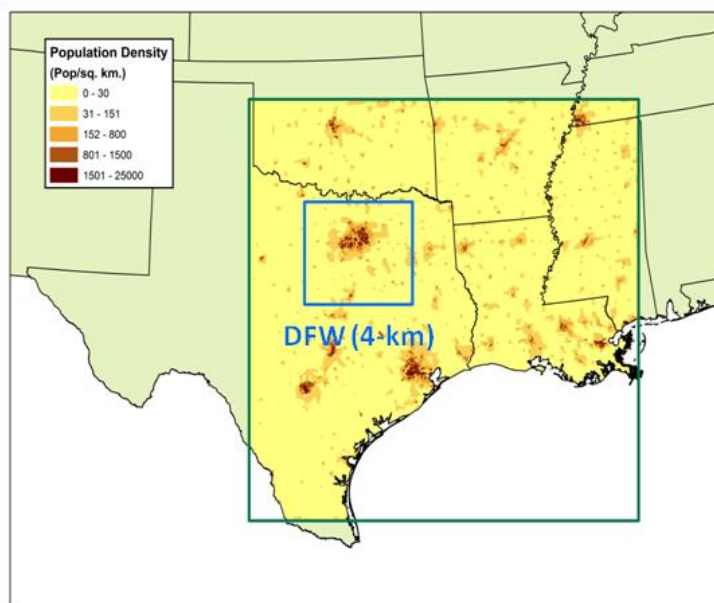


Figure 4.2 – Population density in the study region.

4.2.2. Health Benefit Estimation

To estimate health benefits that result from reductions in O₃ concentrations, we use the C-R function developed by *Bell et al.* (2004) for all-cause short-term premature mortality [*Bell et al.*, 2004], by which the actual number of averted mortalities, $M_{\Delta C,t}$, due to reduction in O₃ concentration, ΔC over a time period, t , can be estimated as,

$$M_{\Delta C,t} = [\exp(\Delta C)\beta - 1]I_t \quad (4.1)$$

In this study, we address averted mortalities from reduced O₃ levels; however, alternatively eq 4.1 could be expressed as additional mortalities for an increase in O₃. No threshold concentration is applied, because epidemiological studies have found a continuous association between daily mortality rates and O₃ even down to very low O₃ concentrations [*Bell et al.*, 2006]. I_t denotes the *baseline* number of health responses per year. *Bell et al.* [2004] quantified the *health risk estimate*, β , based on the change in mortality associated with short-term exposure to ambient O₃ for 95 large cities in the U.S. from 1987-2000. The baseline incidence rates are obtained from U.S. EPA's Environmental Benefits Mapping and Analysis Program (BenMAP) [*Abt Associates Inc.*, 2005] database, which provides county-level mortality rates for the years 2000 through 2050 projected from the rates reported by U.S. Centers for Disease Control for the years 1996-1998. Area-weighted averaging is used to map the county-level incidence data to the air quality

model grid. Finally $M_{\Delta C,t}$ is integrated over the Eastern Texas TCEQ modeling domain as shown in Figure 4.2 (total effect over the 4-km sub-domain where the control is applied, plus the total downwind effect in the area outside the 4-km domain but inside the 12-km domain) and averaged over the episode to estimate the net overall health benefits in eastern Texas. Health benefits are assumed to accrue for five summer months (May to September) but not in other seasons when O_3 concentrations tend to be lower and less responsive to emission controls; thus, $M_{\Delta C,t}$ is scaled by 153/365 to determine total benefits per summer season.

4.2.3. Characterization of Uncertainty

From eq 4.1, it can be seen that uncertainty in $M_{\Delta C,t}$ can arise from uncertainty in ΔC (photochemical uncertainty) and/or β (epidemiological uncertainty). Photochemical uncertainty arises due to uncertain model formulation (*structural uncertainty*) [Pinder et al., 2009] or uncertain input parameters (*parametric uncertainty*) [Fine et al., 2003; Russell and Dennis, 2000].

4.2.3.1. Structural Uncertainty

We apply an ensemble method to address the structural uncertainty in the photochemical modeling. Screening was conducted to test the relative impacts of alternate choices for biogenic emission model, chemical mechanism, vertical deposition scheme, and global model for boundary conditions. The screening revealed that the greatest impact on O_3 sensitivities came from the choice of

chemical mechanism and biogenic emission model. Here, we construct an ensemble of three *structural scenarios* regarding choices of mechanisms and inputs for the CAMx model:

- **'BASE CASE'** which uses the RADM dry deposition scheme [Wesely, 1989], the Carbon Bond 5 (CB-05) chemical mechanism [Yarwood *et al.*, 2005], boundary conditions from the MOZART global model [Brasseur *et al.*, 1998], and GloBEIS-generated biogenic emission inventory [Guenther *et al.*, 1995; Yarwood *et al.*, 1999].
- **'MEGAN'** which substitutes a biogenic emission inventory provided by the Model of Emissions of Gases and Aerosols from Nature (MEGAN) [Guenther *et al.*, 2006] (all other inputs same as the BASE CASE).
- **'CB-6'** which substitutes the Carbon Bond 6 chemical mechanism [Yarwood *et al.*, 2010], using an updated rate constant for the reaction $\text{NO}_2 + \text{OH} \rightarrow \text{HONO}_2$ [Mollner *et al.*, 2010].

4.2.3.2. Parametric Uncertainty

To study the effect of *parametric uncertainties* within each of these members of the structural ensemble, lognormal probability distribution functions (PDF) with uncertainty ranges described in Table 4.1 are assigned to specific model input parameters selected based on their strong contributions to uncertainty in O_3 -emission sensitivities [Digar and Cohan, 2010; Digar *et al.*, 2011]. Domain-wide NO_x and VOC emission rates, and the rate constants for all photolysis reactions,

(NO₂+OH), (NO+O₃), and all (VOC+OH) reactions were found to most influence O₃ sensitivity to DFW ANO_x. For O₃ sensitivity to AVOC, the boundary condition for O₃ was also found to be important, so this was considered in addition to the aforementioned emission and reaction rates (Table 4.1).

Parameter ¹	Uncertainty ² (1 σ)	Reference	Impact ³ on O ₃ sensitivity to ANO _x	Impact ³ on O ₃ sensitivity to AVOC	Range of perturbations ⁴ 1 + ϕ_k used in this study
<i>Emission Rates:</i>					
Domain-wide NO _x	0.336	50	-0.463	0.496	0.60 to 1.67
Domain-wide biogenic VOC	0.405	50	0.216	-0.319	0.56 to 1.80
Domain-wide anthropogenic VOC	0.336	50	0.073	-0.150	0.60 to 1.67
<i>Reaction Rate Constants:</i>					
All photolysis frequencies	0.347	49	0.401	0.091	0.59 to 1.69
R(OH+NO ₂)	0.131	52	-0.057	0.029	0.79 to 1.26
R(NO+O ₃)	0.095	49	-0.058	-0.024	0.84 to 1.19
R(All VOCs+OH)	0.095	50	0.021	0.014	0.84 to 1.19
<i>Boundary Conditions:</i>					
BC (O ₃)	0.203	50	0.006	-0.042	0.71 to 1.41

¹Parameters selected based on the impact analysis by Digar and Cohan (2010); [Digar and Cohan, 2010; Digar et al., 2011]

²All distributions are assumed log-normal, with uncertainties based on [Beekmann and Derognat, 2003; Deguillaume et al., 2007; Digar and Cohan, 2010; Hanna et al., 2001; Sander et al., 2006];

³*Impact factor:* The fractional change in first-order sensitivity of O₃ to emissions, due to a 1 σ change in an input parameter. Computed as Impact Factor = $\sigma S_{j,k}^{(2)} / S_j^{(1)}$ where $S_j^{(1)}$ is the first-order sensitivity of O₃ to emission j (either ANO_x or AVOC) and $S_{j,k}^{(2)}$ is the cross sensitivity of $S_j^{(1)}$ with an uncertain parameter k .

⁴Uncertainty factors based on $\pm 2\sigma$ (i.e., 95%) confidence interval.

Table 4.1 – Uncertainties assumed in the input parameters for Monte Carlo analysis.

Cohan et al., [2005] introduced a method to use HDDM second-order sensitivity coefficients to adjust a baseline estimate of per-ton O₃ sensitivity to emission j ($s_j^{(1)}$) to account for a fractional perturbation φ_k in uncertain input parameter k :

$$\Delta C = s_j^{(1)*} \approx s_j^{(1)} + \varphi_k s_{j,k}^{(2)} \quad (4.2)$$

where $s_j^{(1)*}$ denotes the adjusted value of the sensitivity $s_j^{(1)}$, corrected for the perturbation in parameter k , and $s_{j,k}^{(2)}$ is the cross-sensitivity of O₃ to parameters j and k . We extend this method to adjust $s_j^{(1)}$ for perturbations in multiple input parameters k (which may include j) by assuming that the influences are additive, as shown in eq 4.3:

$$\Delta C = s_j^{(1)*} \approx s_j^{(1)} + \sum_k \varphi_k s_{j,k}^{(2)} \quad (4.3)$$

Eq 4.3 is found to be highly accurate in predicting actual modeled first-order O₃ sensitivities directly calculated by HDDM (normalized mean bias <2%, and normalized mean error <10%, when compared against sensitivities computed by brute force method) up to $+2\sigma$ level of simultaneous perturbations in all the uncertain input parameters considered here.

4.2.3.3. Epidemiological Uncertainty

Uncertainty in epidemiological estimates of health risk (β) are reported in a variety of forms including an estimated standard error, $\sigma(\beta)$. *Bell et al.*, [2004] reports β with $\sigma(\beta)$ in parenthesis for daily (i) 1-h max: 3.33E-04 ($\pm 6.32\text{E-}05$), (ii) 8-h max: 4.22E-04 ($\pm 7.76\text{E-}05$), and (iii) 24-h average: 5.18E-04 ($\pm 1.25\text{E-}04$). We assign a Gaussian PDF to β based on its range of standard errors for alternate temporal metrics. Finally, combining eqs 4.1 and 4.3, we can estimate health benefits as follows,

$$M_{\Delta C,t} = \left[\exp \left\{ \left(s_j^{(1)} + \sum_k \varphi_k s_{j,k}^{(2)} \right) \beta \right\} - 1 \right] I_t \quad (4.4)$$

We apply Monte Carlo to randomly select 10,000 φ_k 's (from log-normal PDF of input parameter k within a range of $\pm 2\sigma$) and β 's (from PDF of β) in eq 4.4 to characterize the probability distribution of $M_{\Delta C,t}$. Each of the three structural scenarios is assumed to have equal probability of occurrence (sample size = 3 x 10,000).

4.3. Results and Discussion

The Monte Carlo results show that the health benefits of O_3 reduction (eq 4.4) are more strongly affected by uncertainties in model inputs (φ) than by uncertainties in health risk estimates (β). As seen in Figure 4.3, PDFs of 8-h O_3

health benefits exhibit a wider spread when only ΔC is uncertain than when only β is uncertain. Moreover, inspection of results shows that uncertainty in health benefits is driven primarily by uncertainty in NO_x and VOC emission inventories and in photolysis rates. Variations in the formulation of emission inventories and chemical mechanism strongly influence O_3 responses to emission changes. The MEGAN inventory estimates higher rates of biogenic VOC emissions and lower rates of soil NO than the base (GloBEIS) [Carlton and Baker, 2011], making O_3 more sensitive to anthropogenic NO_x in scenario B (Figure 4.4).

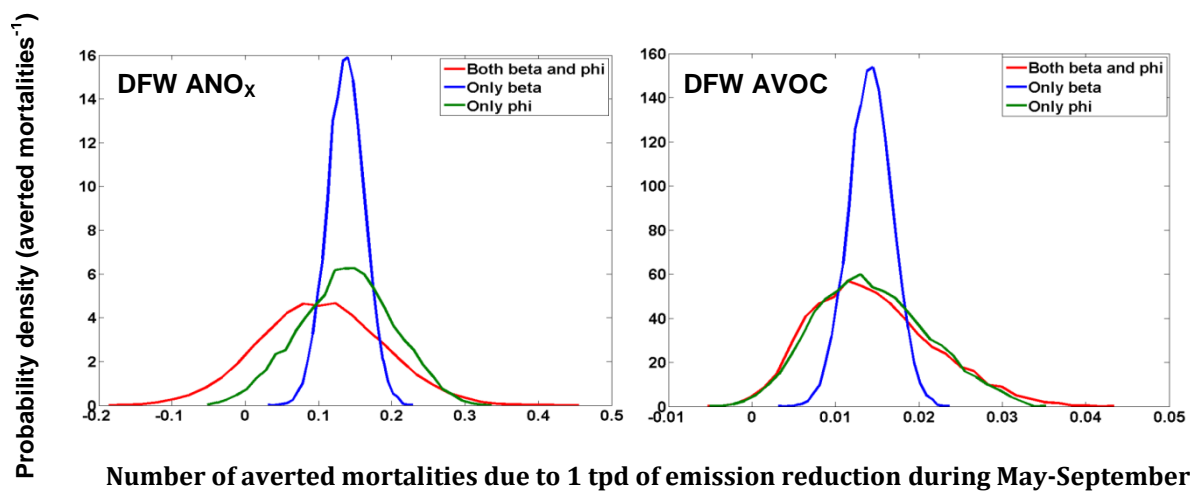


Figure 4.3 – Probability density of averted premature mortalities per ozone season per ton per day reduction in anthropogenic NO_x or VOC emission from DFW under uncertain ϕ and/or β . Modeling results are shown for 8-h O_3 metrics, averaged over the episode and integrated over the domain for the base-case simulation.

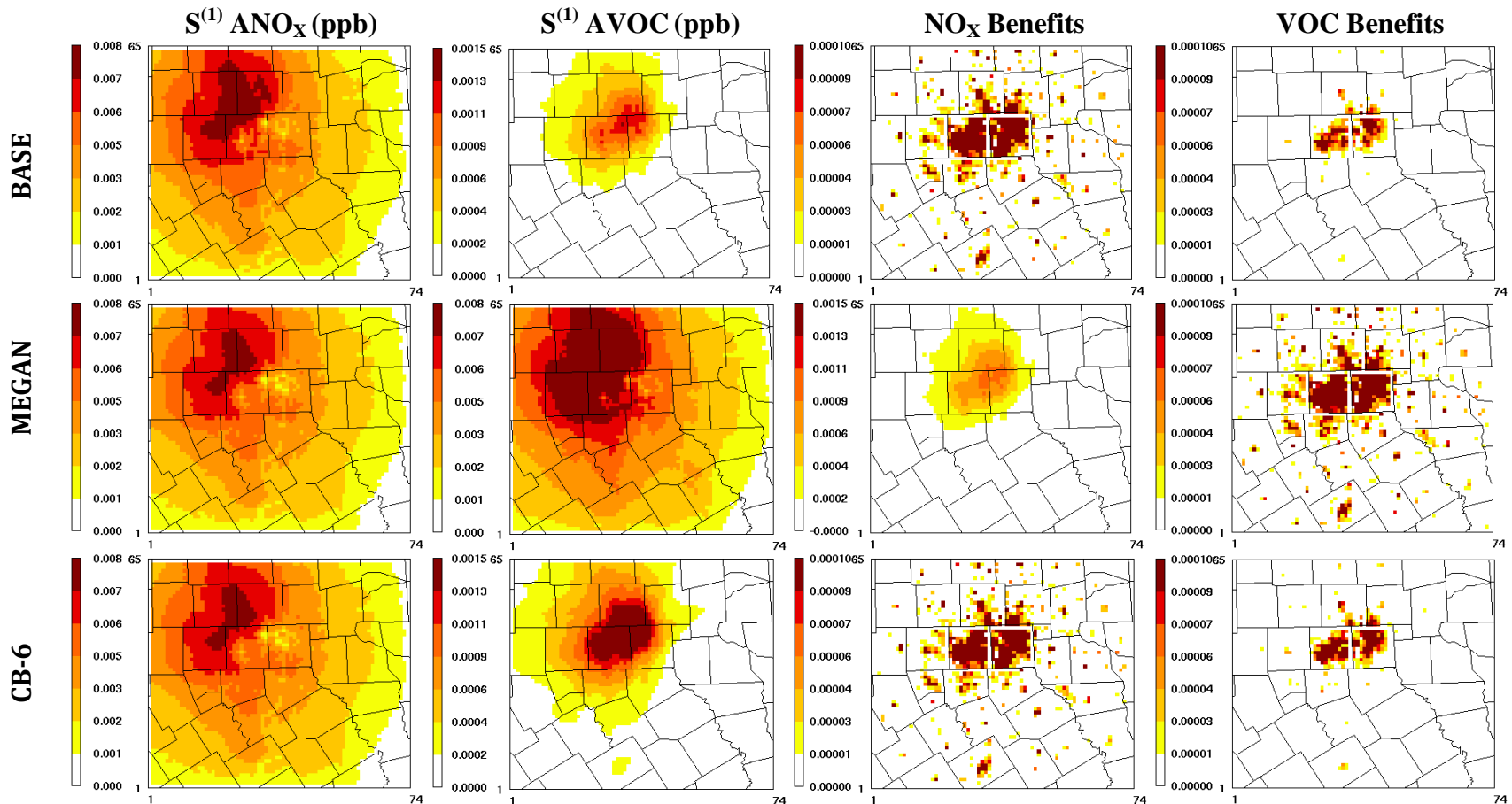


Figure 4.4 – Max 8-h O_3 sensitivity to DFW emission and health benefits (averted mortalities) per ton of reduction in NO_x or VOCs for each of the 3 structural model scenarios when inputs are considered to be perfectly known. Episode average results are shown for the 4-km DFW sub-domain.

In most of the Monte Carlo simulations, more 8-h O₃ benefits are obtained per ton of NO_x control than per ton VOC control, but the benefits from NO_x control are more uncertain (Figure 4.5). Figure 4.6 shows the cumulative likelihood distribution for the ratio between the per-ton impact of 8-h O₃ for pairs of control options when the photochemical model assumptions (structural scenarios) and inputs (parametric estimates) are simultaneously considered uncertain. The uncertainties in health risk estimates (β) considered here do not affect ratios of per-ton impacts, since they affect each control option proportionally. Benefit-ratios computed by this method can be compared with cost-ratios of emission controls (benefit-cost-analysis) to select options that are most cost-effective. This will help to better inform the prioritization and ranking of emission control options [Cohan *et al.*, 2007]. For example, deterministic modeling in DFW shows per-ton reduction of NO_x emission from low-level sources to be 1.42 times as beneficial as controlling per-ton emission from elevated NO_x sources. Under this condition, surface NO_x control would be preferred provided its per-ton control costs are less than 1.42 times the cost of controlling elevated NO_x sources. Incorporating uncertainties via the Monte Carlo analysis shows 96% likelihood that the per-ton benefits of surface NO_x controls will exceed those of elevated NO_x controls (Figure 4.6a). Similarly, comparing benefits of total anthropogenic NO_x and VOC controls, the deterministic modeling shows 9.23 times as much health benefit from NO_x controls as from VOC controls. However, the Monte Carlo analysis finds a 5.7% probability that the per-ton benefits of VOC control will surpass those of NO_x control, including the 2.8% of

cases in which NO_x controls turns out to be unfavorable as it causes additional mortalities (Figure 4.6b).

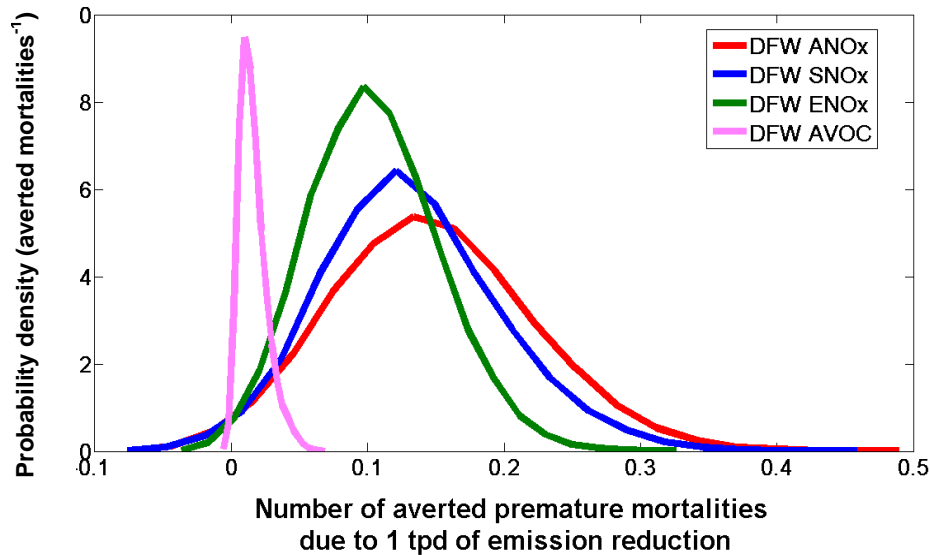


Figure 4.5 – Health Impacts of 8-h O₃ reduction due to NO_x and VOC controls from DFW (9-county), considering uncertainties in photochemical modeling and in the health response relationship.

While the comparisons in Figure 4.6 are evaluated on an 8-h daily maximum basis, consistent with the form of the health-based U.S. ambient O₃ standards, it may be asked how prioritization of control options would differ under alternate temporal metrics. As noted in the Introduction, some epidemiological meta-analyses have used scaling factors to interchangeably consider overall O₃-health relationships reported on a variety of temporal metrics [Anderson and Bell, 2008; Bell et al., 2005a], but the choice of metric may influence the rankings of control strategies [Bell et al., 2005b]. If control measures display dissimilar temporal

signatures in influencing O_3 concentrations, then estimates of their relative health benefits may depend on the choice of temporal metric.

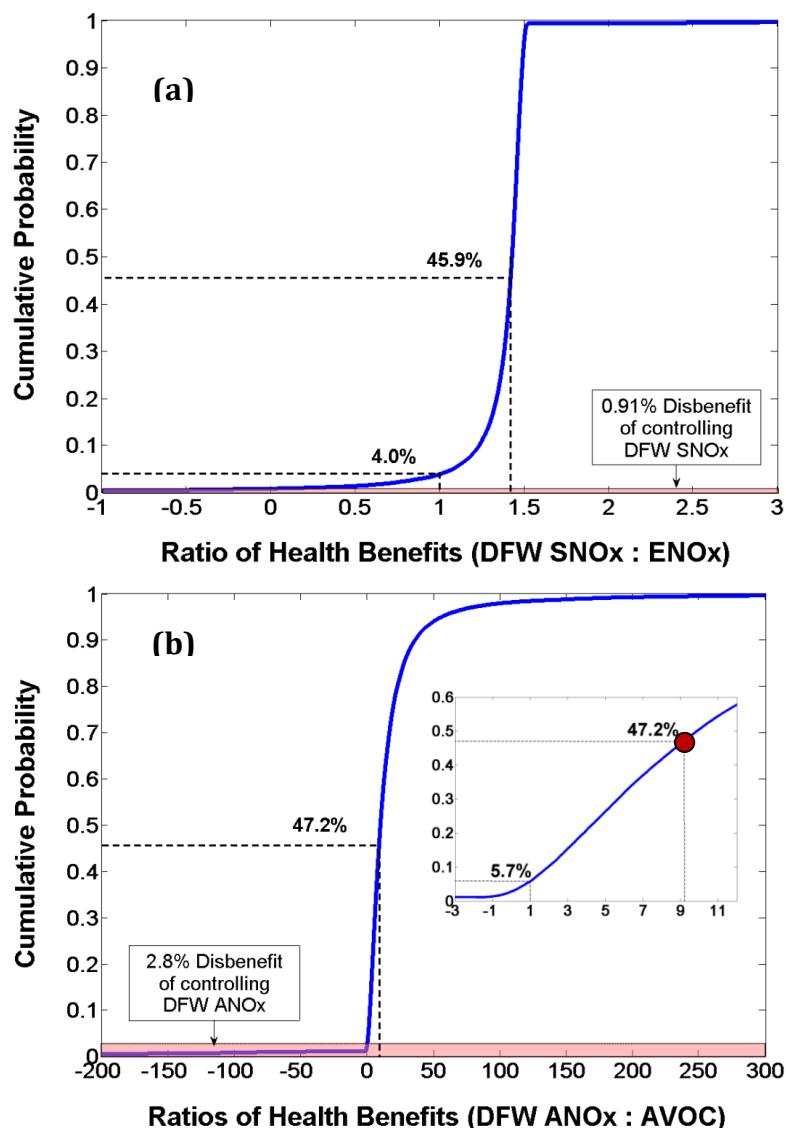


Figure 4.6 – Relative health benefits from 8-h O_3 reduction due to (a) surface NO_x vs. elevated NO_x controls, and (b) total anthropogenic NO_x vs. VOC controls from DFW (9-county), considering uncertainties in photochemical modeling. The red dot denotes results from the deterministic modeling and pink regions represent negative impacts.

Diurnal profiles indeed show distinct temporal signatures for the first-order sensitivities of O_3 to the source categories (Figure 4.7), consistent with those reported in earlier studies [Kim *et al.*, 2009]. O_3 sensitivities to VOCs typically peak in the morning, before biogenic VOC emissions (which peak in early afternoon) push photochemistry toward more NO_x -limited conditions; O_3 sensitivities to NO_x peak in the afternoon coincident with hours of peak O_3 concentrations, and turn negative at night.

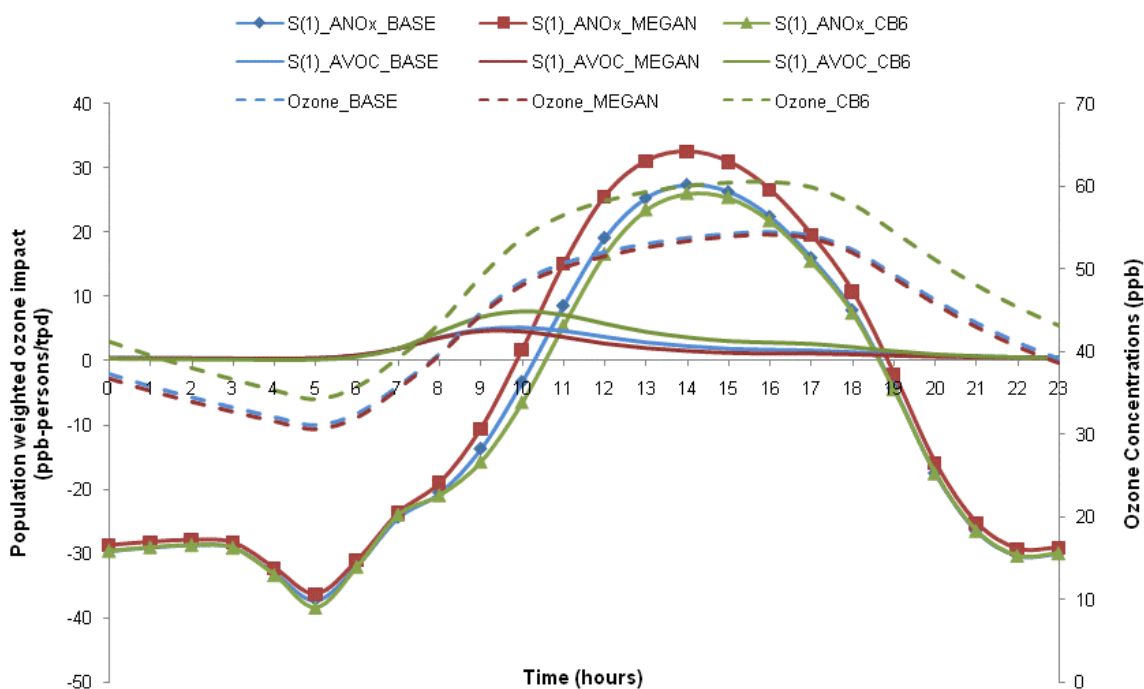


Figure 4.7 - Diurnal profile of ozone concentrations and sensitivities for DFW sub-domain. Results are averaged over domain and episode.

Thus, NO_x controls appear more effective on the 1- and 8-h metrics, while 24-h averaging favors VOC controls (Figure 4.8). Also, NO_x from elevated sources (smokestack of power plants and other chemical facilities) are emitted above the shallow nocturnal planetary boundary layer (PBL) and do not titrate surface O_3 at night. As such, based on the 24-h metric, controlling ENO_x emission is better than SNO_x controls.

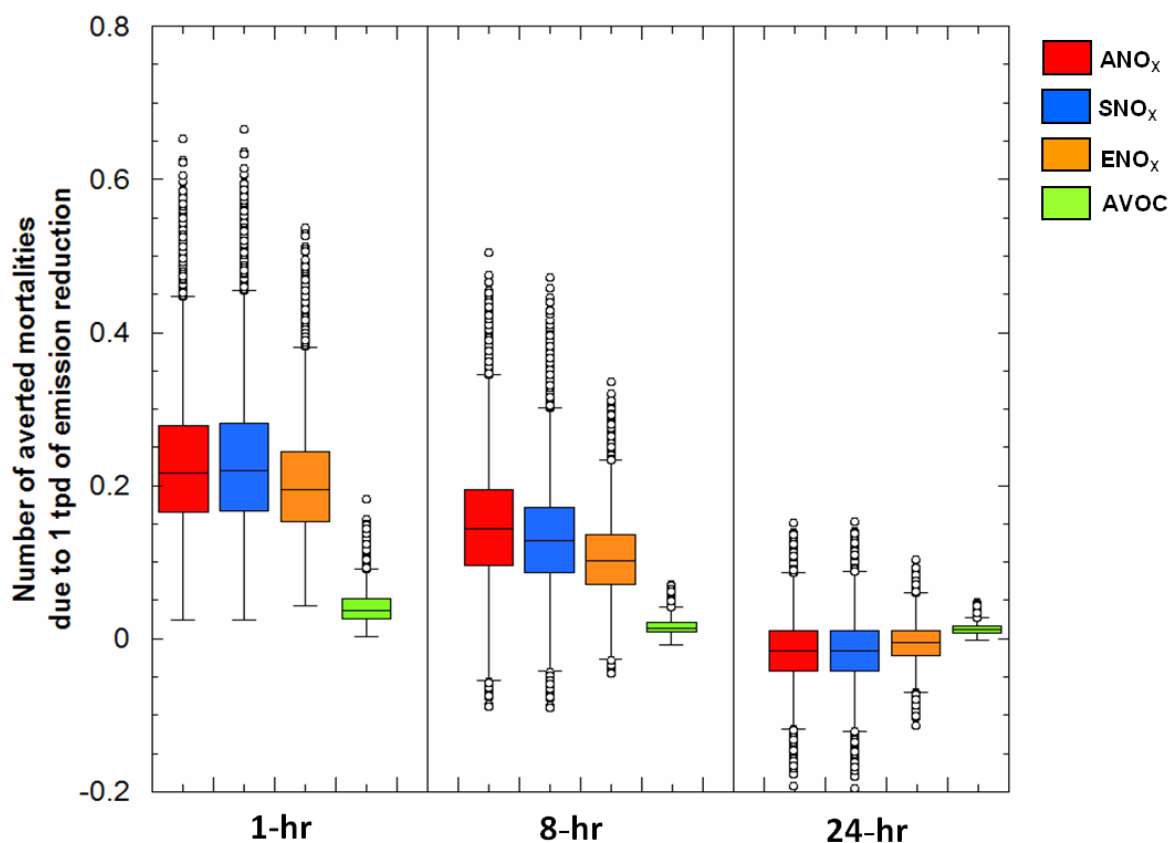


Figure 4.8 - Averted mortalities per O_3 season due to 1 tpd reduction in NO_x or VOC emissions from various sources in DFW when both air quality model inputs (ϕ) and health risk estimates (β) are uncertain. Results are averaged over the episode and integrated over the inner two modeling domains.

The results show health-based prioritization of O₃ control measures to be highly sensitive to uncertainties in photochemical modeling and to the choice of temporal metric for O₃ exposure. However, in this study we considered equal probability for the alternate structural assumptions in the photochemical O₃ modeling. Future work could explore whether the photochemical uncertainties could be narrowed by applying Bayesian approaches to constrain the relative likelihood of the Monte Carlo cases between individual structural simulations [Bergin and Milford, 2000]. Rankings using the max 1- and 8-h metrics are quite similar, but differ dramatically on the 24-h metric that includes nocturnal periods of disbenefit from NO_x controls. This highlights the need for further epidemiological research to clarify which temporal metric is most determinative of health responses to O₃. While only mortality impacts were considered here, similar uncertainties in control measure rankings would likely be found for other health endpoints such as hospital admissions or respiratory incidents, for which associations with O₃ have been reported in C-R functions of similar form to eq 1. Future research could consider morbidity impacts of O₃ as well as the non- O₃ health consequences of O₃ precursors (VOCs and NO_x), which have their own suite of adverse health effects and influence secondary particle formation.

Although there are challenges in incorporating stochastic results rather than deterministic modeling into environmental decision-making, the novel approaches introduced here for characterizing the uncertainty of relative health benefit ratios could be linked with other analyses to usefully inform the selection of control

strategies. For example, health benefit probability distributions such as those depicted in Figure 4.8 could be linked with control cost estimates to assess the likelihood that a given control measure would be more cost-effective than another. Such analyses could be further linked with modeling of impacts at regulatory monitors to enable joint optimization of control strategies for health and attainment objectives.

Chapter 5

Using observations to constrain probabilistic predictions of ozone-precursor responsiveness

5.1. Introduction

Secondary air pollutants like ozone (O_3) are formed as a result of complex nonlinear chemistry between various primary pollutants emitted directly into the atmosphere due to anthropogenic and natural activities. Understanding the responses of ambient pollutant concentrations to emission changes is therefore crucial for the development of effective pollution abatement strategies. Photochemical models are used to estimate the sensitivity of secondary air pollutants to their precursor emissions, and thus serve as useful tools for determining the amount of emission reduction needed to attain ambient air quality standards and informing the selection of control strategies.

Models for informing air quality management are typically run deterministically with a single best-available setting for model formulation and inputs. However, there has been a growing interest in probabilistic representations of model results that account for model uncertainty [Dennis *et al.*, 2010; Hogrefe and Rao, 2001]. Uncertainties in pollutant-emission response (sensitivity) can arise from choices of numerical representations of atmospheric processes such as chemical mechanism, vertical mixing scheme, and emission model (*structural uncertainty*), and/or from the values of input parameters such as emission rates, reaction rate constants, boundary conditions and deposition velocities (*parametric uncertainty*) [Deguillaume *et al.*, 2008; Fine *et al.*, 2003; Pinder *et al.*, 2009].

Recent work by Digar and Cohan [2010] and Tian *et al.* [2010] introduced efficient Monte Carlo techniques for characterizing *parametric* uncertainties in O₃ and PM responses to emission controls. Pinder *et al.* [2009] jointly considered *parametric* and *structural* uncertainties to develop probabilistic estimates of O₃ concentrations. However, none of these studies evaluated the relative likelihoods of the various Monte Carlo cases.

Previous work by Bergin and Milford [2000] had shown that a Bayesian inference approach can weight the relative likelihood of each Monte Carlo model formulation based on its performance in simulating observed concentrations and thus yield probability distributions for predicting the actual values of pollutant-emission sensitivities as well as model inputs. That study used a simplified 2-dimensional trajectory model, and only a handful of studies have applied Bayesian

Monte Carlo approaches to characterize O₃ responsiveness in more computationally intensive 3-dimensional regional models [Beekmann and Derognat, 2003; Deguillaume et al., 2008].

The aim of this study is to develop probabilistic representations of O₃ responsiveness to emission changes constrained by actual measurements of pollutant concentrations. The Monte Carlo Reduced Form Model approach of Digar and Cohan [2010] has been used to generate a large ensemble of model predictions of O₃ concentrations and responsiveness to emission controls in the Dallas-Fort Worth (DFW) region of Texas, which is currently a nonattainment area for the 1997 8-hour O₃ National Ambient Air Quality Standard (NAAQS) [USEPA, 2011]. The simulated concentrations of O₃ and its precursor nitrogen oxides (NO_x ≡ NO and NO₂) are compared against observations to yield adjusted (*a posteriori*) probabilistic representations of photochemical model inputs and output predictions. Use of both Bayesian and non-Bayesian statistical techniques allow us to evaluate the consistency of our results across various observational metrics and methods of comparison. Sections 5.2 and 5.3 describe the modeling and measurements used for this work and section 5.4 describes the statistical methodology and metrics considered here. Important findings are elaborated in the results and discussion section (Section 5.5), followed by conclusions.

5.2. Photochemical Model description

5.2.1. Base Case Modeling

The Comprehensive Air Quality Model with Extensions (CAMx) v5.32 [ENVIRON, 2010] is used here to study a 2006 summer episode in DFW spanning from May 31 to July 02, which includes numerous days with meteorological conditions favoring O₃ formation. Results for the first five days were neglected for model initialization. This period was identified by the Texas Commission on Environmental Quality (TCEQ) based on its prevalence of observed 8-hour daily maximum O₃ concentrations exceeding the 8-hour O₃ 1997 NAAQS of 84 ppb [TCEQ, 2011a; b]. Sensitivity of O₃ to its precursor emissions is computed using the High-order Decoupled Direct Method (HDDM) [Dunker, 1984; Hakami et al., 2003] within the CAMx model. The modeling domain covers an area of 4896 km² in the Eastern U.S. with a horizontal grid resolution of 36 km, encompassing nested finer domains of 12 km (East Texas – area 2136 km²) and 4 km (DFW subdomain - area 556 km²) spatial grid resolution (Figure 5.1). The vertical configuration for the model domain consists of 28 layers of varying thickness (for details see Table 2-2 of [TCEQ, 2011a], Appendix C), sufficient enough to examine the effect of vertical mixing within the typical planetary boundary layer height.

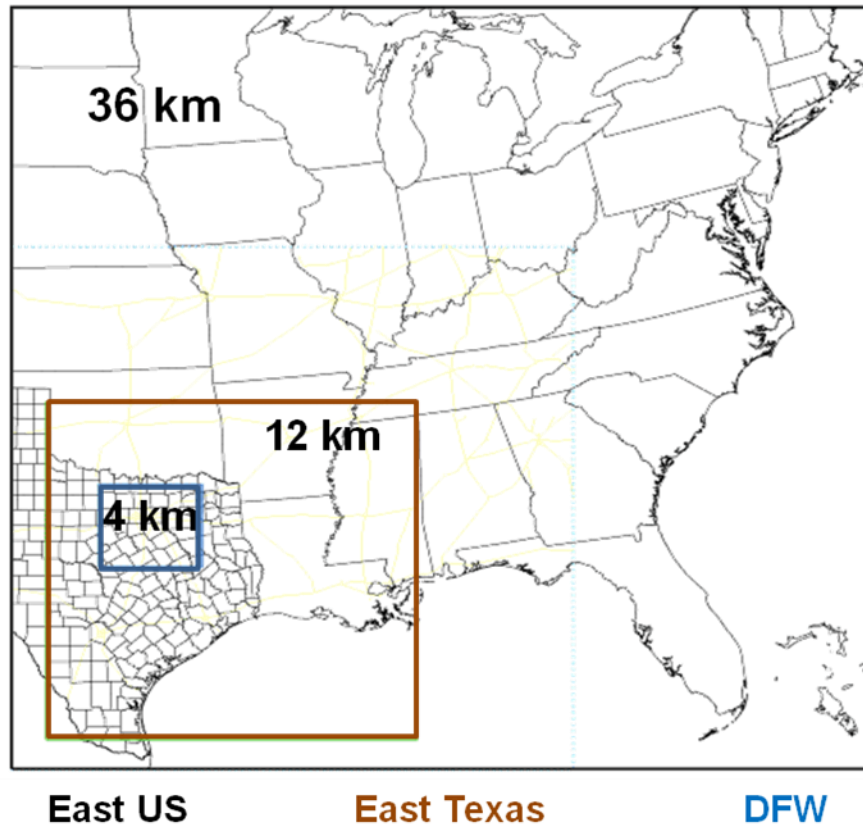


Figure 5.1 –Modeling domain used in the study [TCEQ, 2011a].

The CAMx model inputs (emissions, meteorological conditions, initial and boundary concentrations, chemical mechanism and deposition scheme) were taken from the TCEQ’s Base Case Modeling for the 8-hour O₃ SIP in DFW [TCEQ, 2011a]. The mobile emission (on-road and non-road) inputs obtained from EPA MOBILE6.2 emission factor model, EPA’s National Mobile Inventory Model (NMIM) and the Texas NONROAD (TexN) mobile source models, were processed to a model-ready format by the Emissions Processing System version 3 (EPS3) [ENVIRON, 2007]. Base case biogenic emissions were derived from the Global Biosphere Emissions and

Interactions System (GloBEIS3.13.1) model [Yarwood *et al.*, 1999]. The Fifth Generation Meteorological Model (MM5 version 3.7.4) [Dudhia, 1993] was used to generate the meteorological inputs to CAMx including wind speed, wind direction, temperature, humidity, etc. [Emery *et al.*, 2009]. Details regarding the meteorological and emission modeling and their performance evaluations can be found in Appendix A and B of [TCEQ, 2011a]. The Base Case model uses the Carbon Bond version 05 (CB-05) chemical mechanism [Yarwood *et al.*, 2005], a dry deposition scheme based on the works of Wesely [1989] and Slinn and Slinn [1980], and the global Model for Ozone and Related Chemical Tracers (MOZART) to generate episode-specific boundary condition concentrations for the coarse-grid (36 km) modeling domain [ENVIRON, 2008].

5.2.2. Model Uncertainty Scenarios

This study jointly considers uncertainties in both model formulation (*structural uncertainties*) and in model input parameters (*parametric uncertainties*).

5.2.2.1. Structural Scenarios

Structural scenarios were constructed by choosing either the Base Case setting explained above (section 5.2.1) or the alternate setting described below for each of four features: chemical mechanism, biogenic emissions model, dry deposition scheme, and boundary conditions model.

Alternate chemical mechanism (CHEM): In this setting, the 5th version of the Carbon Bond chemical mechanism (CB05) in the BASE model is replaced by the 6th version (CB6) [Yarwood *et al.*, 2010]. In CB6, several long-lived, abundant organic compounds namely propane, acetone, benzene and ethyne (acetylene), are added explicitly to improve oxidant formation from these compounds as they are oxidized slowly at the regional scale. Compared to the CB05 mechanism, CB6 increases the number of model species (from 51 to 76) and the number of reactions (from 156 to 218). We adjust the rate constant for the reaction (OH+NO₂) in CB6 to be consistent with the most recent findings of Mollner *et al.* [2010] (CB6 also includes several updates for organic and inorganic aerosol chemistry). Detailed discussion of the differences between CB05 and CB6 is provided by Cohan *et al.*, [2011].

Alternate biogenic emissions (BIO): The GloBEIS-derived biogenics inventory is replaced by alternate biogenic emissions from the Model of Emissions of Gases and Aerosols from Nature (MEGAN) [Guenther *et al.*, 2006], which employs updated land cover data based on satellite and ground observations. Guenther *et al.* [2006] reports that the global annual isoprene emission, as estimated by MEGAN, approximately ranges from 500 – 750 Tg. Strong differences (about a factor of 2) between biogenic emission estimates from BEIS and MEGAN have been documented by Carlton and Baker [2011]. For our study region and episode, MEGAN estimated about 60% lower NO_x emissions and 20% higher non-methane volatile organic compound (NMVOC) and carbon monoxide (CO) emissions than GloBEIS (for detailed difference see [Cohan *et al.*, 2011]).

Alternate dry deposition scheme (DEP): The original BASE case that uses land use inputs and a dry deposition scheme based on the work of *Wesely* [1989] and *Slinn and Slinn* [1980] is replaced here by an updated approach [*Zhang et al.*, 2001; 2003]. The Zhang scheme incorporates vegetation density effects via leaf area index (LAI), possesses an updated representation of non-stomatal deposition pathways, has more land use categories, and has been tested extensively through its use in daily air quality forecasting.

Alternate boundary conditions (BC): Here, the MOZART boundary conditions used in the BASE case model are replaced by alternate boundary conditions from the GEOS-Chem global model [*Schubert et al.*, 1993; *Bey et al.* 2001] that exhibit higher O₃ concentrations (0.7 to 8 ppb) than MOZART at all model layers [*Cohan et al.*, 2011].

5.2.2.2. Parametric Uncertainties

For *parametric* uncertainties, we target the model input parameters identified by *Digar and Cohan* [2010] as most likely to influence model predictions of O₃ concentrations and their sensitivities to NO_x and volatile organic compound (VOC) emission controls. These parameters include specific emission rates, reaction rate constants, and boundary conditions (Table 3.1).

Sections 5.4.1.1 and 5.4.1.2 describe additional screening that was conducted to further narrow the structural cases and input parameters that most influence O₃ concentrations and sensitivities for the episode considered here.

5.3. Ground-level Measurements of Ozone and its Precursors

Measurement data were obtained from the U.S. Environmental Protection Agency's (EPA) Air Quality System (AQS) database for ground-level concentrations of O₃ and NO_x. These monitors record hourly concentrations of ambient air pollutants through a nationwide monitoring network [<http://www.epa.gov/ttn/airs/airsaqs/index.htm>]; the monitors in Texas are operated by TCEQ. The raw data were then post-processed to obtain daily maximum 8-hour O₃ and 24-hour average NO_x concentrations at all the monitors that fall within the nine-county DFW nonattainment area (based on 1997 8-hour O₃ NAAQS) – Denton, Collin, Parker, Tarrant, Dallas, Rockwall, Kaufman, Johnson and Ellis Counties. We considered 11 monitors that measure both O₃ and NO_x concentrations (Figure 5.2).

Measurements of O₃ are conducted by well-established techniques, and thus instrumental error is relatively small [US EPA 2006]. However, due to lack of direct measurement technique for nitrogen dioxide (NO₂), NO_x measurements tend to have significant instrumental bias and monitor interferences [Demerejian, 2000; Dunlea et al., 2007]. NO_x concentrations are therefore bias-corrected for interference with other nitrogen species. We apply a bias-correction factor (β) adapted from [Lamsal et al., 2008] computed using modeled species concentrations to correct reported NO_x observations,

$$\beta = \frac{[\text{NO}] + [\text{NO}_2]}{[\text{NO}] + [\text{NO}_2] + 0.95 \times [\text{PAN}] + 0.35 \times [\text{HNO}_3] + [\text{N}_2\text{O}_5] + [\text{PNA}] + [\text{HONO}] + [\text{NO}_3]} \quad (5.1)$$

where PAN is peroxy acetyl nitrate and PNA is peroxy nitric acid.

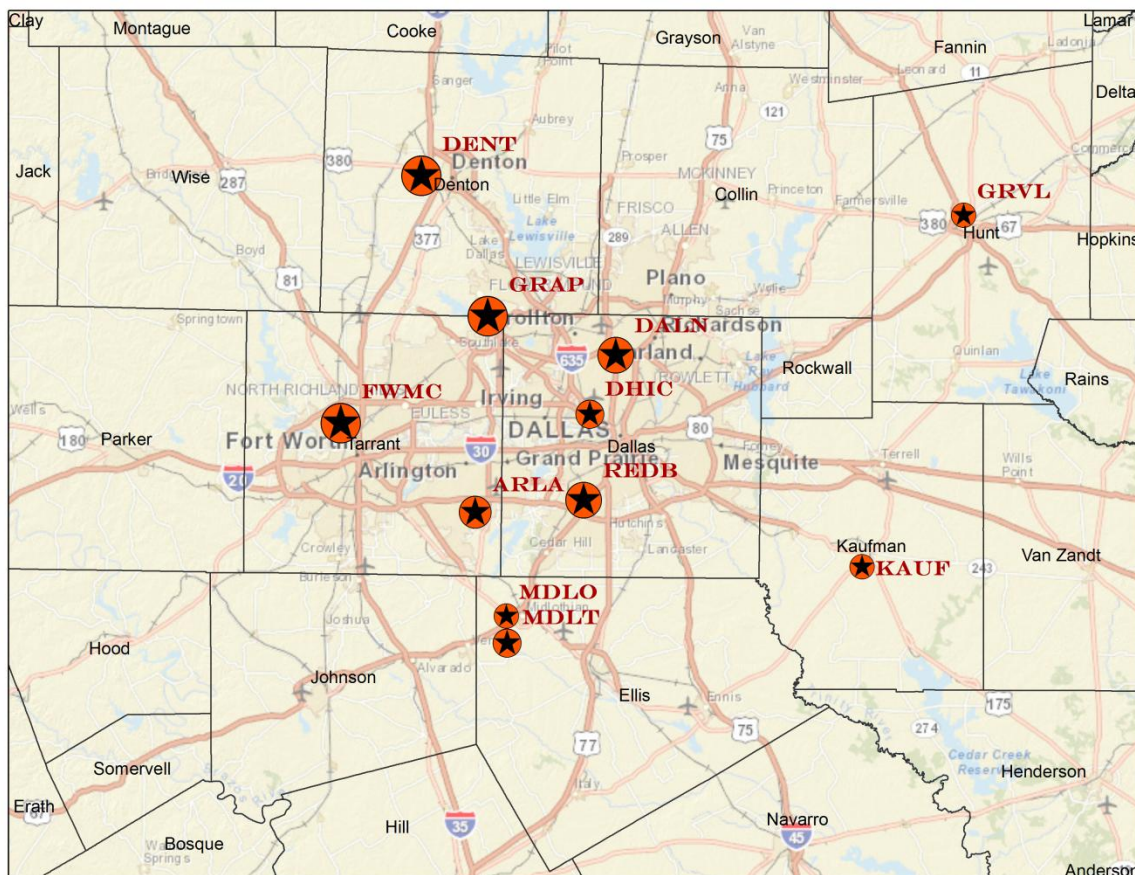


Figure 5.2 – Map showing the locations of the monitoring sites used in this study. The size of the circles are proportionate with their 2006 8-hour O₃ Design Values given in Table A.2 (Appendix A).

5.4. Method

5.4.1. Model Uncertainty Analysis

In this section, we detail the methodology adopted for incorporating *structural* and *parametric* uncertainties in the photochemical air quality modeling.

5.4.1.1. Screening for Structural Uncertainty

To assess the effect of model *structural uncertainty*, we first run the photochemical model with the base-case scenario (BASE), and then with each of the alternate assumptions of atmospheric processes detailed in section 5.2.2.1. To recap, these include alternate chemical mechanism (CHEM), biogenic emission inventory (BIO), dry deposition scheme (DEP), and boundary conditions (BC). Figure 5.3 shows how the diurnal patterns of O_3 sensitivities change with each of these different model assumptions. Afternoon ozone in DFW is primarily NO_x -limited in all of the structural cases, with O_3 about an order of magnitude more sensitive to DFW anthropogenic NO_x (ANO_x) than anthropogenic VOC (AVOC). In general, use of MEGAN biogenic emission increases O_3 sensitivities to ANO_x (S_{NO_x}) and decreases sensitivity to AVOC (S_{VOC}) relative to the base case during daytime because of its stronger biogenic VOC emissions. The alternate CB-6 chemical mechanism also affected daytime O_3 sensitivities but in the opposite direction, yielding stronger sensitivities to AVOC, though conditions remain predominantly NO_x -sensitive under either structural configuration. The alternate BC case did not significantly affect O_3 sensitivities, and DEP affected sensitivities mostly during night.

In order to select the most important structural factors that influence predictions of O_3 concentrations, we compare each structural scenario against the observations. For screening scenarios that most strongly affect O_3 sensitivities, we

compare each alternate scenario against the base-case simulation results. The statistical measures that serve as the bases for the comparisons are detailed below:

$$\text{Root Mean Square Error (ppb), RMSE} = \sqrt{\frac{\sum_{j=1}^N (Y_j - O_j)^2}{N}} \quad (5.2)$$

$$\text{Mean Bias (ppb), BIAS} = \frac{1}{N} \sum_{j=1}^N (Y_j - O_j) \quad (5.3)$$

$$\text{Normalized Mean Bias (\%), NMB} = \frac{\sum_{j=1}^N (Y_j - O_j)}{\sum_{j=1}^N O_j} \cdot 100\% \quad (5.4)$$

$$\text{Normalized Mean Error (\%), NME} = \frac{\sum_{j=1}^N |Y_j - O_j|}{\sum_{j=1}^N O_j} \cdot 100\% \quad (5.5)$$

where N is the number of observations (site/days) and 'Y_j' denotes each of the model structural cases considered above. For screening considering concentrations, 'O_j' represents the observations and for sensitivity, 'O_j' represents the BASE case simulation results.

The comparison results (Table 5.1) show that alternate chemical mechanism (CB6 vs. CB-05) and biogenic model (MEGAN vs. GloBEIS) most strongly influence the predicted O₃ concentrations and sensitivities. Therefore, we build an ensemble of models with the following *structural members* – (1) BASE, (2) CHEM, (3) BIO, and

(4) a combination of alternate chemical mechanism (CB6) and biogenics (MEGAN) (hereafter abbreviated as CHEM + BIO). Figure 5.4 shows the spatial plots for O₃ sensitivities to each of these four structural members. NO_x-limited conditions for daily maximum 8-hour O₃ persist even in the urban center regardless which structural scenario is considered.

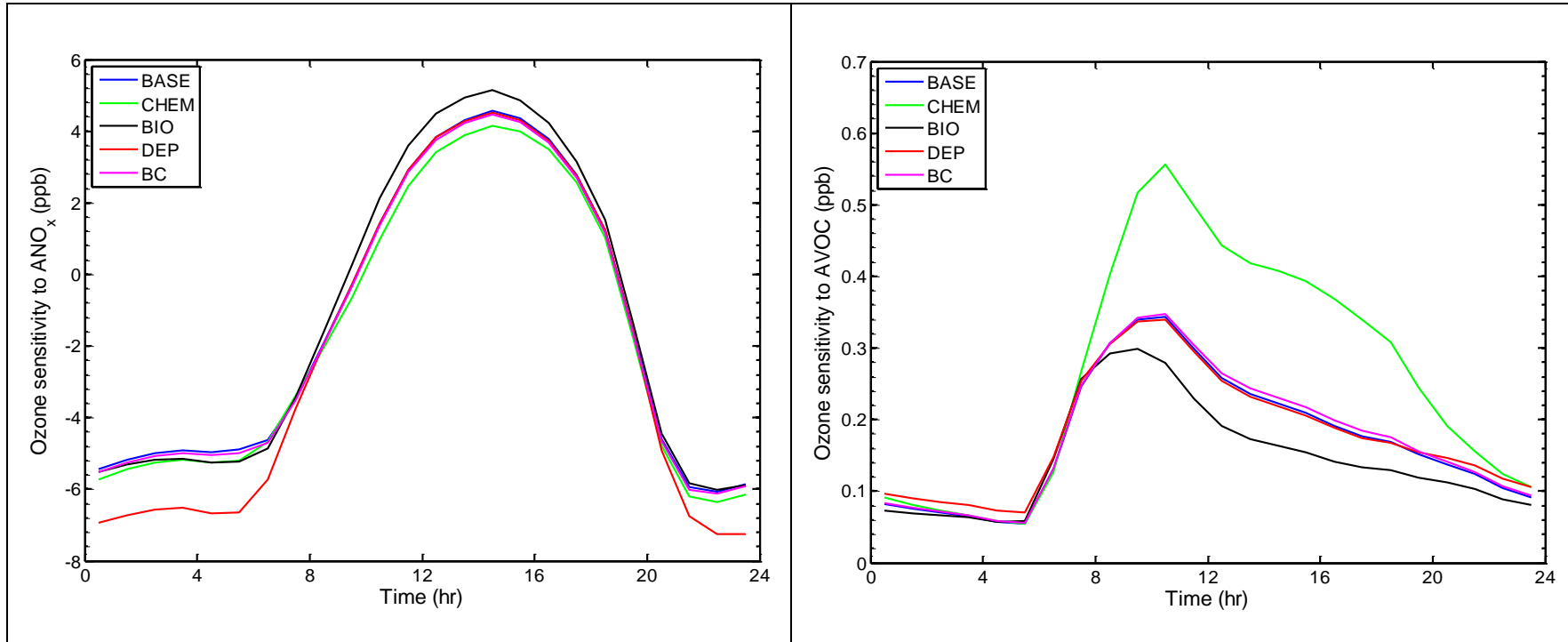


Figure 5.3 - Diurnal profile of ozone sensitivities to DFW ANO_x (left) and AVOC (right) emissions, averaged over the episode and the grid-cells covering the DFW region.

	STRUCTURAL CASES				
	Base	CHEM	BIO	DEP	BC
Comparison of each structural case against the observations for <u>8-hour O₃ concentration in DFW</u>					
RMS (ppb)	13.01	13.21	13.63	12.95	13.01
BIAS (ppb)	-0.61	4.59	-1.06	1.88	0.02
NMB (%)	-1.04	7.83	-1.82	3.22	0.04
NME (%)	17.79	16.88	18.85	17.08	17.76
Comparison of each alternate case against the Base case for <u>8-hour DFW O₃ sensitivity to DFW ANO_x</u>					
RMS (ppb)	-	0.79	1.37	0.12	0.16
BIAS (ppb)	-	-0.40	0.75	-0.01	-0.09
NMB (%)	-	-12.07	22.81	-0.25	-2.81
NME (%)	-	15.35	26.08	2.13	2.83
Comparison of each alternate case against the Base case for <u>8-hour DFW O₃ sensitivity to DFW AVOC</u>					
RMS (ppb)	-	0.44	0.17	0.02	0.02
BIAS (ppb)	-	0.26	-0.08	-0.00	0.01
NMB (%)	-	63.35	-19.33	-0.80	1.88
NME (%)	-	63.45	21.90	2.04	2.14

Table 5.1 – Screening test for the selection of uncertain model structural assumptions.

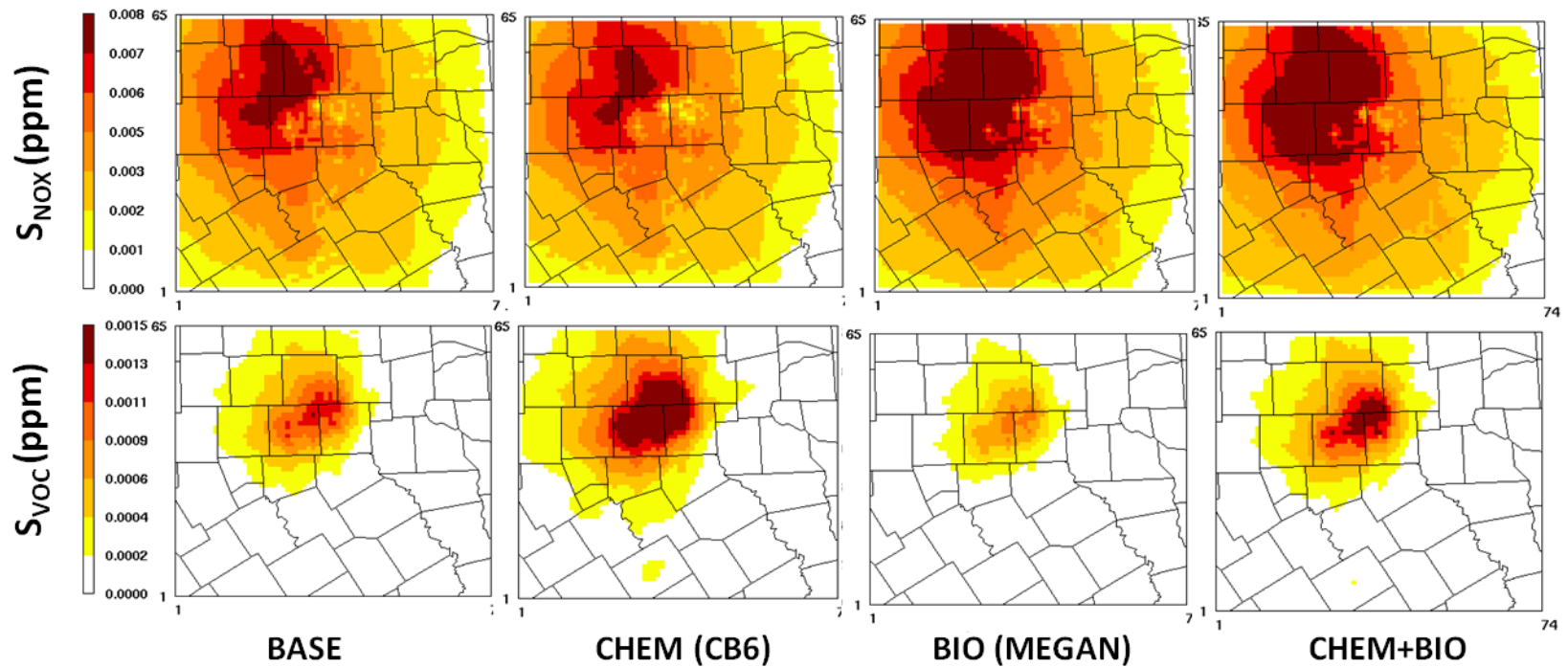


Figure 5.4 – Sensitivity of 8-hour O_3 to anthropogenic NO_x and VOC emissions from DFW for different structural model scenarios under default settings of input parameters. Episode average results are shown for the 4-km resolution domain.

5.4.1.2. Screening for Parametric Uncertainty

Uncertainties in input parameters (*parametric uncertainties*) are characterized by Monte Carlo analysis, where values of input parameters are selected randomly from the probability distribution assumed for each input based on their standard deviations. For computational efficiency we use a Reduced Form Model (RFM) to compute adjusted concentrations (C^*) and sensitivities ($S_j^{(1)*}$) based on the uncertainties in input parameters using the relationships given by *Cohan et al.*, [2005] and *Digar and Cohan* [2010],

$$C^* = C_0 + \sum_j \varphi_j S_j^{(1)} + \sum_k \varphi_k S_k^{(1)} + \frac{1}{2} \sum_j \varphi_j^2 S_{j,j}^{(2)} + \frac{1}{2} \sum_k \varphi_k^2 S_{k,k}^{(2)} + \sum_{j,k} \varphi_j \varphi_k S_{j,k}^{(2)} \quad (5.6)$$

$$S_j^{(1)*} = 1 + \varphi_j \left(S_j^{(1)} + \varphi_j S_j^{(1)} + \sum_k \varphi_k S_{j,k}^{(2)} \right) \quad (5.7)$$

where C_0 is the concentration modeled under default setting of the parameters, φ_j and φ_k are the perturbations in parameters 'j' and 'k' respectively. $S_j^{(1)} = \frac{\partial C}{\partial \varphi_j}$ and

$S_j^{(2)} = \frac{\partial^2 C}{\partial \varphi_j^2}$ denote semi-normalized first- and second-order sensitivities of

concentrations to the parameter 'j'. $S_{j,k}^{(2)} = \frac{\partial^2 C}{\partial \varphi_j \partial \varphi_k}$ denotes cross-sensitivity between

two input parameters 'j' and 'k'. In the RFMs, the value of each φ is restricted to

within a 2-sigma range for that parameter to avoid extreme values of input parameters.

As discussed in section 5.2.2, we use a suite of uncertain model input parameters listed in Table 5.2. Each parameter was assumed to have a lognormal probability distribution, characterized by the uncertainty value (1σ) reported in the table. To screen parameters that strongly influence O_3 concentration (C) and sensitivity to emission ($S^{(1)}$), we perform an impact analysis where relevant ‘impact factors’ were evaluated as follows,

$$\text{Impact Factor (IF) for the influence of parameter 'j' on 'C': } IF_C = \frac{\sigma S_j^{(1)}}{C} \quad (5.8)$$

$$\text{Impact Factor (IF) for the influence of parameter 'k' on } S_j^{(1)}: IF_S = \frac{\sigma S_{j,k}^{(2)}}{S_j^{(1)}} \quad (5.9)$$

Although there was considerable overlap in the selected parameters, there were also some differences in those found to have a greater impact on concentrations and the two sensitivities (Table 5.2). Domain-wide NO_x and biogenic VOC emissions (ENO_x and EBVOC), photolysis rates (hv), and the reaction rate constants R(NO₂+OH) and R(NO+O₃) significantly impacted all three categories. Meanwhile, boundary conditions (BC) of NO_y (= NO_x + HNO₃ + PAN + HONO + N₂O₅) were not major influences on any of the results. However, the BC(O₃) parameter significantly impacted concentrations and sensitivity to VOC but not to NO_x, whereas anthropogenic VOC emissions (EAVOC) impacted sensitivities but not concentrations.

Parameter ¹	Uncertainty ² (1 σ)	Reference	Impact ³ on O ₃ concentration	Impact ³ on O ₃ sensitivity to ANO _x	Impact ³ on O ₃ sensitivity to AVOC
Emission Rates:					
Domain-wide NO _x	0.336	Deguillaume, 2007	<u>0.105</u>	<u>-0.463</u>	<u>0.496</u>
Domain-wide biogenic VOC	0.405		<u>0.026</u>	<u>0.216</u>	<u>-0.319</u>
Domain-wide anthropogenic VOC	0.336		0.006	<u>0.073</u>	<u>-0.150</u>
Reaction Rate Constants:					
All photolysis frequencies	0.347	Hanna, 2001	<u>0.091</u>	<u>0.401</u>	<u>0.091</u>
R(OH+NO ₂)	0.131	Sander, 2006	<u>-0.017</u>	<u>-0.057</u>	<u>0.029</u>
R(NO+O ₃)	0.095	Hanna, 2001	<u>-0.023</u>	<u>-0.058</u>	<u>-0.024</u>
R(All VOCs+OH)	0.095	Deguillaume, 2007	0.003	<u>0.021</u>	<u>0.014</u>
Boundary Conditions:					
BC (O ₃)	0.203	Deguillaume, 2007	<u>0.036</u>	0.006	<u>-0.042</u>
BC (NO _x)	0.549		0.002	-0.001	-0.001
BC (HNO ₃)	0.549		0.001	-0.000	-0.000
BC (PAN)	0.549		0.008	-0.003	-0.002
BC (HONO)	0.549		0.000	-0.000	-0.000
BC (N ₂ O ₅)	0.549		0.000	-0.000	0.000

¹Parameters selected based on the impact analysis by *Digar and Cohan* [2010] and *Digar et al.* [2011];

²All distributions are assumed log-normal;

³*Impact factor*: The fractional change in concentrations and first-order sensitivity of ozone to emissions, due to a 1 σ change in an input parameter as detailed in Section 4.1.2.; Uncertainty factors based on $\pm 2\sigma$ (i.e., 95%) confidence interval.

Table 5.2 - Screening test for the selection of uncertain input parameters.

5.4.1.3. Joint consideration of structural and parametric uncertainty

We construct an ensemble consisting of the four targeted structural members based on the screening test in Table 5.1 (BASE, CHEM, BIO and CHEM+BIO) each coupled with 1000 Monte Carlo samplings from the probability distributions for the selected model input parameters underlined in Table 5.2. Total sample size of the final ensemble was therefore 4000. The final set of *parametric* factors considered in this study are summarized below,

For O₃ concentration: ENO_x, EBVOCs, photolysis frequencies, R(NO₂+OH), R(NO+O₃) and BC(O₃);

For O₃ sensitivity to anthropogenic NO_x emissions: ENO_x, EBVOCs, EAVOC, photolysis frequencies, R(NO₂+OH), R(NO+O₃), and R(all VOCs+OH);

For O₃ sensitivity to anthropogenic VOC emissions: ENO_x, EBVOCs, EAVOC, photolysis frequencies, R(NO₂+OH), R(NO+O₃), R(all VOCs+OH) and BC(O₃).

5.4.2. Constraining Model Predictions using Measurements

A key limitation of the traditional Monte Carlo analysis of the model ensemble [e.g. *Pinder et al.*, 2009; *Digar et al.*, 2011] is the assumption that each of the cases is equally likely. This study uses actual observations to prioritize cases that show good agreement with measured concentrations over those that do not perform well. Figure 5.5 shows the framework of the observation-constrained Monte Carlo analysis, where initially 4000 Monte Carlo simulations are conducted to

develop the *a priori* distribution of O₃ and NO_x concentrations at all the DFW monitors, where the prior probability of each simulation is assumed to be 1/4000. We then compare concentration estimates from each simulation with actual measurements at the monitors to evaluate the adjusted (*a posteriori*) probability distribution of the ensemble. Various techniques are used to weight (Bayesian) or screen (model performance and hypothesis testing) the best-performing model cases to construct adjusted (observation-constrained) posterior distributions. The methods and observation metrics used in this study are elaborated below.

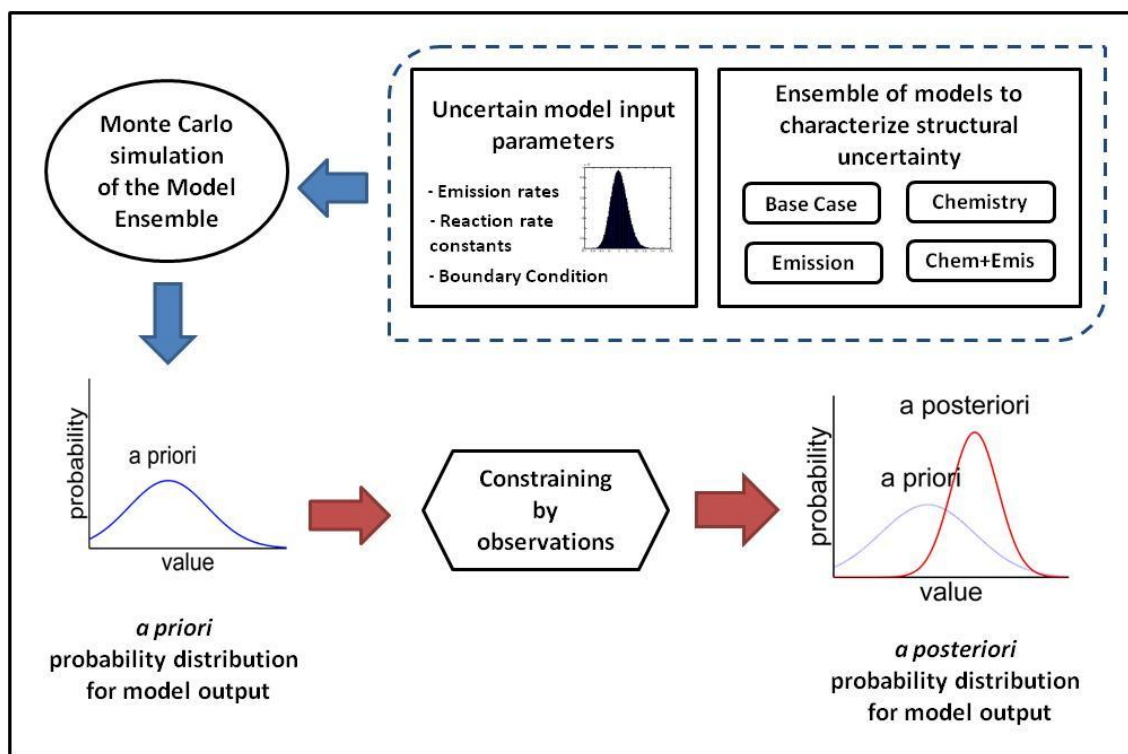


Figure 5.5 - Flowchart for the observation-constrained Monte Carlo analysis.

5.4.2.1. Metric 1 (M1): Bayesian Analysis

A Bayesian inference approach [Bergin and Milford, 2000; Deguillaume et al., 2007] is applied to assign relative weightings to each case based on its performance in simulating observed O_3 and NO_x . For evaluating the likelihood of model prediction ($C_{m,n}^*$) for the m^{th} simulation of the n^{th} observation ($n = 1, 2, \dots, N$, where N denotes total number of observations), a Gaussian likelihood function is used (as defined by Bergin and Milford, [2000]). Errors (θ) in the interpolated observed O_3 and NO_x concentrations at all monitor/days are assumed to be independent and normally distributed with mean zero. The likelihood of model prediction $C_{m,n}^*$ given observation O_n can be expressed as,

$$L(C_{m,n}^* | O_n) = \frac{1}{\theta\sqrt{2\pi}} \exp \left\{ -\frac{1}{2} \left[\frac{(O_n - C_{m,n}^*)^2}{\theta^2} \right] \right\} \quad (5.10a)$$

The total likelihood for all observations can then be computed by the product of likelihoods of individual simulations, that is,

$$L(C_m^* | O) = \frac{1}{\sqrt{2\pi}^N \prod_{n=1}^N \theta} \exp \left\{ -\frac{1}{2} \sum_{n=1}^N \left[\frac{(O_n - C_{m,n}^*)^2}{\theta^2} \right] \right\} \quad (5.10b)$$

$L(C_m^* | O)$ is computed for both O_3 and NO_x and are then multiplied together to get the overall likelihood based on both the observational constrains. Finally,

Bayes' theorem is applied to compute the *a posteriori* probability distribution (p') from the *a priori* probabilities ($p = 1/M$).

$$p'(C_m^* | O) = \frac{L(C_m^* | O)p(C_m^*)}{\sum_{m=1}^M L(C_m^* | O)p(C_m^*)} \quad (5.11)$$

The mean (μ') and standard deviation (σ') of the resulting posterior ensemble distribution can be computed by,

$$\mu' = \sum_{j=1}^M Y_j \times p'_j \quad (5.12)$$

$$\sigma' = \sqrt{\sum_{j=1}^M Y_j - \mu'^2 \times p'_j} \quad (5.13)$$

where Y_j denotes j^{th} value of the simulation and p'_j denotes the respective posterior probability for that iteration (obtained from eq 10) and M is the total size of the ensemble (= 4000).

An aggregated observation metric is used for the Bayesian analysis following the works of *Bergin and Milford* [2000], and *Deguillaume et al.* [2008]. Episode averages of the daily 8-hour O_3 and of the 24-hour NO_x concentrations at each of the 11 monitors were considered ($N = 11$). The consideration of episode-average concentrations on a site-by-site basis tests the ability of each model case to simulate overall levels and spatial patterns in O_3 and NO_x , even if errors in simulating meteorology or emissions variability may have obscured day-to-day comparisons.

Errors and uncertainty in applying measurement data to evaluate model results can arise from instrumental error and from the use of a point measurement to represent a model grid-cell average concentration. The resulting uncertainty can be quantified jointly by examining the variability between pollutant concentrations measured by multiple monitors within the same grid cell. Analysis using five years (centered on our base case model year 2006, i.e. 2004 – 2008) of data for the summer O₃ season (May to September) showed that the error (θ) characterizing the standard deviation of differences between observed 8-hour O₃ values at three pairs of sites falling in the same grid-location ranged from 3.0 to 7.2 ppb; for bias-corrected 24-hour NO_x observations, sigma ranged from 2.2 to 8.2 ppb. Since these estimates are based on a limited number of site pairs, to be conservative we choose the maximum values for sigma (i.e. $\theta = 7.2$ ppb and 8.2 ppb for 8-hour O₃ and 24-hour NO_x respectively).

5.4.2.2. Metric 2 (M2): Screening Based on Model Performance

An alternate approach to developing posterior distributions is to retain only cases that meet specified performance criteria [e.g. *Mallet et al.*, 2006]. Since the base modeling used here was developed for a SIP attainment plan, we formulate a new metric (M2) that screens the 4000 cases based on the three model performance evaluation criteria recommended by EPA [1999; 2007] for determining the acceptability of an O₃ SIP model (Table 5.3). This metric uses all available valid observations of daily 8-hour O₃ at each monitor ($N = 289$). To ensure meaningful results, Mean Normalized Bias (MNB) and Mean Normalized Gross Error (MNGE)

were computed for model results (Model) when O₃ observations (Obs) were greater than the recommended threshold of 60 ppb [USEPA, 2006b]. The screened cases were assigned equal weights to develop the *a posteriori* distribution.

Performance Statistics	Formula	Screening Criteria
Mean Normalized Gross Error (MNGE)	$\frac{1}{N} \sum_1^N \left(\frac{ \text{Model} - \text{Obs} }{\text{Obs}} \right) \times 100\%$	-5% < MNGE < +5%
Mean Normalized Bias (MNB)	$\frac{1}{N} \sum_1^N \left(\frac{\text{Model} - \text{Obs}}{\text{Obs}} \right) \times 100\%$	MNB < 30%
Unpaired Peak Accuracy (UPA)	$\frac{\text{Model}_{\max} - \text{Obs}_{\max}}{\text{Obs}_{\max}} \times 100\%$	-15% < UPA < +15%

Note: MNGE and MNB were computed for model results (Model) when O₃ observations (Obs) were greater than the recommended threshold of 60 ppb [USEPA, 2006b].

Table 5.3 – Statistics for evaluating model performance in Metric 2 [USEPA, 2006b].

5.4.2.3. Metric 3 (M3): Screening Based on Nonparametric Test

Statistical nonparametric tests of significance like the Cramér-von Mises criterion and the Kolmogorov-Smirnov test have been used in the past to test for general differences in predicted and observed distributions of air quality data [Holland and Fitz, 1982; Taylor, Simpson and Jakeman, 1987]. The Cramér-von Mises (CvM) criterion [Anderson, 1962] provides a non-parametric test of the null hypothesis (H₀) that two samples are drawn from the same (unspecified)

distribution. In the CvM two-samples test, the test statistics ‘T’ is computed as follows:

$$T = \frac{AB}{(A+B)^2} \left\{ \sum_{i=1}^A [F_A(x_i) - G_B(x_i)]^2 + \sum_{j=1}^B [F_A(y_j) - G_B(y_j)]^2 \right\} \quad (5.14a)$$

where $F_A(x)$ and $G_B(y)$ are the empirical distribution functions of the two samples $x = x_1, x_2, \dots, x_A$ and $y = y_1, y_2, \dots, y_B$ of size A and B respectively. Note that $G_B(x_i)$ denotes the relative frequency that the observed concentration is at most x_i (i.e. sum of all the elements in the sample less than x_i , divided by the sample size B) and $F_A(y_j)$ denotes the relative frequency that the modeled concentration is at most y_j . The null hypothesis is rejected when T is large, indicating that the two samples are significantly different. For our case, the two samples represent the modeled (x) and observed distribution (y) of pollutant concentrations, and the sample size for the two distributions are equal here (i.e. $A = B = N$, where N denotes total number of observations). Therefore, equation (5.14a) reduces to the form,

$$T = \frac{1}{4} \left\{ \sum_{i=1}^N [F_A(x_i) - G_B(x_i)]^2 + \sum_{j=1}^N [F_A(y_j) - G_B(y_j)]^2 \right\} \quad (5.14b)$$

The test statistic ‘T’ is computed for each of the 4000 members of the model ensemble, separately for available 8-hour O_3 ($N = 289$) and 24-hour NO_x ($N = 303$) concentrations using equation 5.14b. Next, we compute the p-value associated with each test statistic (T), defined as the probability of observing a test statistic greater

than or equal to T , if H_0 is true. A small T will result in a large p-value, indicating that there is NOT significant evidence to reject the null hypothesis (H_0). Screening is then applied to select Monte Carlo cases that generate p-values greater than the 10% significance level, i.e. $\alpha = 0.1$, below which we reject the null hypothesis. We select only those cases that satisfy this test for both of the observational constraints (O_3 and NO_x).

The advantage of this method is that it assesses whether there are any differences in the modeled and observed probability distributions, not just differences in the means of the two samples (e.g. differences in the variance and/or the tail of the samples). Thus a 'well-performing' ensemble will have a small T value, since this indicates that the ensemble prediction is truly consistent with the recorded observations. However, this metric (unlike the other two metrics) does not compare model predictions and ambient observations paired in space and time. Because future meteorology is unpredictable, actual wind fields may be different from model assumptions, which may result in slightly varying (both spatially and temporally) pollutant plume trajectory. Therefore, this metric provides a supplementary test to evaluate the model's ability to predict concentrations irrespective of its location (grid-cell against monitor) in the DFW nonattainment area defined by the 9 counties, and day during the one-month study episode.

5.4.3. Adjusted Ozone Sensitivity

To characterize adjusted O₃ response to emission changes, we use the Reduced Form Model (RFM) given in equation (5.7) to generate the *a priori* (equal-weighted) probability density of O₃ sensitivity to any emission ‘*j*’ for each of the 4 structural case based on the 1000 parametric distribution of input parameters *j* and *k* (= 1, 2, 3, ..., 1000). Since pollutant sensitivities cannot be directly evaluated, the observation-constrained O₃ sensitivities for the full ensemble (all 4000 cases) are estimated based on the model’s performance in reproducing observed concentrations. Therefore for Metric 1, we assume that the *a posteriori* probabilities estimated for O₃ concentrations by equation (5.11) can also be applied to adjust the *a priori* probability distribution of O₃ sensitivities; for Metrics 2 and 3, we select sensitivity values for the simulations that passed the screening test.

5.5. Results

In this section results for input parameter values, O₃ concentrations, and sensitivities to emissions are presented to show how the *a posteriori* probability distributions generated by application of the three observational metrics differ from the *a priori* (equal-weighted) distribution. The evaluation of the quality of the final three *a posteriori* model ensembles is provided in Appendix A.

Application of Metric 1 (Bayesian weightings) to our ensemble of 4000 simulations assigns half of the total weight to the 496 best-performing model

simulations. Most of the spread in weightings results from evaluation against O_3 observations rather than against NO_x observations (Figure 5.6); however, the multiplication of weightings by equation 5.10b leads the joint weightings to differ substantially from those that would have resulted from considering O_3 alone (Table 5.4).

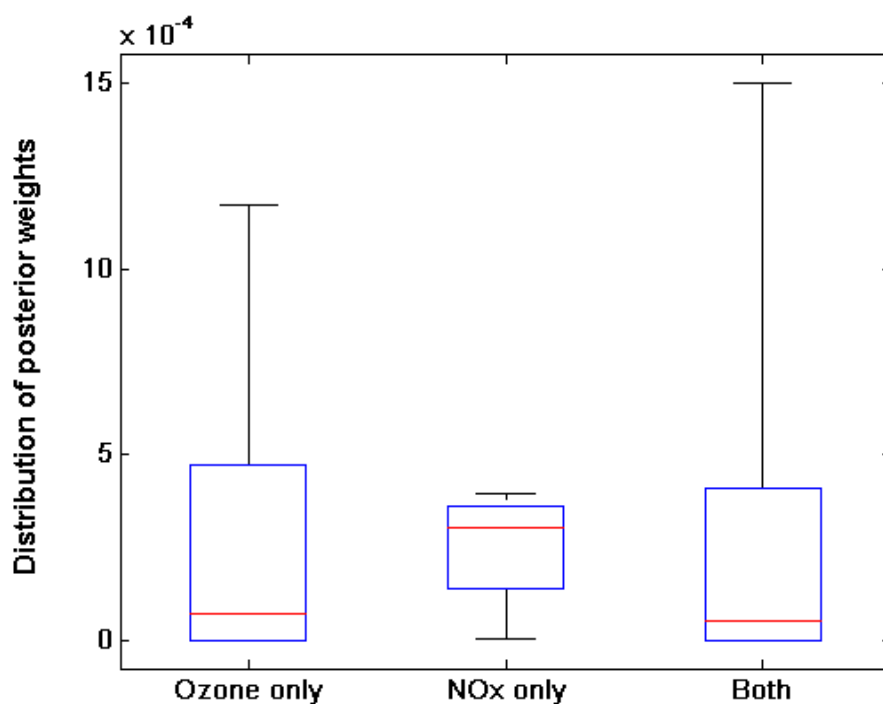


Figure 5.6 - Weights assigned to the 4000 members of the full ensemble under the Bayesian Metric 1 using only 8-hour O_3 , 24-hour NO_x and both (O_3 and NO_x) as the observational constraint.

Metrics	Method	Constrained by Measurements of	Base	CHEM	BIO	CHEM+BIO
Metric 1	Bayesian	O ₃ and NO _x	19.37%	35.37%	16.14%	29.12%
-	Bayesian	O ₃	25.68%	29.55%	21.66%	23.10%
-	Bayesian	NO _x	25.44%	24.73%	25.17%	24.66%
Metric 2	EPA Performance	O ₃	16.14%	33.69%	17.99%	32.19%
Metric 3	CvM Test	O ₃ and NO _x	12.92%	37.08%	16.97%	33.03%
-	CvM Test	O ₃	15.65%	34.60%	18.84%	30.91%
-	CvM Test	NO _x	25.32%	25.32%	24.70%	24.66%

Table 5.4 – Posterior probability of the structural ensemble members.

Metric 2 screened 1134 cases that satisfied all three of EPA’s recommended model performance criteria detailed in Table 5.3. This selection was mainly restricted by the bias term (MNB), which was satisfied by 1137 cases. The other two criteria, namely the Unpaired Peak Accuracy (UPA) and Mean Normalized Gross Error (MNGE), selected nearly all of the 4000 cases, rejecting only 15% and 1% of cases respectively. Metric 3, which selects cases based on the CvM two-sample test, selects only 766 model cases that satisfies the test for both O₃ and NO_x observations. Screening based on only O₃ or NO_x observations would have selected 1003 and 2457 cases, respectively.

Accuracy of the ensemble-mean prediction is tested by evaluating the normalized mean bias (NMB), the normalized mean error (NME), the correlation

and the regression coefficients of the ensemble mean with 8-hour O₃ observations for all site and days ($N = 289$) in the DFW region (Table 5.5). Figure 5.7 shows the difference between the ensemble mean and the observed 8-hour O₃ and 24-hour NO_x concentrations for all site/days in DFW.

Statistics	Base Case (deterministic)	Bayesian (Metric 1)	Non- Bayesian (Metric 2)	Non- Bayesian (Metric 3)
		<i>(a posteriori)</i>		
NMB (%)	-6.08	-0.690	4.52	1.03
NME (%)	17.74	15.76	15.84	15.73
Correlation	0.704	0.720	0.716	0.714
R Square	0.495	0.518	0.513	0.510

Table 5.5 – Performance of the posterior model ensemble-mean against 8-hour O₃ at all site and days in DFW.

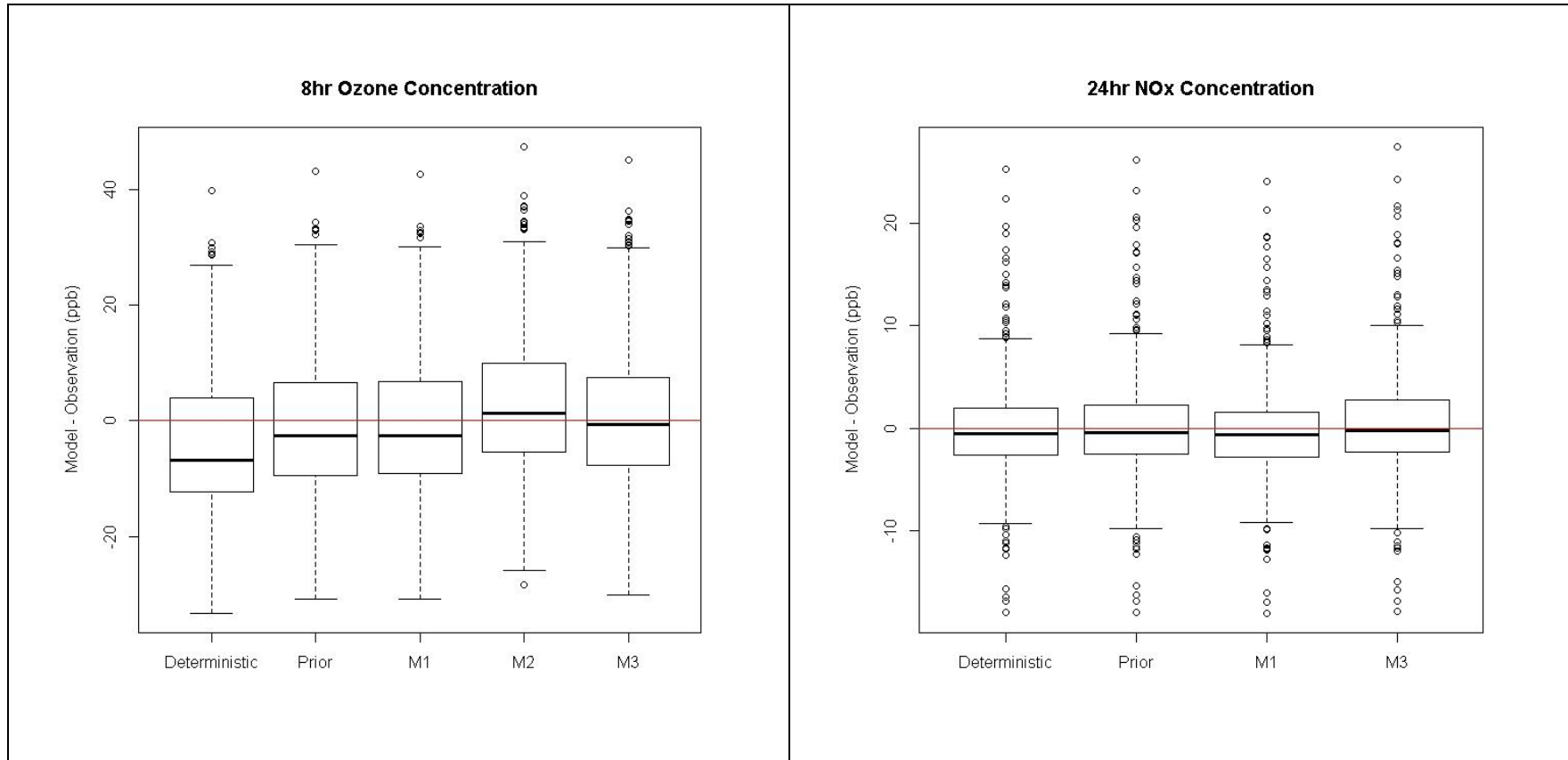


Figure 5.7 – Boxplot evaluating performance of model ensemble mean against 8-hour O₃ and 24-hour NO_x observations at each site-day within DFW.

As expected, the model performance improves when the ensemble is constrained based on the observations. All the observational metrics help to minimize the model bias and error, and to some extent increase the overall correlation and regression (Table 5.5). The base case model underpredicts O₃ concentrations by 6%. The non-Bayesian metrics on the other hand tend to slightly overpredict O₃, although they reduce the overall error by 11%.

To further evaluate the performance of the ensemble in simulating episode-average conditions (similar to the scenario used in Metric 1) at a given location, results for observation-constrained O₃ concentrations are probed for the Denton monitor (Table 5.6). This monitor recorded the highest 8-h O₃ design values (DVs) among all the DFW sites in 2006. Figure 5.8(a) shows the probability density functions (PDFs) of episode-average O₃ concentrations at Denton. The blue curve in the figure depicts the *a priori* (equal-weighted) probability density. The other solid curves show the final *a posteriori* distributions resulting from joint consideration of the full 4000 case ensemble under the 3 observational metrics. The deterministic model (BASE) is found to underpredict (62.0 ppb) the recorded episode-average daily 8-hour O₃ observation of 70.1 ppb at Denton during the study period. The *a priori* equal-weighted ensemble predicts a mean concentration of 65.5 ppb with a standard deviation of 7.3 ppb (Table 5.6). Application of each of the 3 metrics narrowed the spread of the ensemble predictions, as can be seen by the curves in Figure 5.8(a) and the smaller standard deviations in

Table 5.6, indicating greater confidence in the ensemble. Metric 2 and 3 yielded ensemble-mean predictions of episode-average O₃ that more closely matched observations at Denton. Similar trends were observed for the other sites in DFW as well (Appendix A).

However, to examine the applicability of this method for regulatory purposes, it is necessary to test whether these posterior ensembles are capable of successfully predicting concentrations at sites that has not been previously considered for constraining the prior ensemble. As such, the *a posteriori* ensembles are re-generated withholding Denton. In other words, we exclude observations from Denton and constrain the *a priori* results based on daily observations from the remaining 10 monitors. The posterior ensemble thus generated is then used to probe concentrations at the withheld monitor – Denton (Figure 5.8b). Comparable results suggest the reliability of this method for regulatory attainment demonstration at ambient monitors.

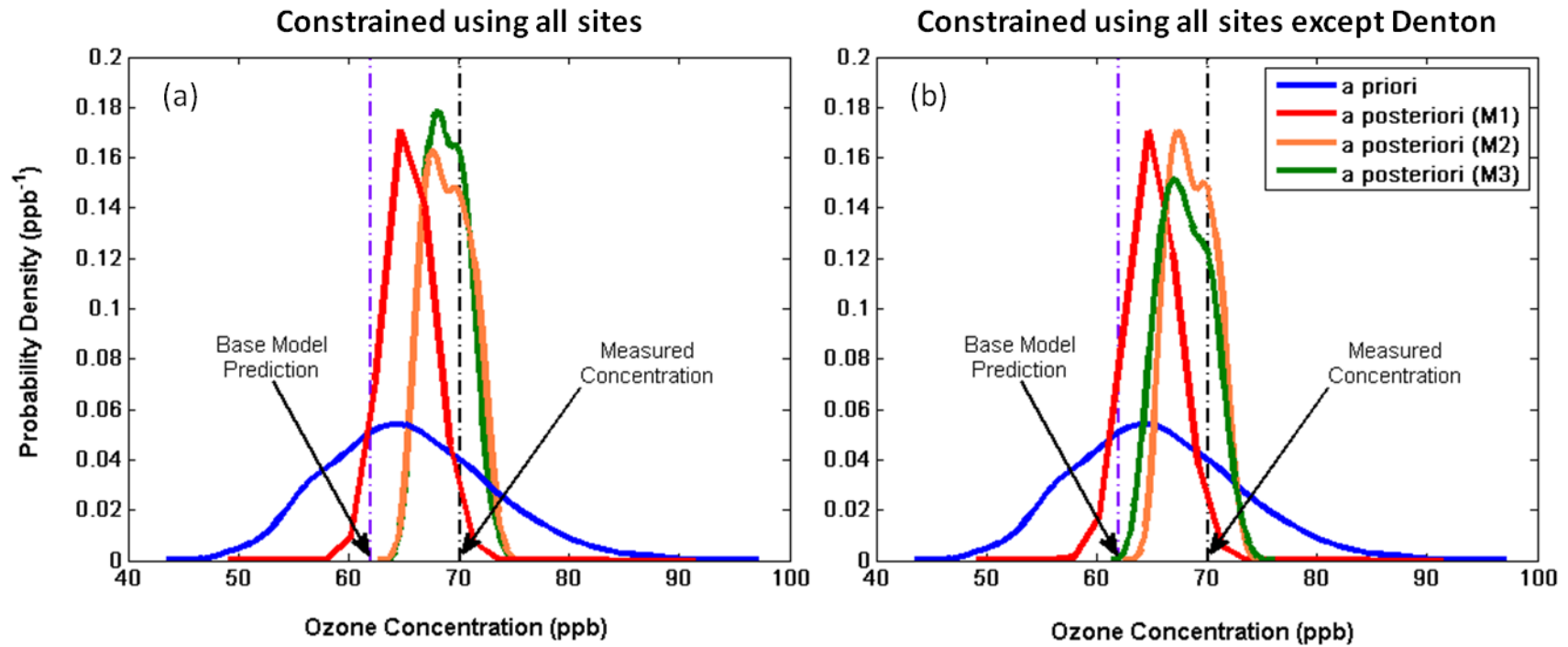


Figure 5.8 - PDFs for episode-average 8-hour ozone concentration at Denton (a) when observations from Denton were used to constrain the *a priori* results and (b) when observations from Denton were withheld.

Metric	O₃ Concentration (ppb) Obs = 70.11 ppb		S_{ANox} (ppb)		S_{AVOC} (ppb)	
	<i>a priori</i> ($\mu \pm \sigma$)	<i>a posteriori</i> ($\mu \pm \sigma$)	<i>a priori</i> ($\mu \pm \sigma$)	<i>a posteriori</i> ($\mu \pm \sigma$)	<i>a priori</i> ($\mu \pm \sigma$)	<i>a posteriori</i> ($\mu \pm \sigma$)
Metric 1	65.51 ± 7.33	65.53 ± 2.16	6.79 ± 2.59	6.98 ± 2.19	1.09 ± 0.81	1.03 ± 0.54
Metric 2		69.04 ± 2.03		6.67 ± 3.01		1.35 ± 0.74
Metric 3		68.85 ± 1.87		6.49 ± 2.83		1.28 ± 0.69

μ and σ denotes mean and standard deviation respectively.

Table 5.6 - Comparison of prior and posterior episode average 8-hour ozone concentrations and sensitivities at Denton.

Although each of these metrics uses different criteria and methods for comparing pollutant concentrations, they each yield similar allocation of posterior probabilities among the structural scenarios (Table 5.4). For the study region and episode, application of each metric tends to prioritize model cases that use the CB6 chemical mechanism. For example, under Metric 1, 384 of the 496 highest-weighted cases used CB6, lending to 64% of overall weight being placed on CHEM and CHEM+BIO scenarios (Table 5.4). The CHEM and CHEM+BIO scenarios were also favored relative to their CB-05 counterparts by Metrics 2 and 3. The metrics do not show a consistent preference between the MEGAN and GloBEIS biogenic inventories.

Application of the three metrics also generated *a posteriori* probability distributions for the scaling factors $(1+\phi)$ for the model input parameters listed in Table 5.2. Figure 5.9 shows the probability density functions (PDFs) for some of the key parameters. The *a priori* PDFs are derived from the 1000 Monte Carlo cases randomly sampled from the truncated lognormal probability distributions assumed for each input parameter, and the *a posteriori* PDFs are generated by applying the same weightings (Metric 1) and screenings (Metrics 2 and 3) used for constraining O₃ concentrations. No significant differences were observed in the *a priori* and *a posteriori* distributions of model input parameters, except for ENO_x. Adjustment under each metric tended to prefer higher levels of NO_x

emission, as indicated by the clear positive shift in the *a posteriori* PDFs, especially for Metrics 2 and 3.

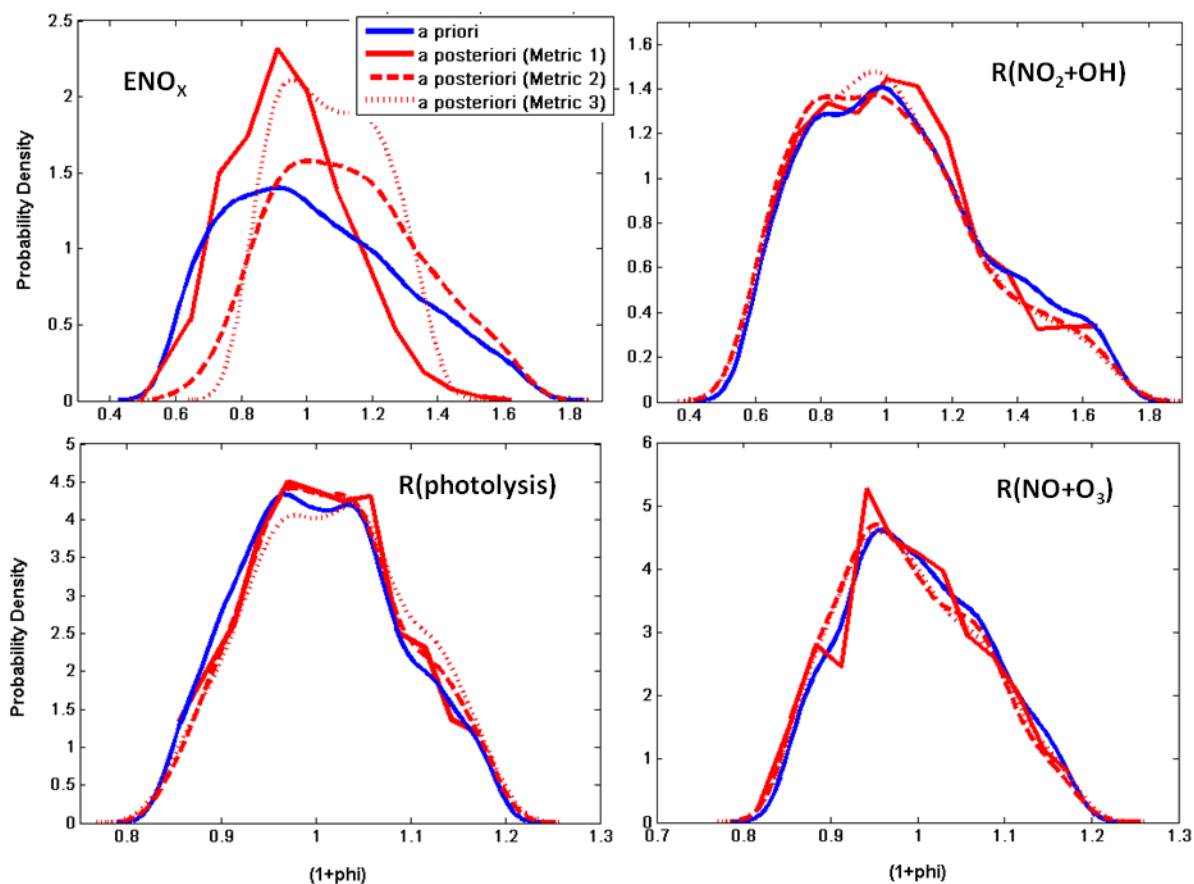


Figure 5.9 – Prior and posterior distributions of selected model input parameters.

Figure 5.10 shows results when O₃ and NO_x are used separately as observational constraints. Constraining the ensemble based only on O₃ observations favors higher levels of NO_x emission, since this helps correct the base model's tendency to underpredict O₃ concentrations during this episode

(Figure 5.10a). On the other hand, adjustments based on only NO_x observations reduce the spread in the NO_x emission scaling factors and favors cases near the original estimate, except for Metric 1 that slightly favor lower ENO_x (Figure 5.10b) to compensate for the extreme over-prediction of episode-average concentration at the Fort Worth Northwest (FWMC) monitor (Figure 5.11). This implies that the higher levels of NO_x emission in the combined results (Figure 5.9) is primarily due to model predictions being constrained based on O_3 observations.

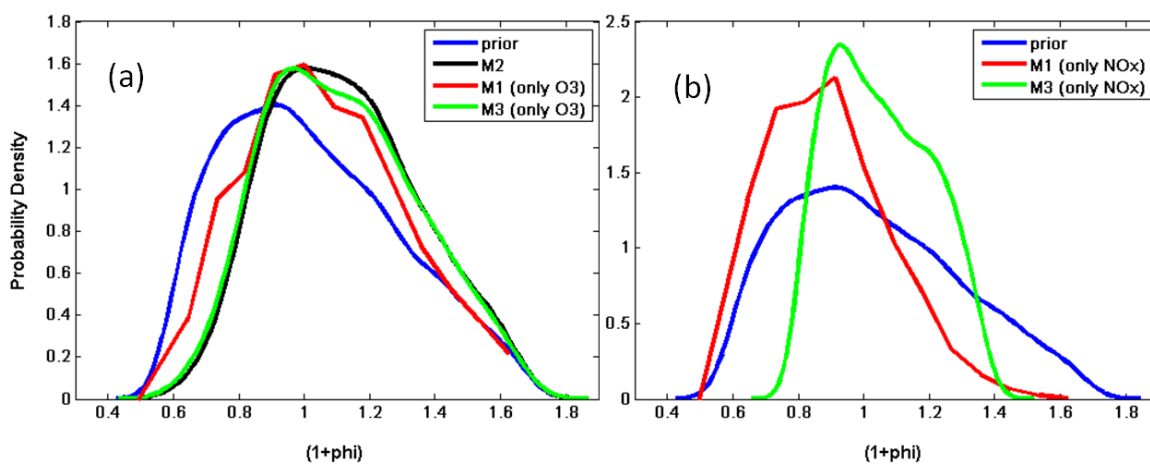


Figure 5.10 – Probability density function of NO_x emission scaling factor showing results when only O_3 (left) or only NO_x (right) are used as observation constraints.

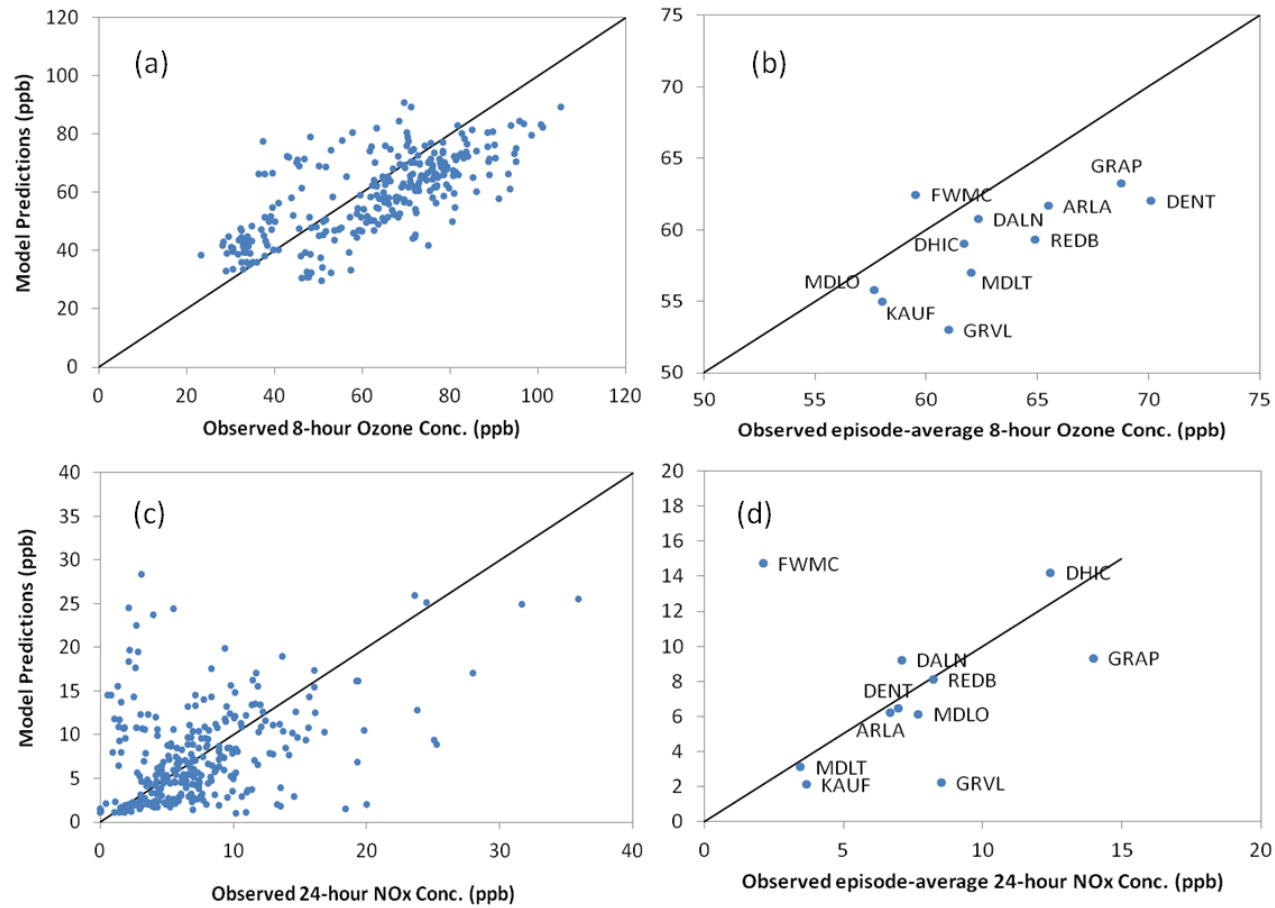


Figure 5.11 – Comparison of 8-hour O₃ (top) and 24-hour NO_x (bottom) predictions against daily observations at all sites (left) and episode-average concentrations at each site (right).

We now examine how the relative sensitivities of O_3 to NO_x (S_{NO_x}) and to VOC (S_{VOC}) change when the uncertainties in photochemical modeling are considered. The base case model (without incorporating uncertainties) predicts that at Denton, S_{NO_x} is 6.56 ppb and S_{VOC} is 0.83 ppb, indicating that ANO_x controls are approximately 7.9 times as effective per ton as $AVOC$ controls for reducing episode-average 8-hour O_3 concentrations (Figure 5.12). The equal-weighted *a priori* ensemble yields a distribution of O_3 sensitivity results and indicates 93% likelihood that O_3 is more sensitive to ANO_x than to $AVOC$, and a 2.3% chance that reducing local ANO_x emission may actually increase O_3 concentrations in the region. A sharp negative correlation is observed between O_3 sensitivities to NO_x and VOC, which leads to a large variability in the ratio of these two sensitivities. This reflects the tendency of changes in model inputs to push the O_3 formation regime towards being more NO_x -limited or more VOC-limited, and hence less sensitive to the other precursor.

The observational metrics also yield *a posteriori* distributions of O_3 sensitivity to ANO_x and $AVOC$ emissions. Metric 1 narrows the spread in the sensitivity predictions but does not substantially change the mean estimate (Figure 5.13 and Table 5.6). However, applications of Metric 2 and 3 shift O_3 sensitivity toward slightly higher S_{VOC} and slightly lower S_{NO_x} than in the equal-weighted ensemble (Figure 5.13 and Table 5.6). This is also seen in the

shift toward lower values of $S_{NO_x} : S_{VOC}$ under Metrics 2 and 3, even as predictions remain primarily NO_x -limited (Figure 5.13). This is because most of the cases accepted by the Metric 2 and 3 screenings used the alternate (CB6) chemical mechanism and higher NO_x emissions (Table 5.4 and Figure 5.9), each of which makes O_3 slightly more sensitive to VOC compared to NO_x (Figure 5.3 and Figure 5.4). Metric 1 favored cases with CB6 (Table 5.4) but gave low weightings to cases with high NO_x emissions (Figure 5.9).

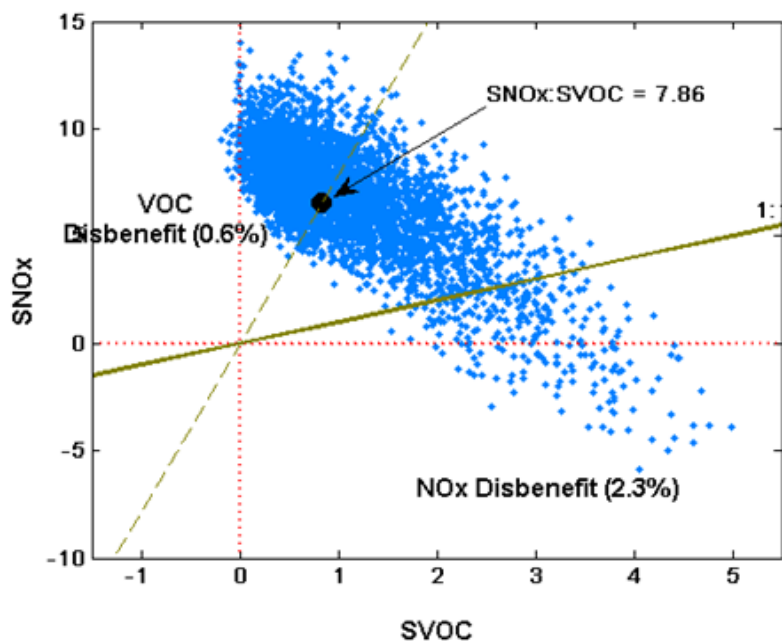


Figure 5.12 - *A priori* episode-average 8-hour ozone sensitivity results at Denton.

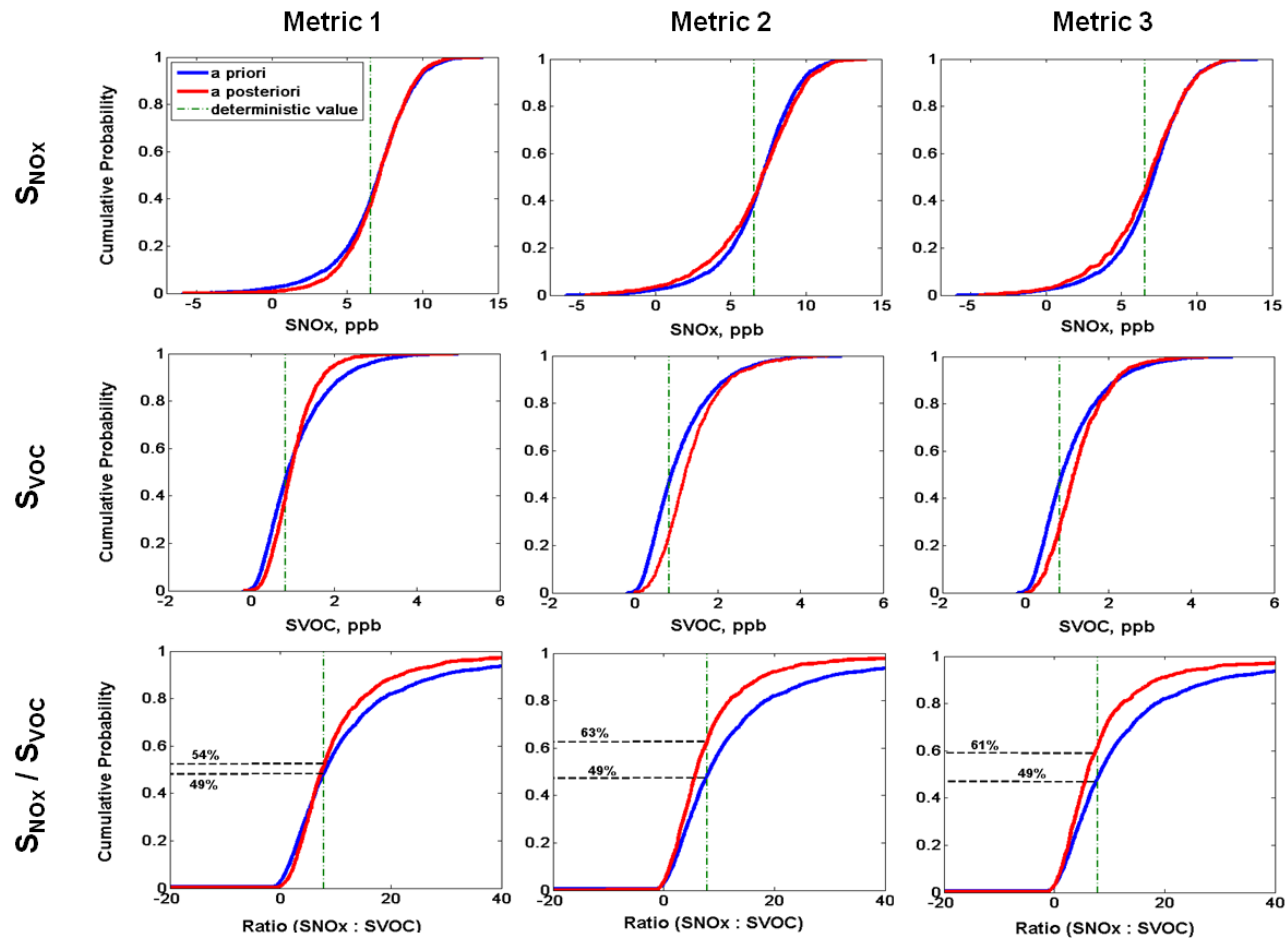


Figure 5.13 - CDFs for the sensitivity of ozone at Denton monitor for the three metrics. Results are averaged over all days of the episode.

5.6. Discussion

In this study, measurements of O₃ and NO_x have been used to adjust model estimates of O₃ concentrations and responsiveness to NO_x and VOC emission changes in the Dallas-Fort Worth (DFW) region. Three distinct observation-based approaches have been applied to weight or screen an ensemble of model simulations that employ alternate model assumptions (*structural uncertainty*) and model input values (*parametric uncertainty*).

Screening analysis of *structural* uncertainties led to a focus on scenarios involving alternate choices for the biogenic emissions model and chemical mechanism. For *parametric* uncertainties, impact analysis identified the specific emission rates, reaction rate constants, and boundary conditions that most influence O₃ concentrations and their sensitivities to NO_x and VOC emissions. Some parameters such as O₃ boundary conditions were found to impact concentrations far more strongly than sensitivities, whereas the converse was true for some other parameters such as anthropogenic VOC emissions.

Deterministic use of a single model formulation with a single set of input parameters yields a false sense of precision that the air quality impacts of emission controls are perfectly known. Traditional Monte Carlo analysis of uncertain inputs or model ensembles yields probabilistic (*a priori*) estimates of model outputs, but naively assumes that each of the scenarios is equally likely. This paper has explored three of the many Bayesian and non-Bayesian approaches that could be used to

adjust these *a priori* estimates by evaluating each case against observations. All three metrics tend to favor the CB6 chemical mechanism for this region and episode, and two of the metrics favor scaling up NO_x emission rates. This resulted in enhanced O₃ responsiveness to VOC emission and dampened sensitivity to NO_x, although the region still remained predominantly NO_x-limited.

A key assumption of this study is that performance of a model case against observed concentrations provides an indicator for the reliability of the input choices and of the output sensitivity predictions associated with case. Since ambient monitors observe concentrations but not sensitivities, that assumption is both necessary and yet unverifiable. Dynamic evaluation of how pollutant concentrations respond to emission changes over weekly (i.e., weekday vs weekend) or inter-annual (e.g., before and after a major emission trend) time scales can provide a proxy for ground-truthing sensitivity estimates [Dennis *et al.*, 2010; Gilliland *et al.*, 2008; Pierce *et al.*, 2010].

The Bayesian analysis considered in Metric 1 multiplies together individual likelihoods from each simulation. Multiplying a large set of data with small likelihood values may favor cases that slightly outperform the rest. This restricted us from considering likelihood based on all the site/days; instead we focused on only average concentrations over the episode to lower the sample size over which the product of likelihoods is computed. This helped to yield a broader distribution of posterior weights, but failed to capitalize upon the spatial and temporal resolution

of the available data. Further research is needed to refine the choice of Bayesian likelihood metric.

Future work could consider observations taken aloft by aircraft, sondes and satellites. Other model constraining methods like Bayesian Model Averaging [Raftery *et al.*, 2005] may be explored to consider both errors in model as well as measurements. Additional structural uncertainties such as use of alternate meteorological inputs or model formulations could expand the ensemble considered here, which tended to be underdispersive in predicting day-to-day variability in O₃ concentrations [Cohan *et. al.*, 2011].

Chapter 6

Conclusion

This thesis presents computationally efficient methods to probabilistically estimate responses of secondary pollutants to emission controls acknowledging that regulatory air quality models are uncertain. This chapter summarizes major findings and presents recommendations for future work.

6.1. Major Findings and Contribution

6.1.1. Key factors influencing ozone-precursor responsiveness

This research characterizes how uncertain assumptions in model formulations (*structural uncertainty*) and input parameters (*parametric uncertainty*) influence predictions of nonlinear responsiveness of O₃ to its precursor controls. Two separate studies focusing on the 8-hour O₃ non-attainment regions in Georgia and Texas showed that among the model input parameters that are reported to be uncertain in

existing literatures, NO_x and biogenic VOC emission rates, photolysis frequencies and the reaction rate constants $R(\text{NO}_2+\text{OH})$ and $R(\text{NO}+\text{O}_3)$ were found to be the leading contributors to uncertainty in O_3 concentration and sensitivity to anthropogenic NO_x and VOC emissions. Interestingly, anthropogenic VOC emissions only impacted sensitivities but not concentrations, and boundary conditions of O_3 impacted O_3 concentrations and sensitivity to man-made VOCs much significantly compared to O_3 sensitivity to anthropogenic NO_x emissions.

6.1.2. Computationally efficient characterization of model uncertainties

Characterization of air quality model uncertainty for regulatory attainment demonstration is computationally challenging. To greatly reduce the computational burden of formal model uncertainty analysis, this thesis contributes two Reduced Form Models (RFMs) that efficiently characterize the impact of uncertainties in model input parameters on O_3 response to precursor emissions within a single base model run. These two RFMs were targeted specifically for 'fixed' (analogous to installing a device at a point source) and 'flexible' (corresponding to percentage changes in area or mobile sources) amounts of emission reductions. The accuracy and applicability of these RFMs has been tested by validating their results against the underlying photochemical model. The RFMs proved to be extremely accurate in predicting O_3 and PM (sulfate and ammonium) response to large amounts of emission reductions (50% from area-sources and 85%, 99.8% from point-sources) in the presence of model uncertainties. For all test cases, extremely low bias (<10%) and error (<15%), and high regression coefficients (>99%) were observed,

indicating high confidence in the RFM's performance in reproducing results similar to that of the underlying model.

6.1.3. Probabilistic framework for ozone attainment

Chapter 2 demonstrates how Monte Carlo analysis of these validated RFMs could reliably predict the likelihood that an emission control measure will yield regulatory attainment considering models to be uncertain. Application of this method to 8-hour O₃ non-attainment regions in Georgia shows that under uncertain conditions, the ranking of the predicted effectiveness of control strategies may differ between *probabilistic* (considering model uncertainties) and *deterministic* (neglecting model uncertainties) analyses.

The framework is expanded to incorporate both model and epidemiological uncertainties to study how control measures could benefit public health. A case-study for assessing averted premature mortalities due to short-term O₃ exposure in the Dallas-Fort Worth (DFW) region shows that uncertainty in photochemical modeling greatly influences health-based prioritization of O₃ control options. The effectiveness of control measures is also found to vary with the duration of O₃ exposure (1-hour / 8-hours / 24-hours).

Irrespective of the basis of air pollution control evaluation (i.e. regulatory attainment or health benefits), the probabilistic approach enables more confident selection of control strategies by considering uncertainties in air quality model inputs. This probabilistic approach is further extended to incorporate the effect of

uncertainties in model formulations on O₃-precursor response predictions. A model ensemble with varying *structural* and *parametric* assumptions is simulated using an observation-constrained Monte Carlo technique to generate probabilistic distributions of pollutant concentrations and sensitivities at each monitor in the DFW region. Realizing that air quality impacts of emission controls cannot be directly evaluated, we assume that the model simulations that are capable of replicating observed concentrations can be used to adjust sensitivities and input parameter values as well. Hence, each concentration value in the resulting distribution is evaluated against observations, and the 'best-performing' simulations are used to constrain model inputs and pollutant response to emission reductions. This method of constraining model results based on observations generated *a posteriori* distributions with smaller standard deviations indicating precise prediction with greater confidence in the ensemble. This type of probabilistic evaluation of pollutant-precursor responsiveness can serve as a supplementary test to the deterministic approach used for developing secondary air pollutant control strategies.

6.2. Recommendations for Future Research

Our contributions of air quality model uncertainty analysis in this thesis open potential avenues for further research.

6.2.1. Additional Uncertainties

Future meteorology is unknowable and therefore prediction of future air quality involves great uncertainties that need to be explored for reliable control strategy development. This thesis presents methods to jointly consider *parametric* and *structural* uncertainties in photochemical modeling for regulatory attainment demonstration. Analysis of uncertain scenarios beyond the ones considered here, such as using alternate meteorological models, and uncertain meteorological inputs (like wind speed, sea breeze circulation, ambient temperature, rainfall, cloud cover, boundary layer height, etc.), could be explored. Chapter 3 employs a simple way to investigate the effect of hypothetical meteorological uncertainties on the likelihood of NAAQS attainment. Other creative and more comprehensive approaches such as dynamic evaluation of models [Dennis *et al.*, 2010; Gilliland *et al.*, 2008; Pierce *et al.*, 2010] studying the model's ability to predict air quality changes as a result of changing emission sources over temporally varying meteorological episodes could also be explored in the future. The sensitivity results obtained from these dynamic model evaluations could be used as alternative basis for constraining model simulations.

6.2.2. Observation-constrained Model Predictions

In this research, we use ground-based measurements of O₃ and NO_x concentrations to constrain model simulations. Observations recorded at higher altitudes (ozonesonde and aircraft) and in space (satellite) could be used in the

future to adjust model predictions. Moreover, the *a posteriori* estimates of emission inputs obtained from our study could be compared with the adjusted emission inventory based on model inversion techniques like Kalman Filter and adjoint methods.

6.2.3. Economic Evaluation for Control Strategy Selection

Regulatory attainment for ground-level O₃ is a headache for many states. With the enforcement of more stringent federal standards, development of cost-effective O₃ abatement will remain to be an intriguing field of research. This thesis demonstrates how the ratio of O₃ control effectiveness varies with uncertainty in regulatory modeling. These results could be considered jointly with the cost of these controls to optimally choose the most cost-effective option. In addition, uncertainty in control costs could also be considered for such analysis.

6.2.4. Applicability

Although our research primarily focuses on ground-level O₃ pollution, the methods and models presented here could be readily applied to other secondary pollutants as well, because the RFMs can successfully predict the non-linearity in pollutant-precursor responsiveness. In Chapter 2, we show that the RFM is capable of accurately characterizing parametric uncertainty for inorganic PM (sulfate and ammonium) responsiveness to changes in SO₂ emissions. The sensitivity coefficients that the RFM uses may be computed by HDDM or by brute force method. Also we found that second-order approximation of the Taylor expansion was sufficient for

representing O₃ and inorganic PM responses to emission changes, and assumed the impacts of multiple emission controls to be additive. One could also validate and if needed adjust the RFM accordingly for other pollutants depending on the capability of the underlying model.

The regions for our O₃ case-analysis were primarily NO_x-sensitive. Photochemical uncertainty analysis in regions with a mix of NO_x- and VOC-limited conditions may yield insightful results on how pollutant responses change with drastically different O₃-formation regimes. Since we were studying O₃ sensitivities, we purposefully looked at summer episodes, as O₃ is observed to be high during this season. O₃ tends to be more VOC-limited in other seasons and on non-peak days with lower biogenic VOCs. It will be interesting to extend this study for other seasons as well to see how the O₃-precursor responsiveness changes over temporal scales. Moreover, to address PM pollution, it might be meaningful to consider winter conditions.

6.2.5. Valuable Extension

The ranking of O₃ controls based on the likelihood of NAAQS attainment in Chapter 2 only considers model *parametric* uncertainties. It would be interesting to know how these rankings might change as a result of inclusion of *structural* uncertainties highlighted in Chapter 5 and beyond.

Findings from Chapter 4 show that the propensity of O₃ controls to save human lives (avert mortality) vary with the duration of exposure. This demands

further epidemiological research to understand which temporal metric (1-hour, 8-hours or 24-hours) is most determinative of human health responses to O₃ exposure.

6.3. Closing Remarks

To conclude, my PhD research presents a promising approach to efficiently characterize uncertainties in regulatory air quality planning and management, with particular focus on the mitigation of ground-level O₃ pollution. Results from this work provide important insights on the prioritization of O₃ abatement efforts in urban regions of Georgia and Texas, where elevated O₃ concentrations still remain to be an issue of grave concern. These methods could be readily applied for other regions and for other pollutants as well.

References

- Abt Associates Inc., (2005), BenMAP environmental benefits mapping and analysis program user's manual, *Prepared for U.S. EPA. Available at www.epa.gov/ttn/ecas/benmodels.html.*
- Anderson, T. W. (1962), On the distribution of the two-sample Cramer-von Mises criterion, *The Annals of Mathematical Statistics*, 33, 1148-1159.
- Anderson, G. B., and M. L. Bell (2008), Does one size fit all? The suitability of standard ozone exposure metric conversion ratios and implications for epidemiology, *J Expos Sci Environ Epidemiol*, 20(1), 2-11.
- Associates, E. H. P. (2005), AirControlNET version 4.1 development report. Prepared for U.S. EPA.
- Beekmann, M., and C. Derognat (2003), Monte Carlo uncertainty analysis of a regional-scale transport chemistry model constrained by measurements from the atmospheric pollution over the Paris area (ESQUIF) campaign, *J. Geophys. Res.*, 108.
- Bell, M. L., et al. (2004), Ozone and short-term mortality in 95 US urban communities, 1987-2000, *Journal of the Air & Waste Management Association*, 292(19), 2372-2378.
- Bell, M. L., et al. (2005a), A Meta-Analysis of Time-Series Studies of Ozone and Mortality With Comparison to the National Morbidity, Mortality, and Air Pollution Study, *Epidemiology*, 16(4), 436-445.
- Bell, M. L., et al. (2005b), Metric matter: Conflicting air quality rankings from different indices of air pollution., *Journal of the Air & Waste Management Association*, 55, 97-106.
- Bell, M. L., et al. (2006), The exposure-response curve for ozone and risk of mortality and the adequacy of current ozone regulations., *Environmental Health Perspective*, 114(4), 532-536.
- Bell, M. L., et al. (2007), Climate change, ambient ozone, and health in 50 U.S. cities., *Climate Change*, 82(1-2), 61-76.
- Bergin, M. S., et al. (1999), Formal uncertainty analysis of a Lagrangian photochemical air pollution model, *Environmental Science & Technology*, 33(7), 1116-1126.
- Bergin, M. S., and J. B. Milford (2000), Application of Bayesian Monte Carlo analysis to a Lagrangian photochemical air quality model, *Atmospheric Environment*, 34(5), 781-792.
- Bey I. et al. (2001), Global modeling of tropospheric chemistry with assimilated meteorology: Model description and evaluation, *J. Geophys. Res.*, 106, 23, 073-23, 096.
- Boylan, J. W., et al. (2006), 8-hour ozone and PM_{2.5} modeling to support the Georgia SIP, paper presented at Proceedings of the Air & Waste Management Association's Annual Conference and Exhibition.
- Brasseur, G. P., et al. (1998), MOZART, a global chemical transport model for ozone and related chemical tracers 1. Model description, *J. Geophys. Res.*, 103(D21), 28265-28289.
- Breiman, L., et al. (1984), *Classification and Regression Trees.*, Wadsworth and BrooksCole. , Belmont, CA.
- Brunekreef, B., and S. T. Holgate (2002), Air pollution and health, *Lancet*, 360(9341), 1233-1242.

- Byun, D. W., and K. L. Schere (2006), Review of the governing equations, computational algorithms, and other components of the Models-3 Community Multiscale Air Quality (CMAQ) modeling system, *Applied Mechanics Review*, 59, 51-77.
- Carlton, A. G., and K. R. Baker (2011), Photochemical Modeling of the Ozark Isoprene Volcano: MEGAN, BEIS, and Their Impacts on Air Quality Predictions, *Environmental Science & Technology*, 45(10), 4438-4445.
- Chang, J. S., et al. (1987), A Three-Dimensional Eulerian Acid Deposition Model: Physical Concepts and Formulation, *J. Geophys. Res.*, 92(D12), 14681-14700.
- Chestnut, L. G., et al. (2006), Cost-benefit analysis in the selection of efficient multipollutant strategies., *Journal of the Air & Waste Management Association*, 56(4), 530-536.
- Cohan, D., et al. (2006), Control strategy optimization for attainment and exposure mitigation: Case study for ozone in Macon, Georgia, *Environmental Management*, 38(3), 451-462.
- Cohan, D., et al. (2007), An integrated framework for multipollutant air quality management and Its application in Georgia, *Environmental Management*, 40(4), 545-554.
- Cohan, D., et al. (2010), Influence of uncertain reaction rates on ozone sensitivity to emissions in Houston, *Atmospheric Environment*, 44(26), 3101-3109.
- Cohan, D. S., et al. (2005), Nonlinear response of ozone to emissions: Source apportionment and sensitivity analysis, *Environmental Science & Technology*, 39(17), 6739-6748.
- Cohan, D. S., et al. (2011), Factors influencing ozone-precursor response in Texas attainment modeling, Final Report, Texas Air Quality Research Program, Project 10-008.
- Collins, W. J., et al. (1997), Tropospheric Ozone in a Global-Scale Three-Dimensional Lagrangian Model and Its Response to NO_x Emission Controls, *Journal of Atmospheric Chemistry*, 26(3), 223-274.
- Cox, W. M., and S.-H. Chu (1993), Meteorologically adjusted ozone trends in urban areas: A probabilistic approach, *Atmospheric Environment. Part B. Urban Atmosphere*, 27(4), 425-434.
- D'Ottone, L., et al. (2005), Kinetic and mechanistic studies of the recombination of OH with NO₂: Vibrational deactivation, isotopic scrambling and product isomer branching ratios, *Faraday Discussions*, 130, 111-123.
- Deguillaume, L., et al. (2007), Bayesian Monte Carlo analysis applied to regional-scale inverse emission modeling for reactive trace gases, *J. Geophys. Res.*, 112.
- Deguillaume, L., et al. (2008), Uncertainty evaluation of ozone production and its sensitivity to emission changes over the Ile-de-France region during summer periods, *J. Geophys. Res.*, 113.
- Demerjian K. L. (2000), A review of national monitoring networks in North America, *Atmospheric Environment*, 34, 1861-1884.
- Dennis, R., et al. (2010), A framework for evaluating regional-scale numerical photochemical modeling systems, *Environ. Fluid Mech.*, 10(4), 471-489.
- Derwent, R. G., and T. J. Davies (1994), Modelling the impact of NO_x or hydrocarbon control on photochemical ozone in Europe, *Atmospheric Environment*, 28(12), 2039-2052.
- Digar, A., and D. S. Cohan (2010), Efficient characterization of pollutant-emission response under parametric uncertainty, *Environmental Science & Technology*, 44(17), 6724-6730.

- Digar, A., et al. (2011), Likelihood of achieving air quality targets under model uncertainties., *Environmental Science & Technology*, 45(1), 189-196.
- Dockery D. W. and Pope III C. A. (1994), Acute respiratory effects of particulate air pollution, *Annu. Rev. Public Health*, 15, 107-32.
- Dudhia, J. (1993), A Nonhydrostatic Version of the Penn Stateâ€“NCAR Mesoscale Model: Validation Tests and Simulation of an Atlantic Cyclone and Cold Front, *Monthly Weather Review*, 121(5), 1493-1513.
- Dunker, A. M. (1981), Efficient calculation of sensitivity coefficients for complex atmospheric models, *Atmospheric Environment (1967)*, 15(7), 1155-1161.
- Dunker, A. M. (1984), The decoupled direct method for calculating sensitivity coefficients in chemical kinetics, *J. Chem. Phys.*, 81(5), 2385-2393.
- Dunker, A. M., et al. (2002), The Decoupled Direct Method for Sensitivity Analysis in a Three-Dimensional Air Quality Model Implementation, Accuracy, and Efficiency, *Environmental Science & Technology*, 36(13), 2965-2976.
- Dunlea E. J. et al. (2007), Evaluation of nitrogen dioxide chemiluminescence monitors in a polluted urban environment, *Atmos. Chem. Phys.*, 7 (10), 2691-2704.
- Emery, C., et al. (2009), MM5 Meteorological Modeling of Texas for June 2006. Final Report prepared for Texas Commission on Environmental Quality.
- ENVIRON (2007), User's Guide to Emissions Processor, Version 3. , ENVIRON International Corporation., Novato, CA.
- ENVIRON (2008), Boundary Conditions and Fire Emissions Modeling, Final Report to the Texas Commission on Environmental Quality (TCEQ). ENVIRON International Corporation., Novato, CA.
- ENVIRON (2010), User's Guide - Comprehensive Air-Quality Model with Extensions, Version 5.30., ENVIRON International Corporation, Novato, CA.
- European Environmental Agency (2011), Air Quality in Europe, Technical report No. 12/201.
- Feng, Z., and K. Kobayashi (2009), Assessing the impacts of current and future concentrations of surface ozone on crop yield with meta-analysis, *Atmospheric Environment*, 43(8), 1510-1519.
- Fine, J., et al. (2003), Evaluating uncertainties in regional photochemical air quality modeling *Annual Review of Environment and Resources*, 28(1), 59.
- Fine, P. M., et al. (2008), Secondary particulate matter in the United States: Insights from the particulate matter supersites program and related studies, *Journal of the Air & Waste Management Association*, 58(2), 234-253.
- Finlayson-Pitts, B. J., and N. Pitts (1993), VOCs, NO_x and ozone production., *Journal of the Air & Waste Management Association*, 43, 1093-1101.
- Frost, G. J., et al. (2006), Effect of changing power plant NO_x emissions on ozone in the eastern United States: Proof of concept, *Journal of Geophysical Research*, 111.
- Fuhrer, J. (2002), Ozone impacts on vegetation, *Ozone-Science & Engineering*, 24(1), 69-74.
- Gao, D., et al. (1996), Global uncertainty analysis of a regional-scale gas-phase chemical mechanism, *J. Geophys. Res.*, 101.
- Georgia Department of Natural Resources, E. P. D., Air Protection Branch (2009), Proposed Georgia's State Implementation Plan for the Atlanta 8-Hour ozone nonattainment area.

- Gery, M. W., et al. (1989), A photochemical kinetics mechanism for urban and regional scale computer modeling *J. Geophys. Res.*, 94.
- Gilliland, A. B., et al. (2008), Dynamic evaluation of regional air quality models: Assessing changes in O₃ stemming from changes in emissions and meteorology, *Atmos Environ*, 42(20), 5110-5123.
- Godowitch, J. M., et al. (2008), Modeling assessment of point source NO_x emission reductions on ozone air quality in the eastern United States, *Atmospheric Environment*, 42(1), 87-100.
- Grantz D. A., Garner J. H. B., and Johnson, D. W. (2003), Ecological effects of particulate matter, *Environment International*, 29 (2-3), 213-239.
- Grell, G. A., et al. (1994), A description of the fifth-generation Penn State/NCAR mesoscale model (MM5).
- Guenther, A., et al. (1995), A global model of natural volatile organic compound emissions, *J. Geophys. Res.*, 100 (D5), 8873-8892.
- Guenther, A., et al. (2000), Natural emissions of non-methane volatile organic compounds, carbon monoxide, and oxides of nitrogen from North America, *Atmospheric Environment*, 34(12-14), 2205-2230.
- Guenther, A., et al. (2006), Estimates of global terrestrial isoprene emissions using MEGAN (Model of Emissions of Gases and Aerosols from Nature), *Atmos. Chem. Phys.*, 6(11), 3181-3210.
- Hagerman, L. M., et al. (1997), Characterization of non-methane hydrocarbons in the rural southeast United States, *Atmospheric Environment*, 31(23), 4017-4038.
- Hakami, A., et al. (2003), High-order, direct sensitivity analysis of multidimensional air quality models, *Environmental Science & Technology*, 37(11), 2442-2452.
- Hakami, A., et al. (2004), Nonlinearity in atmospheric response: A direct sensitivity analysis approach, *Journal of Geophysical Research-Atmospheres*, 109(D15), DOI: 10.1029/2003JD004502.
- Hanna, S. R., et al. (1998), Monte carlo estimates of uncertainties in predictions by a photochemical grid model (UAM-IV) due to uncertainties in input variables, *Atmospheric Environment*, 32(21), 3619-3628.
- Hanna, S. R., et al. (2001), Uncertainties in predicted ozone concentrations due to input uncertainties for the UAM-V photochemical grid model applied to the July 1995 OTAG domain, *Atmospheric Environment*, 35 (5), 891-903.
- Harley, R. A., et al. (1997), Updated Photochemical Modeling for California's South Coast Air Basin: Comparison of Chemical Mechanisms and Motor Vehicle Emission Inventories, *Environmental Science & Technology*, 31(10), 2829-2839.
- Hart J. E. et al. (2011), Long-term ambient multipollutant exposures and mortality, *Am. J. Respir. Crit. Care Med.*, 183, 73-78.
- Hill, J., et al. (2009), Climate change and health costs of air emissions from biofuels and gasoline., *Proceedings of the National Academy of Sciences of the United States of America*, 106(6), 2077 - 2082. doi:2010.1073/pnas.0812835106
- Hippler, H., et al. (2006), Reaction of OH+NO₂: High pressure experiments and falloff analysis. , *Journal of Physical Chemistry A*, 110, 6781-6788.

- Hogrefe, C., and S. T. Rao (2001), Demonstrating attainment of the air quality standards: Integration of observations and model predictions into the probabilistic framework, *Journal of the Air & Waste Management Association* 51(7), 1060-1072.
- Hogrefe, C., et al. (2008), Rethinking the assessment of photochemical modeling systems in air quality planning applications, *Journal of the Air & Waste Management Association*, 58(8), 1086-1099.
- Holland, D. M. and T. Fitz-Simons (1982), Fitting statistical distributions to air quality data by the maximum likelihood method, *Atmospheric Environment* 16(5), 1071-1076.
- Hubbell, B. (2005), Response surface metamodeling for Ozone and PM2.5, in *EPA Modeling Workshops, 3rd Particulate Matter/Regional Haze/Ozone Modeling* edited, New Orleans, LA.
- Hubbell, B. J., et al. (2004), Health-Related Benefits of Attaining the 8-Hr Ozone Standard, *Environ Health Perspect*, 113(1).
- Ito, K., et al. (2005), Associations between ozone and daily mortality - Analysis and meta-analysis, *Epidemiology*, 16(4), 446-457.
- Jerrett, M., et al. (2009), Long-term ozone exposure and mortality., *New England Journal of Medicine*., 360(11), 1085-1095.
- Jin, L., et al. (2008), Sensitivity Analysis of Ozone Formation and Transport for a Central California Air Pollution Episode, *Environmental Science & Technology*, 42(10), 3683-3689.
- Jones, J. M., et al. (2005), An assessment of the sensitivity and reliability of the relative reduction factor approach in the development of 8-hr ozone attainment plans, *Journal of the Air & Waste Management Association*, 55(1), 13-19.
- Kim, S., et al. (2009), Contributions of inter- and intra-state emissions to ozone over Dallas-Fort Worth, Texas, *Civil Engineering and Environmental Systems*, 26, 103-116.
- Koo, B., et al. (2007a), Implementing the decoupled direct method for sensitivity analysis in a particulate matter air quality model, *Environmental Science & Technology*, 41(8), 2847-2854.
- Koo, B., et al. (2007b), Incorporation of High-order Decoupled Direct Method (HDDM) Sensitivity Analysis Capability into CAMx, Prepared for Texas Commission on Environmental Quality.
- Lamsal, L. N., et al. (2008), Ground-level nitrogen dioxide concentrations inferred from the satellite-borne Ozone Monitoring Instrument, *J. Geophys. Res.*, 113(D16), D16308.
- Lei W. et al. (2008), Characterizing ozone production and response under different meteorological conditions in Mexico City, *Atmos. Chem. Phys.*, 8, 7571-7581. DOI: 10.5194/acp-8-7571-2008.
- Lin, X., et al. (1988), On the Nonlinearity of the Tropospheric Ozone Production, *J. Geophys. Res.*, 93(D12), 15879-15888.
- Loeppky, J. L., et al. (2009), Choosing the sample size of a computer experiment: A practical guide, *Technometrics*, 51(4), 366.
- MACTEC Engineering and Consultancy, I. (2008), Documentation of the Base G2 and Best & Final 2002 Base Year, 2009 and 2018 Emission Inventories for VISTAS.

- Mallet, V. and B. Sportisse (2006), Ensemble-based air quality forecasts: A multimodal approach applied to ozone, *Journal of Geophysical Research-Atmospheres*, 111(D18302), 11 PP.
- Malm, W. C., et al. (1994), Spatial and seasonal trends in particle concentration and optical extinction in the United States, *Journal of Geophysical Research-Atmospheres*, 99(D1), 1347-1370.
- McConnell, R., et al. (2002), Asthma in exercising children exposed to ozone: a cohort study, *The Lancet*, 359(9304), 386-391.
- Mollner, A. K., et al. (2010), Rate of Gas Phase Association of Hydroxyl Radical and Nitrogen Dioxide, *Science*, 330(6004), 646-649.
- Moore, G. E. and Londergan, R. J. (2001), Sampled Monte Carlo uncertainty analysis for photochemical grid models, *Atmospheric Environment*, 35(28), 4863-4876.
- Morris, R. E., et al. (2008), Final Report: Technical support document for the Association for Southeastern Integrated Planning (ASIP) emissions and air quality modeling to support PM_{2.5} and 8-Hour ozone State Implementation Plans.
- Napelenok, S. L., et al. (2006), Decoupled direct 3D sensitivity analysis for particulate matter (DDM-3D/PM), *Atmospheric Environment*, 40(32), 6112-6121.
- Napelenok, S. L., et al. (2008), Extension and evaluation of sensitivity analysis capabilities in a photochemical model, *Environmental Modelling & Software*, 23(8), 994-999.
- NRC (2008), Estimating Mortality Risk Reduction and Economic Benefits from Controlling Ozone Air Pollution., National Research Council (NRC) of the National Academies, Committee on Estimating Mortality Risk Reduction Benefits from Decreasing Tropospheric Ozone Exposure, Washington, DC.
- Olerud, D., and A. Sims (2004), MM5 2002 modeling in support of VISTAS (Visibility Improvement – State and Tribal Association), Swannanoa, NC.
- Ostro, B. D., et al. (2006), The health benefits of reduced tropospheric ozone in California., *Journal of the Air & Waste Management Association*, 56(7), 1007-1021.
- Pierce, T., et al. (2010), Dynamic evaluation of a regional air quality model: Assessing the emissions-induced weekly ozone cycle, *Atmos Environ*, 44(29), 3583-3596.
- Pinder, R. W., et al. (2009), Efficient Probabilistic Estimates of Surface Ozone Concentration Using an Ensemble of Model Configurations and Direct Sensitivity Calculations, *Environmental Science & Technology*, 43(7), 2388-2393.
- Raftery, A. E., T. Gneiting, F. Balabdaoui, and M. Polakowski (2005), Using Bayesian Model Averaging to Calibrate Forecast Ensembles, *Monthly Weather Review*, 133, 1155-1174.
- Rappengluck, B. (2009), Air Quality Modeling of TexAQS-II Episodes with Data Assimilation, TERC Project H98, Final Report, edited.
- Renaut, J., et al. (2009), The impact of atmospheric composition on plants: A case study of ozone and poplar, *Mass Spectrometry Reviews*, 28(3), 495-516.
- Rodriguez, M. A., and D. Dabdub (2003), Monte Carlo uncertainty and sensitivity analysis of the CACM chemical mechanism, *J. Geophys. Res.*, 108(D15), 4443.
- Russell, A., and R. Dennis (2000), NARSTO critical review of photochemical models and modeling, *Atmospheric Environment*, 34(12-14), 2283-2324.

- Ryerson, T. B. et al. (2001), Observations of ozone formation in power plant plumes and implications for ozone control strategies, *Science*, 292(5517), 719-723. DOI: 10.1126/science.1058113.
- Sander S P, F. R. R., Ravishankara A R, Golden D M, Kolb C E, Kurylo M J, Molina M J, Moortgat G K, Rudek H K, Finlayson-Pitts B J, Wine P H, Huie R E (2006), Chemical kinetics and photochemical data for use in atmospheric studies, NASA JPL.
- Schubert S. D., Rood R. B., and Pfaendtner J. (1993), An assimilated data set for Earth Science applications, *Bull. Am. Meteorol. Soc.*, 74, 2331-2342.
- Seinfeld, J. H., and S. N. Pandis (2006), *Atmospheric Chemistry and Physics*, Second ed., John Wiley & Sons, Inc.
- Shih, J.-S., et al. (1998), An optimization model for photochemical air pollution control, *European Journal of Operational Research*, 106(1), 1-14.
- Sillman, S., et al. (1995), Photochemistry of ozone formation in Atlanta, GA - Models and measurements *Atmospheric Environment*, 29(21), 3055-3066.
- Sistla, G., et al. (2004), An operational assessment of the application of the Relative Reduction Factors in the demonstration of attainment of the 8-Hr ozone National Ambient Air Quality Standard *Journal of the Air & Waste Management Association*, 54(8), 950-959.
- Slinn, S. A., and W. G. N. Slinn (1980), Predictions for particle deposition on natural waters, *Atmos Environ*, 14(9), 1013-1016.
- Solomon, P. A., et al. (2003), Overview of the 1999 Atlanta Supersite Project, *Journal of Geophysical Research-Atmospheres*, 108(D7), 24.
- Srivastava, R. K., and W. Jozewicz (2001), Flue gas desulfurization: The state of the art, *Journal of the Air & Waste Management Association*, 51(12), 1676-1688.
- Srivastava, R. K., et al. (2005), Nitrogen oxides emission control options for coal-fired electric utility boilers, *Journal of the Air & Waste Management Association*, 55(9), 1367-1388.
- Talagrand, O. R., et al. (1997), Evaluation of probabilistic prediction systems, *Proceedings, ECMWF Workshop on Predictability*, 1-25.
- Taylor, J. A., R. W. Simpson, and A. J. Jakeman (1987), Statistical modeling of restricted pollutant data sets to assess compliance with air quality criteria, *Environmental Monitoring and Assessment*, 9(1), 29-46.
- TCEQ (2011a), Dallas-Fort Worth attainment demonstration SIP revision for the 1997 eight-hour ozone standard nonattainment area. Prepared for Texas Commission on Environmental Quality as part of the revisions to the state of Texas air quality implementation plan for the control of ozone air pollution in Dallas-Fort Worth eight-hour ozone nonattainment area.
- TCEQ (2011b), Dallas-Fort Worth reasonable further progress state implementation plan revision for the 1997 eight-hour Ozone standard. Prepared for Texas Commission on Environmental Quality as part of the Revisions to the State of Texas air quality implementation plan for the control of ozone air pollution in Dallas-Fort Worth 1997 eight-hour Ozone nonattainment area.

- Tian, D., et al. (2010), Uncertainty analysis of ozone formation and response to emission controls using higher-order sensitivities, *Journal of the Air & Waste Management Association*, 60, 797 - 804.
- Tonnesen, G. S. (1999), Effects of uncertainty in the reaction of the hydroxyl radical with nitrogen dioxide on model-simulated ozone control strategies, *Atmospheric Environment*, 33(10), 1587-1598.
- US-EPA (1999), The Benefits and Costs of the Clean Air Act, 1990-2010.
- US-EPA (2007), Guidance on the use of models and other analyses for demonstrating attainment of air quality goals for ozone, PM2.5, and regional haze.
- USEPA (1999), Draft report on the use of models and other analyses in attainment demonstrations for the 8-hr Ozone NAAQS, U.S. Environmental Protection Agency, Research Triangle Park, NC.
- USEPA (2006a), Documentation for EPA Base Case 2006 (V.3.0) using the Integrated Planning Model.
- USEPA (2006b), Air Quality Criteria for Ozone and Related Photochemical Oxidants., edited.
- USEPA (2007), Guidance on the use of models and other analyses for demonstrating attainment of air quality goals for Ozone, PM2.5, and Regional Haze.
- USEPA (2010), National Ambient Air Quality Standards for Ozone, in *Proposed Rules*, edited.
- USEPA (March, 2010), Policy Assessment for the Review of the Particulate Matter National Ambient Air Quality Standards., in - *First external review draft.*, edited.
- USEPA (2011), Green Book Nonattainment Areas for Criteria Pollutants.
- Wang, L., and J. B. Milford (2001), Reliability of Optimal Control Strategies for Photochemical Air Pollution, *Environmental Science & Technology*, 35(6), 1173-1180.
- Wesely, M. L. (1989), Parameterization of surface resistances to gaseous dry deposition in regional-scale numerical models, *Atmospheric Environment (1967)*, 23(6), 1293-1304.
- Wesely, M. L., and B. B. Hicks (2000), A review of the current status of knowledge on dry deposition, *Atmospheric Environment*, 34, 2261-2282.
- West, J. J., et al. (1999), Marginal PM2.5: Nonlinear aerosol mass response to sulfate reductions in the Eastern United States, *Journal of the Air & Waste Management Association*, 49(12), 1415-1424.
- Yang, Y.-J., et al. (1997), Fast, direct sensitivity analysis of multidimensional photochemical models, *Environmental Science & Technology*, 31(10), 2859-2868.
- Yang, Z., et al. (2006), A Decision-Making Framework for Ozone Pollution Control, *Operational Research*, 57(2), 484-498.
- Yarwood, G., et al. (1999), Development of the GloBEIS—a state of the science biogenic emissions modeling system. Final Report to the Texas Natural Resource Conservation Commission., Austin, TX.
- Yarwood, G., et al. (2005), Updates to the Carbon Bond chemical mechanism: CB05. Final Report to the U.S. EPA.
- Yarwood, G., et al. (2010), Development, Evaluation and Testing of Version 6 of the Carbon Bond Chemical Mechanism (CB6), Final Report prepared for Texas Commission on Environmental Quality.
- Zhang, L. M., et al. (2001), A size-segregated particle dry deposition scheme for an atmospheric aerosol module, *Atmos Environ*, 35(3), 549-560.

- Zhang, L., et al. (2003), A revised parameterization for gaseous dry deposition in air-quality models, *Atmospheric Chemistry and Physics*, 3, 2067-2082.
- Zhou, Y., et al. (2010), Risk-Based Prioritization among Air Pollution Control Strategies in the Yangtze River Delta, China, *Environ Health Perspect*, 118(9).

Appendix A

SUPPLEMENTARY INFORMATION TO CHAPTER 5: USING GROUND-BASED OBSERVATIONS TO CONSTRAIN PROBABILISTIC PREDICTIONS OF OZONE-PRECURSOR RESPONSIVENESS

A1. Ensemble Quality

Brier Score & Sharpness:

The quality of the final *a posteriori* model ensembles is evaluated by computing two properties that are often used to assess probabilistic forecasts: the *Brier Score* (which is a combined measure for the forecast *Reliability*, *Resolution* and *Uncertainty*), and the *Sharpness*. The *Brier Score* is the mean squared error of the probability forecast and can be expressed as “*Reliability – Resolution + Uncertainty*” as explained in *Wilks* [2006]. *Reliability* represents the conditional bias of the forecast ensemble and *Resolution* is a measure of the degree to which the ensemble sorts observed events into groups that are different from each other. *Sharpness* is an indication of the variance (or spread) of the predicted ensemble density and is independent of the observations. Therefore, for both *Brier Score* and *Sharpness*, a lower value implies better performance of the ensemble.

Table A.1 reveals that although the base model, by definition, has the maximum *Sharpness*, the adjusted ensembles have relatively lower *Brier Scores* (for predicting 8-hour O₃ concentrations to exceed a threshold of 75 ppb) than the base-case deterministic model, thereby indicating a good-performing ensemble, particularly for attainment demonstration.

Statistics	Base Case Model (deterministic)	Adjusted <i>a posteriori</i> ensemble		
		Metric 1	Metric 2	Metric 3
Brier Score for predicting 8-hour O₃ > 75 ppb	0.253	0.195	0.204	0.205
Sharpness in predicting 8-hour O₃ > 75 ppb	0	0.049	0.041	0.033

Table A.1 – Comparison of prior and posterior episode average ozone concentrations and sensitivities at Denton.

Rank Histogram:

The *Talagrand* diagram, popularly known as the rank histogram [Talagrand *et al.*, 1997], is a statistical tool to assess the measure of differences in the ensemble predictions (spread). The ensemble is distributed into $(M + 1)$ bins, where $M =$ number of ensemble predictions (4000). For each of the N observations (site and days), the ensemble predictions are ranked along with the observed value to find out the bin in which the observation is falling. A rank histogram is then constructed by tallying over these N observed dataset and plotting the frequency of the rank of

the observation. A rank histogram therefore evaluates whether the model-ensemble is able to predict the actual observations such that the occurrence of the observation within each bin is equally likely, and a flat rank histogram would indicate that the ensemble has the correct spread (rank uniformity).

The ensemble used in this study has an *underforecasting bias*, reflected in the preponderance of observations that fall on the right of the rank histogram (Figure A.1, a), above the majority of the model cases. The rank histogram also shows the prior ensemble spread to be too narrow (*underdispersive*), as reflected in the U shape. Note both the large first bin, which shows that many observations fall below most or all of the model cases and the large bins toward the right.

For the *a posteriori* ensembles, the U shape of the rank histograms (overconfidence) becomes even more pronounced (Figure A.1, b-d). Although these metrics (especially Metrics 2 and 3) strive to make majority of the distribution uniform (central bins), they fail to adjust the extreme bins that were present in the prior ensemble. Thus, the bulk of each ensembles lie above some observations (leading to the large left-most column), and below other observations (leading to the large right-most column).

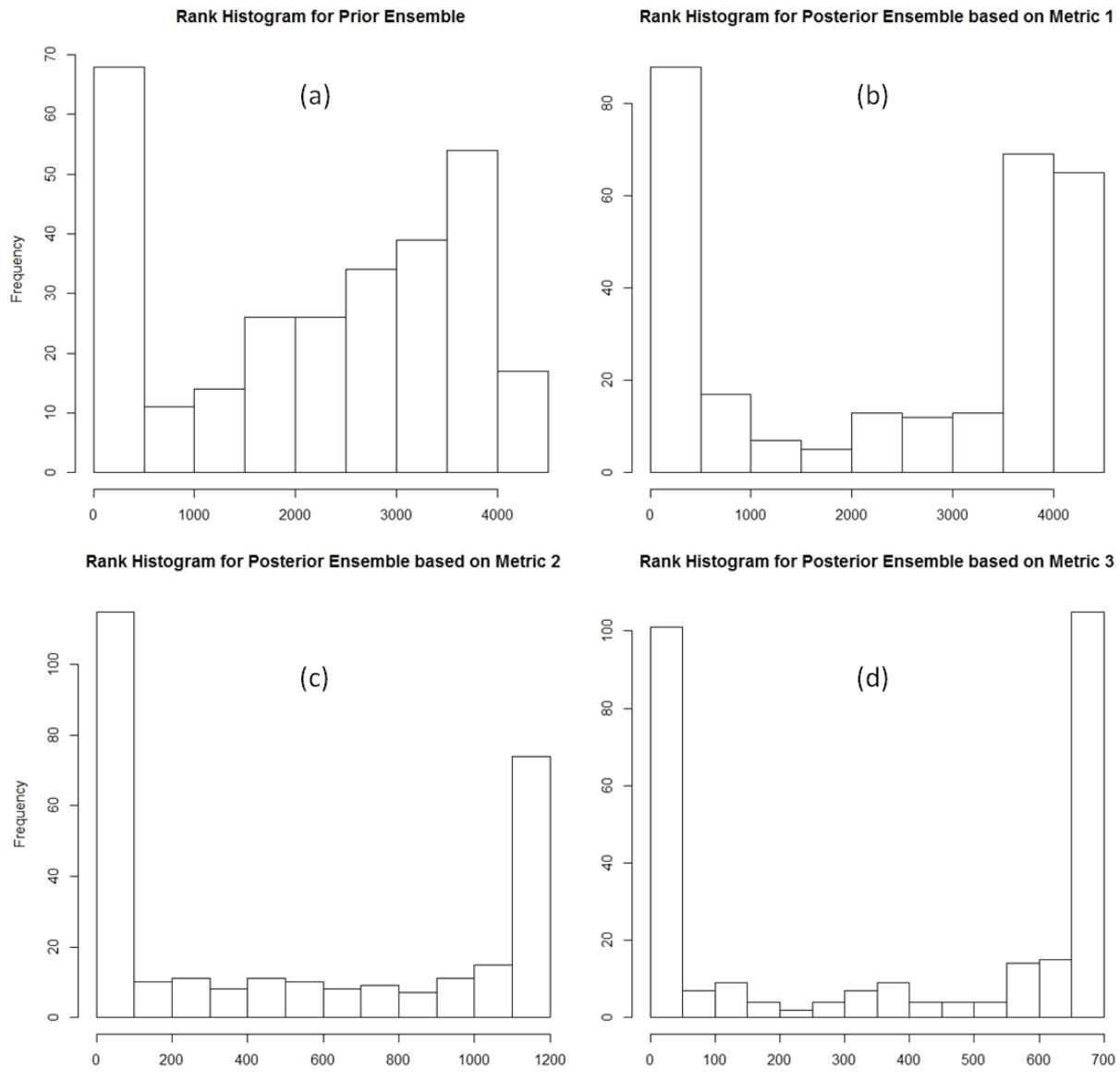


Figure A.1 – Rank histogram for the prior and the posterior ensembles.

A2. Ensemble Performance

The ensemble-mean predictions for episode-average 8-hour O₃ concentration at all the 11 DFW sites considered for our study are listed in Table A.2. In an effort to adjust the prior underprediction of the base model (Figure 5.7 and Figure 5.11), the ensemble prefers higher NO_x emissions (Figure 5.9), which results in an overall increase in 8-hour O₃ concentrations at all sites. Therefore, the posterior adjustments improved the prediction accuracy for the sites that had large underpredictions in the base-case modeling (Table A.2).

Site	2006 DV (ppb)	Episode-average 8-hour O ₃ concentration (ppb)					
		Observation	Base-Model Prediction	<i>a priori</i> ($\mu \pm \sigma$)	<i>a posteriori</i> ($\mu \pm \sigma$)		
					Metric 1	Metric 2	Metric 3
DENT	93.33	70.11	61.98	65.51 \pm 7.33	65.53 \pm 2.16	69.04 \pm 2.03	68.85 \pm 1.87
GRAP	90.67	68.79	63.20	66.62 \pm 7.21	66.76 \pm 2.21	70.02 \pm 2.17	69.98 \pm 2.03
FWMC	89.33	59.54	62.42	66.10 \pm 7.17	66.23 \pm 2.22	69.50 \pm 2.17	69.43 \pm 2.01
DALN	85.00	62.34	60.52	64.09 \pm 7.00	64.25 \pm 2.11	67.42 \pm 1.99	67.36 \pm 1.84
REDB	85.00	64.91	59.26	62.73 \pm 7.07	62.75 \pm 2.09	66.13 \pm 1.91	65.94 \pm 1.74
ARLA	83.33	65.51	61.63	65.12 \pm 7.27	65.12 \pm 2.17	68.61 \pm 2.01	68.43 1.86
DHIC	81.67	61.70	59.53	63.08 \pm 6.75	63.33 \pm 2.09	66.27 \pm 2.04	66.26 \pm 1.88
MDLT	80.50	62.03	56.57	59.77 \pm 6.76	59.77 \pm 2.00	63.01 \pm 1.91	62.77 \pm 1.75
MDLO	75.00	57.68	55.96	59.23 \pm 6.50	59.35 \pm 1.94	62.32 \pm 1.82	62.19 \pm 1.71
GRVL	75.00	61.02	53.96	57.04 \pm 6.70	56.96 \pm 2.10	60.29 \pm 2.11	59.96 \pm 1.79
KAUF	74.67	58.04	55.22	58.31 \pm 6.88	58.20 \pm 2.14	61.64 \pm 2.14	61.29 \pm 1.81

Table A.2 – Comparison of episode average 8-hour ozone concentrations at the DFW sites.

Appendix B

PUBLICATIONS RELATED TO THE RESEARCH DESCRIBED IN THIS THESIS

1. **Digar, A.**, and Cohan D. S. (2010), Efficient characterization of pollutant-emission response under parametric uncertainty, *Environmental Science & Technology*, 44(17), 6724-6730. **DOI:** 10.1021/es903743t.
2. Cohan D. S., **Digar A.** and Bell M. L. (2010). Influence of concentration-response temporal metrics on control strategy optimization. *Air Pollution Modeling and Its Application XX*, Eds. D.G. Steyn and S.T. Rao, Springer Publishing, 421-425.
3. **Digar, A.**, Cohan D. S., Cox D. D., Kim B., and Boylan J. W. (2011), Likelihood of Achieving Air Quality Targets under Model Uncertainties, *Environmental Science & Technology*, 45(1), 189-196. **DOI:** 10.1021/es102581e.
4. **Digar, A.**, Cohan D. S., and Bell M. L. (2011), Uncertainties Influencing Health-Based Prioritization of Ozone Abatement Options, *Environmental Science & Technology*, 45(18), 7761-7767. **DOI:** 10.1021/es200165n.
5. **Digar, A.**, Cohan D. S., Xiao, X., Foley, K. M., Koo, B. and Yarwood G., Constraining ozone-precursor responsiveness using ground-based measurements. In preparation for *Journal of Geophysical Research*.

Appendix C

PRESENTATIONS RELATED TO THE RESEARCH DESCRIBED IN THIS THESIS

1. **Digar A.**, Cohan D. S. and Foley K. (2011). Bayesian probabilistic evaluation of emissions and pollutant sensitivities; AGU Fall Meeting, San Francisco, California, USA.
2. **Digar A.**, Cohan D. S. and Foley K. (2011). Bayesian analysis of uncertainties in ozone response estimates; 10th Annual CMAS Conference, Chapel Hill, North Carolina, USA.
3. Cohan D. S. and **Digar A.** (2011). Characterizing uncertainty in atmospheric response modeling; AEESP Education and Research Conference, Florida, USA.
4. Cohan D. S. and **Digar A.** (2010). Assessing attainment likelihood of State Implementation Plans; *90th Annual AMS Meeting*, Atlanta, GA, USA.
5. Cohan D. S., **Digar A.**, Bell M. L. and Tang W. (2010). Uncertainties influencing health-based prioritization of ozone abatement options; *9th Annual CMAS Conference*, North Carolina, USA.
6. **Digar A.** and Cohan D. S. (2009). Efficient characterization of uncertainty in control strategy impact predictions; *8th Annual CMAS Conference*, North Carolina, USA.
7. Cohan D. S. and **Digar A.** (2009). Accuracy of multi-parameter response surfaces generated using sensitivity coefficients; *8th Annual CMAS Conference*, North Carolina, USA.

8. Cohan D. S. and **Digar A.** (2009). Uncertainty in integrated air quality planning; *2nd Georgia Air Policy Symposium*, Atlanta, GA USA.
9. Cohan D. S. and **Digar A.** (2009). Influence of Concentration-Response Temporal Metrics on Control Strategy Optimization; *NATO/SPS International Technical Meeting on Air Pollution Modelling and its Application*, San Francisco, CA, USA.
10. Cohan D. S. and **Digar A.** (2008). Reaction rate uncertainty in the development of control strategies; *International Conference on Atmospheric Chemical Mechanisms*, Davis, CA, USA.
11. **Digar A.**, Cohan D. S., Boylan J. W., Khan M., Cox D. D. (2008). Incorporating uncertainty into air quality modeling and planning—A case study for Georgia; *7th Annual CMAS Conference*, North Carolina, USA.